ERDC TR-22-21

US Army Corps
of Engineers®
Engineer Research and
Development Center

ERDC
ENGINEER RESEARCH & DEVELOPMENT CENTER

Development and Validation of a Balanced Mix Design Approach for CIR Mixtures Using Full-Scale Testing

Ayman Ali, Ahmed Saidi, Yusuf Mehta, Christopher J. DeCarlo,
Mohamed H. Elshaer, Ben C. Cox, and Wade A. Lein

October 2022

Approved for public release; distribution is unlimited.

Engineer Research and
Development Center

The U.S. Army Engineer Research and Development Center (ERDC) solves the nation's toughest engineering and environmental challenges. ERDC develops innovative solutions in civil and military engineering, geospatial sciences, water resources, and environmental sciences for the Army, the Department of Defense, civilian agencies, and our nation's public good. Find out more at www.erdc.usace.army.mil.

To search for other technical reports published by ERDC, visit the ERDC online library at https://erdclibrary.on.worldcat.org/discovery.

ERDC TR-22-21
October 2022

Development and Validation of a Balanced Mix Design Approach for CIR Mixtures Using Full-Scale Testing

Ayman Ali, Ahmed Saidi, and Yusuf Mehta

Center for Research and Education in Advanced Transportation Engineering Systems (CREATEs)
Rowan University
201 Mullica Hill Rd.
Glassboro, NJ 08028

Christopher J. Decarlo, Mohamed H. Elshaer and Wade A. Lein

US Army Engineer Research and Development Center (ERDC)
Cold Regions Research and Engineering Laboratory (CRREL)
72 Lyme Road
Hanover, NH 03755-1290

Ben C. Cox

US Army Engineer Research and Development Center (ERDC)
Geotechnical and Structure Laboratory (GSL)
3909 Halls Ferry Road
Vicksburg, MS 39180

Final Report

Prepared for Headquarters, US Army Corps of Engineers
Washington, DC 20314-1000

Under PE 0602784A, Project T53, Task 09, “Military Engineering Applied Research”

Abstract

The main goal of this study was to improve the performance of cold in-place recycling (CIR) mixtures by using a balanced mix design (BMD) approach. This study involved preparing and testing CIR mixtures in the lab at varying contents of bituminous additives and constant content of 1% cement and 3% water. Eight combinations of CIR mixtures were produced for this study using two binders (emulsion and foamed asphalt), compaction efforts (30 and 70 gyrations), and curing processes (72 hours at 140°F and 50°F). Results showed that asphalt pavement analyzer, semicircular bend, and indirect tensile strength tests presented the highest correlation with the change of binder contents. The study successfully used the developed BMD for designing CIR mixtures and selecting their optimum binder contents. It then used three balanced CIR mixtures to construct full-scale pavement sections to validate the BMD approach in the field. A heavy vehicle simulator was used to apply different accelerated loadings on each section. Results showed that the CIR section with 2% binder presented the best rutting performance under truck loading and the highest rutting susceptibility under aircraft loading. Conversely, the CIR section with 3% binder presented the highest cracking resistance under both truck and aircraft loading.

Contents

Figures and Tables

Figures

Tables

Preface

This study was conducted for Headquarters, US Army Corps of Engineers, under PE 0602784A, Project T53, Task 09, "Military Engineering Applied Research."

The work was performed by the Engineering Resources Branch (Dr. Melisa Nallar, acting chief) and the Force Projection and Sustainment Branch (Dr. Wade Lein, acting chief) of the Research and Engineering Division, US Army Engineer Research and Development Center (ERDC), Cold Regions Research and Engineering Laboratory (CRREL). At the time of publication, Dr. Caitlin A. Callaghan was division chief. The acting deputy director of ERDC-CRREL was Mr. Bryan E. Baker, and the director was Dr. Joseph L. Corriveau.

This work was also performed by the Airfields and Pavements Branch of the Engineering Systems and Materials Division, ERDC Geotechnical and Structures Laboratory (GSL). At the time of publication, Ms. Anna Jordan was branch chief; Mr. Justin S. Strickler was division chief; and Mr. R. Nicholas Boone was the technical director for Force Projection and Maneuver Support. The deputy director of ERDC-GSL was Mr. Charles W. Ertle II, and the director was Mr. Bartley P. Durst.

COL Christian Patterson was commander of ERDC, and Dr. David W. Pittman was the director.

Executive Summary

This study aimed to develop a performance-based laboratory design approach for cold in-place recycling (CIR) asphalt mixtures. In addition, the study involved validating the laboratory mix design approach through full-scale accelerated pavement testing. In particular, eight CIR mixtures were prepared using two bituminous additives (foamed and emulsified asphalts), cured for three days at two temperatures (either hot curing at 140°F [60°C] or cold curing at 50°F [10°C]), and compacted at two gyration levels (30 or 70 gyrations). The CIR mixtures were prepared at a constant water and cement content of 3% and 1%, respectively. A balanced CIR mix design approach was developed and used successfully to design eight CIR mixtures and to select the optimum binder content for each mix. Experimental and statistical evaluation was also conducted on CIR mixtures prepared at optimum binder contents.

Furthermore, three full-scale CIR sections were constructed at the Center for Research and Education in Advanced Transportation Engineering Systems (CREATEs) through reclaiming and recycling the existing asphalt pavement structure. All CIR sections were prepared using 3% water (by total weight), 0% cement, and neat PG64-22 foamed asphalt at 2% (CIR2%FAC section), 3% (CIR3%FAC section), and 4% (CIR4%FAC section) bituminous additives' contents. Each of the sections was instrumented with four asphalt strain gauges and two pressure cells placed at the bottom of the CIR layer. Heavy weight deflectometer (HWD) testing and rutting (through measuring transverse depth profiles) were conducted before and after the placement of the hot mix asphalt layer. A heavy vehicle simulator was also used to apply full-scale accelerated loading on the balanced CIR sections for (1) 150,000 cycles using a truck tire to simulate low to medium traffic level and (2) 50,000 passes using an aircraft tire to simulate airfield loading conditions.

The laboratory and full-scale accelerated testing results and the subsequent analyses conducted resulted in the following conclusions:

- The BMD approach was used successfully in designing eight CIR mixtures. This was evidenced with performance-testing results that highlighted the importance of rutting measures, which generally previous

mix design methods for CIR mixtures did not consider, and the dependence of rutting measures on the binder content of emulsified and foamed asphalt binder content.

- Emulsified and foamed asphalt CIR mixtures presented similar rutting performance at different compaction efforts and curing processes. With regard to cracking, emulsified asphalt CIR mixtures exhibited higher fracture energy than that of foamed asphalt CIR mixtures, indicating better cracking resistance than foamed asphalt CIR mixtures.

- In general, the HWD backcalculated moduli values indicated that the CIR4%FAC section had the highest structural responses before and after accelerated loading. This is because the moduli values for the CIR layer of this section were higher than those for the other two sections before and after the application of loading.

- The recorded transverse pavement profiles showed that the three CIR sections had similar rut-depth values (i.e., within 0.1 in. [3 mm] rut depth) after the application of truck loading (i.e., 9,000 lb [40 kN] and 115 psi [0.8 MPa]).

- Under aircraft loading (i.e., 22,500 lb [100 kN] and 196 psi [1.35 MPa]) applied immediately after the truck loading, the recorded rut-depth values increased meaningfully for all three sections, exceeding the rutting failure criteria of 1 in. (25 mm) within 11,000 loading passes. The rate of failure was fastest for the CIR2%FAC section, when compared to the other two CIR sections, indicating that the increase in loading and tire pressure caused higher shear strain movements, which increased the susceptibility of this section to rutting. Under aircraft loading, the CIR layer behaved more like an unbound granular layer as opposed to a bound pavement layer. This may explain why the CIR2%FAC section (i.e., one with lowest CIR binder) was the most susceptible to rutting under aircraft loading.

This page intentionally left blank.

1 Introduction

1.1 Background

Cold in-place recycling (CIR) is a rehabilitation technique that involves processing and treating deteriorated asphalt pavements by using either bituminous or cementitious stabilization agents or both. As the name implies, CIR does not require heat when restoring a damaged pavement layer (AASHTO [American Association of State Highway and Transportation Officials] 1998) because the CIR mix is produced at ambient site temperatures. CIR has successfully rehabilitated all kinds of pavements, such as city and county roads and highways with different traffic volumes (Lewis and Collings 1999; Forsberg et al. 2002; Fišer and Varaus 2004; Modarres et al. 2014; Cox and Howard 2013; Lane and Kazmierowski 2014). The use of CIR offers several construction, economic, and environmental advantages over other conventional rehabilitation techniques (Kim et al. 2009; Chen et al. 2010). For instance, CIR involves milling existing deteriorated pavement and reusing reclaimed millings to produce a stabilized base pavement layer. The CIR process leads to reduced construction time and eliminates the need to use virgin aggregates, thus persevering resources.

CIR is a solution for constructing pavements in remote locations, such as the Arctic region, as it allows construction materials to be obtained from existing pavements. CIR provides meaningful savings regarding fuel consumption and the number of trucks needed to haul materials. Research has also shown CIR to be an ecofriendly technique since it does not require any heating, which reduces the release of greenhouse gas emission. Moreover, traffic disruption is remarkably low when using CIR compared to other conventional techniques, facilitating rapid repairs and quick opening to traffic (Kim et al. 2011; Black 2013; Turk et al. 2016; Sanger et al. 2017).

Several studies have conducted extensive research to improve the performance of CIR mixtures (Kim and Lee 2006; Kim et al. 2007; Wegman and Sabouri 2016; Ozer 2015; Cox and Howard 2015a). Researchers, agencies, and state departments of transportation (DOTs) on CIR projects developed and utilized different mix design methods. However, previous CIR-related studies had several gaps, discussed further in chapter 2:

- The CIR rehabilitation technique was generally performed on asphalt pavements with low to medium traffic conditions.
- Most CIR mix design procedures did not include air-void measurements of the prepared CIR mixtures.
- CIR mix design methods have relied primarily on Marshall stability or indirect tensile strength, which have both exhibited shortcomings in other works.
- Studies' methods have not addressed how curing should be handled for CIR applications in cold and Arctic regions.
- Studies lacked full-scale testing results for CIR mixtures.

Therefore, there is a need to develop a balanced mix design (BMD) method for designing CIR mixtures to meet heavy loading, especially in airfields. It is also important to validate the efficiency of the BMD approach through a full-scale accelerated pavement testing program. Our research here is valuable as it will help guide the process of updating and modifying the standard practice for pavement recycling that the US Department of Defense currently uses for designing CIR mixtures.

1.2 Objectives

The overall goal of this study was to develop and validate a BMD approach for designing CIR mixtures that can withstand aircraft traffic. To achieve this goal, this study evaluated the impacts of compaction effort (30 vs. 70 gyrations), curing process (hot vs. cold), and bituminous additive type (emulsion vs. foamed asphalt) on the rutting and cracking performance of CIR mixes. In addition, this study constructed three full-scale (60 ft [18.3 m] long by 12 ft [3.7 m] wide) CIR sections to validate the results of the performance-balanced laboratory mix design approach.

The specific objectives established to successfully achieve the goal of this study included the following:

- Develop a laboratory procedure for designing CIR mixtures, focusing on determining the optimal binder content at which both rutting and cracking performances of CIR mixtures are balanced.
- Evaluate, experimentally and statistically, the impact of binding agent type, compaction level, and curing process on rutting and cracking performances of CIR mixtures.

- Construct three fully instrumented CIR pavement sections and subject these sections to accelerated loading and testing using a heavy vehicle simulator (HVS).

1.3 Approach

This report is divided into seven chapters. Following this brief introduction and goals of the project, chapter 2 summarizes current literature pertaining to CIR technologies, benefits of CIR, CIR mix design procedures, and more. Chapter 3 discusses materials used for this study, detailing the selected bituminous additives, curing conditions employed, and compaction levels. Chapter 4 details the BMD approach as well as the experimental program developed to evaluate CIR mixes. Chapter 5 discusses the laboratory performance-testing results and the subsequent statistical analyses. Chapter 6 details the construction activities and testing results of three full-scale CIR test sections constructed as part of this study. Finally, chapter 7 presents a summary of findings, conclusions, and recommended future research.

2 Literature Review

2.1 Introduction

This chapter presents a comprehensive literature review pertaining to CIR asphalt mixtures. The following subsections provide information relevant to the CIR process, the various CIR mix design methodologies, the best CIR field construction practices, and the reported laboratory and field performance of CIR mixtures and pavements.

2.2 General cold in-place recycling process

CIR consists of milling the existing pavement to a certain depth, width, and length, then sizing the reclaimed asphalt pavement (RAP) material to an evenly graded aggregate mix with a maximum size of 1 in (25 mm). Bituminous additives such as emulsified asphalt and foamed asphalt are then added to the graded RAP to obtain a homogeneous and uniformly coated recycled pavement mixture. The RAP material must be put in place, then compacted in conformance with the plans and standard specifications (Davidson and Croteau 2003; ARRA [Asphalt Recycling and Reclaiming Association] 1992; Hicks et al. 1987; Winke 2014). Figure 1 illustrates the CIR construction. The following subsections discuss the CIR construction and practice guidelines and provide information pertaining to the successful construction of a CIR pavement layer.

Figure 1. Cold in-place recycling equipment.

2.2.1 Step 1: Project selection and CIR requirements

Prior to selecting CIR as the method for repairing a deteriorated pavement, a field survey is required to examine the degree of existing distresses and identify their exact locations. In general, a field survey collects the following information (Stroup-Gardiner 2012):

- Records review: assessment of construction and maintenance information and review of past condition surveys
- Visual inspection: determining mode and severity of pavement distresses
- Pavement investigation: additional information on the nature and condition of the asphalt pavement and the extent of the distresses

Generally, CIR is performed on cracked asphalt pavements with sound structure and well-drained bases. CIR is also applicable on pavements featuring load- and non-load-associated distresses (i.e., transverse cracks, longitudinal cracks, fatigue cracks, rutting, raveling, potholes, and polished surfaces). It is important to note that deteriorated asphalt pavement layer should be treated at early stages (i.e., when ruts and cracks begin to appear) to ensure a satisfactory service life of CIR-rehabilitated pavements (Federal Highway Administration 2018).

2.2.2 Step 2: Mix design of CIR

The second major step in the general CIR process is the design of CIR mixture by determining the optimum binder content. A portion of the pavement section is milled, and RAP is collected for further analysis. RAP is then used to prepare CIR mixtures. The mix design process also involves determining the percentages of water and cementitious additives to be used in the mixture. For additional details about the various methods for designing CIR mixtures, refer to section 2.3.

2.2.3 Step 3: Milling the deteriorated surface pavement layer

The field portion of the CIR process begins after finalizing the mix design. An equipment train (Figure 2) is used to complete the process on-site (or in-place). A milling machine is the first piece of equipment used for reclaiming the deteriorated surface pavement layer (Figure 2). The milling machine mills the top 2–4 in. (51–102 mm) of the surface layer of deteriorated pavements.

Figure 2. CIR milling process.

2.2.4 Step 4: Millings sizing and mixing with bituminous and cementitious additives

Crushing and screening equipment is then used to reduce the RAP to desired sizes (i.e., maximum size of 1 in; Kim and Lee 2011; Wirtgen 2016). After crushing and sizing, the RAP is treated in a mixing unit using selected bituminous additives (e.g., emulsified asphalt) with water and cementitious additives. In addition, certain CIR practices call for spreading the cementitious additives (e.g., portland cement) on top of the existing pavement before milling instead of mixing it with RAP, bituminous additives, and water in the mixing unit.

2.2.5 Step 5: Placement of the CIR mix

The CIR mixture is placed over the milled pavement and graded to the desired thickness. Conventional asphalt pavers or self-propelled pavers are used to place the CIR mixture (Figure 3). It is important to note that the lift thickness for a CIR mixture is typically a minimum of 2 in. (51 mm), especially when millings have a larger aggregate size (Wirtgen 2012).

Figure 3. CIR mix placement.

2.2.6 Step 6: Compaction of placed CIR mix

After the CIR mix is placed, primary compactionis applied on the CIR layer by using traditional compaction equipment such as a vibratory steel drum or pneumatic tire rollers (Figure 4). In general, compaction operations should start 15 minutes after placement of the CIR layer when the ambient temperature is above 60°F (15.6°C). Cases where the ambient temperature is below 60°F (15.6°C) require a waiting time of 10 minutes for each 5°F (–15°C) below 60°F (Tario 2010). Nuclear density testing (ASTM D2950) is conducted at regular intervals throughout the compaction process (Wirtgen 2012, n.d.; ASTM 2014).

Figure 4. Compaction process.

2.2.7 Step 7: Curing and maintenance

Prior to placing the final surface, the CIR layer is typically given time to cure. For example, Tario (2010) requires (a) at least 2 days as long as moisture is below 2.0% or (b) at least 10 days without rainfall. Once cured, a hot mix asphalt (HMA) layer is generally paved on top of the CIR layer to provide structural strength to the pavement. A fog seal can also be applied on the CIR layer to prevent the surface of asphalt pavement from oxidizing.

2.3 General laboratory CIR mixture design approach

Prior to treating deteriorated asphalt pavements by using CIR technology, it is necessary to determine the optimum contents of the bituminous and cementitious additives used in preparing CIR mixtures. The goal of a mix design is to prepare a mixture of aggregates and binder that can achieve desired levels of performance in the field. Researchers proposed different procedures for mix designs in the laboratory that are representative of CIR construction practices in the field (Salaices Gomez 2017; Ozer 2015; Buss et al. 2017). It is also important to mention that there is no universally accepted standard for designing CIR asphalt mix (Ozer 2015). Prior to preparing CIR mixtures, CIR materials should be selected and characterized, and then the performance of the prepared mixtures is evaluated. This section discusses in detail a general laboratory procedure for designing and evaluating CIR mixtures. This general procedure is common for all methods available in the literature.

2.3.1 Overview of CIR mix design methods

Various researchers, agencies, and state DOTs have developed several mix design procedures to select an optimal binder content and optimal water content for CIR projects (Salaices Gomez 2017; Ozer 2015; Buss et al. 2017). The process of designing a CIR mix involves obtaining representative RAP materials from existing pavements, which would then be mixed at ambient temperatures with a binding agent (either asphalt emulsion or foamed asphalt) at varying binder and water contents. For each binder content, test specimens are prepared to conduct performance testing (e.g., indirect tensile strength, ITS, or semicircular bend, SCB). The optimum CIR binder content (or the optimum water content) is then determined as the binder content (or the water content) at which the highest ITS (or fracture energy) is obtained (Kim and Lee 2011). The following subsections provide additional details.

2.3.2 Step 1: Collect RAP samples from the field

RAP samples are collected from the milled pavement surface to be analyzed and characterized in the laboratory. There are different ways to collect RAP. For instance, pavement cores or test pits can be collected from the pavement to be rehabilitated, then crushed in the lab into RAP with various sizes. Another method consists of using a CIR milling machine to mill the top 4 in. (102 mm) of the deteriorated asphalt pavement. Random sampling techniques in accordance with AASHTO T 2 (Standard Method of Test for Sampling of Aggregates) are generally used to collect representative samples from the pavement (AASHTO 1991). The collected millings are then allowed to dry before producing the CIR mix (e.g., drying RAP at room temperature for 10 days until the moisture content of the RAP millings is below 0.3%; Epps 1990; Kim and Lee 2011).

2.3.3 Step 2: Determine RAP properties

Several studies focused on determining the characteristics of RAP materials for preparing CIR mixtures. These characteristics included the existing asphalt content of RAP (e.g., penetration and viscosity of the binder recovered from RAP), gradation, moisture content, and density measurements (i.e., maximum specific gravity). It is also optional to assess additional RAP properties such as permeability and abrasion resistance. RAP gradation and extracted aggregates gradation (after recovery of binder) can be useful for determining if virgin aggregates are needed for a CIR mix (Kandhal and Mallick 1997; Alam et al. 2010; Bleakley and Cosentino 2013).

2.3.4 Step 3: Add aggregate (optional)

Virgin aggregate may be added to CIR mixtures to improve the strength of CIR mixtures and to minimize RAP creep (Bleakley and Cosentino 2013). RAP gradation is usually affected by the fines generated during the milling process or due to contamination from underlying layers. Therefore, the gradation of RAP (as received from milling) may not be suitable for the intended recycled base course. In this case, virgin aggregates are added to satisfy the gradation requirement or structural improvement of the recycled mix (Epps 1980; ARRA 2016).

2.3.5 Step 4: Select type, amount, and grade of bituminous and cementitious additives

The most commonly used bituminous additives are emulsified asphalt and foamed asphalt. Various types of polymer are also used to reduce rutting, increase early strength, and reduce thermal cracking of CIR mixtures. Cementitious additives can also be added to CIR mixtures such as portland cement and lime slurry. These additives are used in small amounts to enhance mix cohesion, to shorten the curing time, and to increase the moisture susceptibility resistance of the CIR materials. Below are some descriptions of CIR bituminous and cementitious additives (ARRA 2016):

2.3.5.1 Asphalt emulsions

Cationic and anionic emulsions are the most commonly considered asphalt emulsions in CIR. Dense-graded aggregate (or RAP) gradation containing fines requires slow-setting emulsions. Asphalt emulsion is also selected based on compatibility with RAP milling. Additionally, emulsion selection considers binding properties, coating, initial strength, and breaking time of emulsion. It is important to note that a field coating test (AASHTO T 59) can be used to determine whether asphalt emulsions (anionic or cationic emulsified asphalt) are compatible with RAP and new aggregate (Division of Construction 2009; Yan et al. 2009; AASHTO 2016). Table 1 summarizes the recommended combinations (Asphalt Institute 1983).

Table 1. Guidelines for Selection of Emulsified Asphalt Binders for CIR (Asphalt Institute 1983).

Emulsion	Type	Aggregates
Anionic	Medium-setting emulsions (MS-2 and MS-2h)	Open-graded aggregates
	High-float medium-setting emulsions (HFMS-2, HFMS-2h, and HFMS-2s) Slow-setting emulsion (SS-1 and SS-1h)	Dense-graded aggregate, sand, and sandy soil
Cationic	Cationic medium-setting emulsions (CMS-2 and CMS-2h)	Open-graded aggregate
	Cationic slow-setting emulsions (CSS-1 and CSS-1h)	Dense-graded aggregate, sand, and sandy soil

2.3.5.2 Foamed Asphalt

The use of foamed asphalt offers several economic and construction benefits. As the name indicates, foamed asphalts are produced using a foaming machine, which injects hot asphalt binder (e.g., performance grade [PG] 64-22 asphalt) with cold water. Expansion ratio and half-life values are determined to characterize foamed asphalts and to establish the optimum foaming water content (Kim et al. 2011; Kuna et al. 2014). The water content resulting in the highest values of expansion rate and half-life are used to produce foamed asphalt for CIR mixtures.

2.3.5.3 Recycling additives

Portland cement and lime slurry have been effective additives to CIR mixtures. These chemical additives provide improved early strength, enhanced rutting resistance, and improved moisture-damage protection. Cement and lime have been used successfully in combination with asphalt emulsions (Division of Construction 2009; Yan et al. 2009; Kim et al. 2011).

2.3.6 Step 5: Determine the moisture content required for mixing

Water is a key element in CIR mixes since it assists in coating RAP millings with the bituminous additives and facilitates compaction in the field (Anderson et al. 1985). In general, the typical moisture content for standard CIR is in the range of 2% to 5% (Scholz et al. 1991; Kim et al. 2011; ARRA 2016). Optimum moisture content of a CIR mix is often determined using Proctor compaction tests, which can produce a relatively high moisture content. Other methods consist of using 75 Marshall blows at room temperature or gyratory compaction via the Superpave Gyratory Compactor (SGC) to select the optimum moisture content of CIR mixtures (Carter et al. 2010; Bang et al. 2011; Cox and Howard 2016).

2.3.7 Step 6: Compaction, curing, and density measurements

CIR mixtures (loose and compacted specimens) consisting of emulsions or foamed asphalt, and sometimes low dosage of cement or lime (e.g., 1%), are cured in an oven for a given period of time (e.g., 7 days at 140°F [60°C]) (Cox and Howard 2015a). Table 2 presents compaction and curing procedures adopted by different agencies and DOTs summarized by Apeagyei and Diefenderfer (2013).Once the curing process of CIR specimens is completed, compacted specimens are tested for bulk specific gravity (G_{mb}), while theoretical maximum specific gravity (G_{mm}) is determined

for loose CIR mixtures. Different methods can be used to measure the air-void level of CIR test specimens. The G_{mb} of the compacted CIR specimens is determined in accordance with AASHTO T 331 or AASHTO T 166, while ASTM D6857 or AASHTO T 209 are used to determine the G_{mm} of the loose CIR mixes (AASHTO 2013, 2020c, 2021; ASTM 2018a).

Table 2. Examples of compaction and curing procedures for CIR mixes. (Table adapted from Apeagyei and Diefenderfer 2013.)

Compaction Method	Description	References
Marshall	75 blows	Wirtgen (2006), Fu et al. (2010)
Gyratory	25 gyrations	Buss et al. (2017), Kim et al. (2011)
	30 gyrations	Kim and Lee (2006)
	300 gyrations	Martínez et al. (2007)
Curing Temperature	**Curing Time**	**References**
104°F (40°C)	2 days	Tario (2010)
113°F (45°C)	7 days	Kim et al. (2011)
160°F (71°C)	3 days	Wirtgen (2006), Buss et al. (2017)
77°F (25°C)	7 days	Saleh (2006)
77°F (25°C)	14 days	Kim et al. (2011)
77°F (25°C)	28 days	Bessa et al. (2016)

2.3.8 Step 7: Determine the optimum binder content

A set of trial CIR mixtures are prepared to determine the optimum content for CIR bituminous (foamed asphalt) and cementitious additives. Previous studies accounted for different parameters, including initial and final curing properties and final moisture sensitivity (ARRA 2016; Tario 2010). The IDT test is often used to determine the optimum binder content for CIR mixes (compacted at 30 gyrations in SGC or 75 blows by Marshall hammer) prepared at various binder contents (e.g., 0.5% through 3% at 0.5 percentage-point increments) and using the selected moisture content (e.g., 4%) and additive dosages (Kim et al. 2007).Kim et al. (2007) reported that the optimum content of foamed asphalt ranges between 1.5% and 2.5%. Other studies showed that the optimum binder content varies between 1.5% to 3%, the optimum water content varies from 1.5% to 4%, and optimum cement content varies from 0.5% to 2% (Niazi and Jalili 2009; Brovelli and Crispino 2012; Berthelot et al. 2013; Gao et al. 2014; Bessa et al. 2016; Graziane et al. 2018). It is important to note that when CIR mixtures are prepared using virgin aggregates, higher ranges of bituminous and cementitious additives contents are often necessary (Cox and

Howard 2015a; ARRA 1996; Lee et al. 2016). Finally, a job mix formula can be established and used to reproduce CIR mixtures in the field.

Table 3 briefly summarizes the standard specifications different state DOTs and agencies use to design CIR mixtures and to assess their performance.

Table 3. Example of main specifications for CIR asphalt mix design recommended by ARRA (2016).

Test	Properties
AASHTO T 308	Existing binder content of RAP
AASHTO T 11 AASHTO T 27	Gradation of RAP
AASHTO T 166	Bulk specific gravity of compacted, cured specimen
AASHTO T 209	Maximum theoretical specific gravity
AASHTO T 269	Air voids of compacted, cured specimens
AASHTO T 283	Indirect tensile strength
AASHTO T 245	Marshall stability
ASTM D7196	Tensile-strength ratio and retained Marshall stability based on moisture conditioning

Note: Tests are in AASHTO (2018a, 2020a, 2020b, 2021, 2020c, 2018b, 2015b, 2018c) and ASTM (2018b).

2.4 Laboratory CIR mix design methods

Several agencies and DOTs have successfully established mix design procedures for CIR technology. For example, ARRA proposed three methods to design mixtures for CIR projects: modified Marshall mix design, modified Hveem mix design, and Oregon mix design (ARRA 2016). Other agencies (i.e., Wirtgen and the Asphalt Institute), Departments of Transportation (i.e., Rhode Island, Pennsylvania, New Jersey, and Florida), and the US Department of Defense (DoD) have developed their own mix design procedures, which have many similarities and some differences (i.e., number of gyrations, type of binder, RAP gradation). This section presents the available CIR mix design procedures used by several agencies and DOTs.

2.4.1 Unified Facilities Guide Specifications (UFGS) mix design procedure for CIR (DoD method)

The current mix design procedure developed by DoD (Unified Facilities Guide Specifications [UFGS] 32 01 16.70) consists of obtaining RAP from milling existing asphalt concrete pavement (US Army Corps of Engineers [USACE] 2018). The UFGS specifies that the maximum particle size of RAP millings should be less than half the thickness of the compacted CIR

pavement (i.e., maximum particle size of 1.5 in. [38 mm] with at least 90% of the RAP passing a 1 in. [25 mm] sieve; USACE 2018). UFGS 32 01 16.70 2018 focuses on determining the properties of RAP millings and the binder existing in them. RAP is then mixed with bituminous additives such as cationic emulsions (e.g., cationic slow-setting emulsion [CSS-1h]) in accordance with ASTM D977 (ASTM 2020a). The military mix design determines the amount of asphalt binder (i.e., tolerance of 0.3%) and specifies the amount of water (i.e., 0.5% intervals from 0% to 2.5%) to add to the CIR mixture. Once the optimum contents of asphalt binder and water are determined using a stability test, samples are compacted at higher temperature than the one used for CIR (i.e., 250°F [121°C]) with 75 blows of the typical Marshall hammer according to CRD-C 649 and CRD-C 650 (US Army Corps of Engineers 1995a, 1995b). The compacted CIR specimens are placed in an oven at 140°F (60°C) for 96 hours. Then, the dry density of samples is determined. It is also worth mentioning that DoD (USACE 2018) specifies completing CIR projects in good weather (i.e., no rain, storms, fog, etc.). CIR projects should be completed when the ambient air temperature is above 50°F (10°C), which can help with the curing process of the CIR layer (no delays).

2.4.2 Modified Marshall mix design

Previous studies used the modified Marshall mix design procedure to prepare CIR mixtures at 3% total moisture content (including emulsion water, water remaining in RAP, and water added into the mixture; Epps and Monismith 1986; Asphalt Institute 1983). Emulsions are added to the mixtures at desired contents in 0.5% increments. CIR mixtures are then compacted with 50 blows (per face) using the Marshall compacting hammer and, afterwards, allowed to cure in an oven at 140°F (60°C) for 6 hours. The cured CIR specimens are tested for bulk specific gravity, stability (140°F [60°C]), and flow (140°F [60°C]). The maximum specific gravity for each binder content is also determined using equation (1). CIR specimens' properties (air voids [AV], volume of asphalt binder [VB], voids in mineral aggregate [VMA], and voids filled with asphalt binder [VFB]) are determined using equations (2) through (5) (Epps and Monismith 1986; Asphalt Institute 1983). The Marshall stability test is used to determine the optimum binder content.

$$G_{\mathrm{mm}} = \frac{W_{\mathrm{m}}}{W_{\mathrm{m}} - W_{\mathrm{w}}}, \tag{1}$$

$$\mathrm{AV} = \frac{(\mathrm{G_{mm}} - G_{\mathrm{mb}}) \times 100}{G_{\mathrm{mm}}}, \quad (2)$$

$$\mathrm{VB} = \frac{\frac{W_{\mathrm{b}}}{G_{\mathrm{mb}}}}{\frac{W_1 + W_2 + W_3 + W_{\mathrm{b}}}{G_{\mathrm{mm}}}}, \quad (3)$$

$$\mathrm{VMA} = \mathrm{AV} + \mathrm{VB}, \quad (4)$$

$$\mathrm{VFB} = \frac{\mathrm{VB} \times 100}{\mathrm{VMA}}, \quad (5)$$

where

G_{mm} = the maximum specific gravity of the mix,
W_{m} = the weight of the mix in air,
W_{w} = the weight of the mix in water,
W_1 = the weight of the coarse aggregate,
W_2 = the weight of the fine aggregate,
W_3 = the weight of the filler in the total mix,
W_{b} = the weight of bitumen in the total mix, and
G_{mb} = the specific gravity of bitumen.

2.4.3 Modified Marshall mix design used for Superpave mix design

Lee et al. (2016) developed a mix design procedure using RAP obtained from different locations in the United States. The purpose of their study was to evaluate the effectiveness of CIR material compaction using an SGC rather than a Marshall hammer (Lee et al. 2016). This new mix design uses similar steps to those discussed in the previous section, "Modified Marshall mix design." However, the cured CIR specimens are compacted with 52 gyrations using an SGC at 77°F (25°C) and then allowed to cure for 6 hours at 140°F (60°C). The optimum binder content is determined using the peak ITS of CIR mixtures prepared at different binder contents (Lee et al. 2016).

2.4.4 Modified Hveem mix design

The modified Hveem mix design method of specimen preparation is similar to that of the modified Marshall method except the Marshall compactor is replaced by a kneading compactor, applying 20 tamping blows at 250 psi (1.725 Mpa) pressure to achieve a semicompacted condition. Afterwards, the compaction pressure is raised to 500 psi (3.45 Mpa), and 150

tamping blows are applied to complete compaction. The specimen is subjected to a leveling load with a testing machine at 1,259 lb (5.6 kN) at a head speed of 39 mil/min (1 mm/min). As in the modified Marshall method, this method also determines CIR parameters such as RAP properties and optimum binder-to-water-ratio contents (Epps and Monismith 1986; Asphalt Institute 1983).

2.4.5 Mix design developed for Oregon

This method aims to select an initial asphalt emulsion content to be added into the recycled mix containing 100% RAP (i.e., no virgin aggregates are required). The procedure consists of adjusting from a base emulsion content of 1.2% (by weight of RAP) based on aggregate properties and asphalt binder recovered from RAP. The method is applicable only when the bituminous additive is either a cationic medium setting or anionic high-float medium-setting type 150, also known as HFE-150 emulsion (Asphalt Institute 1983). The gradation of RAP millings is determined only for ½ in. (12.5 mm), ¼ in. (6.4 mm), and no. 10 sieves. Next, the estimated asphalt emulsion content (EC_{EST}) is determined using equation (6).

$$EC_{EST} = 1.2 + A_G + A_{AC} + A_{P/V}, \quad (6)$$

where

EC_{EST} = the estimated added emulsion content,
1.2 = the base emulsion content,
A_G = the adjustment for milling gradations,
A_{AC} = the adjustment for milling residual asphalt content, and
$A_{P/V}$ = the adjustment for millings penetration or viscosity.

In the Oregon mix design method, CIR specimen were produced and tested to determine their mechanical properties and to select the optimum emulsion content. Each specimen was compacted gradually using a hydraulic compaction device with a load of 25,000 psi (172,400 kPa). In this process, the stress level is increased to achieve 20,000 psi (137, 900 kPa) for the first 1 minute, and then an additional 5,000 psi (34,500 kPa) is applied for next 30 seconds to attain a final load of 25,000 psi (172,400 kPa).

2.4.6 Wirtgen mix design

The Wirtgen mix design procedure requires determining the engineering properties of RAP millings, such as gradation (sieves analysis), plasticity, and density, in accordance with ASTM D422, D4318, and AASHTO T 180, respectively (ASTM 2016, 2020b; AASHTO 2020d). RAP gradation for Wirtgen mix design is as follows: 53.6% passing no. 4 (0.187 in. [4.75 mm]), 18.7% passing 0.51 in. (13.2 mm) and retained on sieve no. 4, and 27.7% passing 0.75 in. (19 mm) but retained on a 0.51 in. (13.2 mm) sieve. Afterwards, the moisture content ($W_{\text{air-dry}}$) of selected RAP is determined by placing RAP samples in an oven at between 221°F (105°C) and 230°F (110°C). $W_{\text{air-dry}}$ is determined using equation (7) (Wirtgen 2012, n.d.):

$$W_{\text{air-dry}} = \frac{(M_{\text{air-dry}} - M_{\text{dry}})}{M_{\text{dry}}}, \quad (7)$$

where

$W_{\text{air-dry}}$ = the hygroscopic moisture content (% by mass),
$M_{\text{air-dry}}$ = the mass of air dried material (g), and
M_{dry} = the mass of oven dried material (g).

The prepared CIR mixture is allowed to cure for 7 days at a temperature of 60°F (15.5°C) to 70°F (21.1°C). Also, an accelerated curing can be achieved by placing CIR mixtures in sealed bags and allowing them to cure in an oven at 170°F (76°C) to 180°F (82°C). However, when cement is added to the mix, the curing period is reduced to 45 hours, and the oven temperature is reduced to 140°F (60°C). The optimum binder content of CIR mixtures is generally determined by conducting a test on CIR specimens prepared with varied binder contents (Wirtgen 2012, n.d.).

2.4.7 Mix design method developed for Rhode Island DOT

The University of Rhode Island developed a mix design method that consists of mixing cationic slow-setting emulsions (CSS-1h) with RAP obtained from milling a construction site. Lee et al. (2014) investigated the appropriate number of gyrations for compactions so as to better represent field conditions. CIR mixtures were compacted with 175 gyrations using an SGC. Lee et al. (2014) determined the estimated bulk specific gravity (1) after each gyration and (2) after 175 gyrations. CIR specimens were allowed to cure in an oven at 140°F (60°C) for 1 day (Lee and Mueller 2014).

Finally, CIR specimens were tested for ITS and creep compliance, in accordance with AASHTO T 322, at temperatures of –4°F (–20°C), 14°F (–10°C), and 32°F (0°C) (AASHTO 2007). The optimum binder content was determined from the peak of ITS.

2.4.8 Mix design method developed for Iowa DOT

The Iowa DOT mix design procedure developed by Kim and Lee (2012) consisted of mixing 100% RAP, collected from different CIR projects in the state, with type CSS-1h and HFMS-2 emulsions at different contents (of emulsion by total RAP weight (i.e., 0.5%, 1%, 1.5%, 2%, and 2.5%) and with constant moisture content (i.e., 3%). Prior to mixing, RAP was dried until obtaining a final RAP moisture content between 0.1% and 0.2%. Then, RAP gradations were designed by dividing into six stockpiles the materials retained from the following sieve sizes: 1 in. (25 mm), ¾ in. (19 mm), 3/8 in. (9.5 mm), no. 4 (4.75 mm), no. 16 (1.18 mm), and passing no. 16 (1.18 mm). Millings with size greater than 1 in. (25 mm) were discarded. After mixing the graded RAP with emulsions and water, the CIR mix was compacted using an SGC with 25 gyrations. The compacted mix was allowed to cure in an oven at 104°F (40°C) for 3 days. The optimum binder content of CIR mixtures was determined using wet ITS (Kim and Lee 2011).

2.4.9 Other mix design procedures

Table 4 presents a brief summary of mix design methods developed by Pennsylvania; Minnesota; and Ontario, Canada. These procedures are different in the binder type (anionic or cationic emulsions), the binder-content range, compaction method, curing time, and target volumetric (Salomon and Newcomb 2000).

Table 4. Additional example mix design procedures.

Property	Pennsylvania	Minnesota	Ontario
Binder Type	Use CMF-2 or CSS-1h.	Use CSS-1h, HFMS-2s, or HFMS-2p.	Use HF-150.
Binder Content	Vary the binder content from 2% to 3.5%, in increments of 0.5 percentage points, at optimum water content.	Use the emulsion contents of 1%, 1.5%, 2%, and 3%. Determine the optimum emulsion content.	Vary the binder content from 0.5% to 2.5%, in increments of 0.5 percentage points.
Water Content	Vary the water content from 3% to 7%, in increments of 1 percentage point, at 2.5% binder content. The optimum water content is then determined as the one yielding the best performance.	Vary water content until obtaining 4% total liquid content.	Vary water content until obtaining 4.5% total liquid content.
Compaction	Apply 75 blows with Marshall hammer at 73°F (22.8°C).	Compact at 40 or 150 gyrations using SGC, depending on experiments.	Apply 50 blows with the Marshall hammer before curing and an additional 25 blows after curing in the molds for 24 hours.
Curing	Allow CIR specimens to cure for up to 96 hours at 104°F (40°C).	Allow CIR specimens to cure from 24 to 168 hours.	Allow CIR specimens to cure for 72 hours at 140°F (60°C).
Volumetrics	Determine resilient modulus and bulk specific gravity.	Determine resilient modulus, bulk specific gravity, and maximum specific gravity.	Target air voids between 8% and 12% and a minimum Marshall stability of 2,000 lb (8.9 kN) at 72°F (22.2°C).

2.5 Best practices of CIR field construction

CIR technology has the ability to increase the service life of asphalt pavements by approximately 11 years, provided that certain best practices are followed (Chen et al. 2010; Chesner et al. 2011). CIR performed on pavements with minimal deterioration extends the service life of such pavements by approximately 50% more than when performed on severely damaged pavements (Chesner et al. 2011). Several construction factors affect the long-term CIR performance and the service life of rehabilitated pavements (Chen et al. 2010; Cross et al. 2010). The following subsections detail the best CIR construction practices.

2.5.1 Best practices for CIR mix production

The type and amount of binder and cementitious additives: Anionic and cationic emulsions, recycling additives, and water should not be added to CIR mixtures in excessive amounts. Excessive amounts of binder, additives, or water cause asphalt bleeding or flushing (ARRA 2016).

Mixing of the materials: When there is an inadequate mixing of RAP with binder and additives, or there is insufficient asphalt coating of the RAP, segregation can occur. To prevent this, all CIR materials should be sufficiently held in the mixing chamber until the mixture is homogenous (up to 2 minutes) (ARRA 2016).

RAP gradation: When there is a variation in depth of the milled materials (some of the base layer is also milled), RAP behind the recycling unit is likely poorly graded. Therefore, depth of milling should be regularly checked and adjusted (ARRA 2016).

Size of RAP: During the CIR milling process, RAP materials can be oversized if the screen bar (or breaker) is not properly adjusted. Therefore, the screen bar and all equipment should be carefully checked prior to CIR construction (ARRA 2016).

Emulsion content: After compaction, raveling can occur in the surface of the CIR-rehabilitated pavement when low emulsion content (e.g., 0.5%) is added to the mix. When higher contents of emulsion are used in the CIR mix (e.g., 5%), a shiny black mat can appear after compaction, which can simulate pavement distresses such as rutting. In this case, virgin aggregates can be added to the CIR mix to absorb the extra emulsion in the mix.

2.5.2 Environmental and other considerations

Pavements engineers can encounter additional challenges during the early implementation of CIR with respect to the design approach and construction methodology (Harun et al 2010; ARRA 2016):

- Weather: Rain during CIR operations or during the curing process can affect the performance of the recycled layer (e.g., moisture damage).
- Equipment failure: The contractor's equipment may fail to meet the requirements.
- Storage of bituminous and cementitious additives: Storing asphalt emulsion and cement helps maintain these additives in suspension inside the slurry feed tank.
- Fabric and geosynthetic incorporation into the CIR layer: The presence of foreign materials in the existing pavements (e.g., rubberized crack filler, pavement markers, loop wires, thermoplastic markers, etc.) can affect the performance of CIR pavement by inhibiting its placing and its compaction.

- Curing time: Slow-curing problems may occur when work takes place in damp or cold weather conditions (Tabaković et al. 2016).
- Moisture: Some CIR materials are susceptible to moisture damage, which can negatively affect the performance of the CIR mix. (Tabaković et al. 2016).
- Drainage system: An inadequate or poor drainage system can also aggravate failure of rehabilitated pavement.

There are ways to prevent the above-mentioned challenges when constructing CIR-rehabilitated pavement:

- Weather: Perform CIR operations when the pavement temperature is above 50°F (10°C) with overnight ambient temperatures above 35°F (2°C) (Tario 2010).
- Equipment failure: Prior to construction, check all CIR construction equipment. In addition, evaluate pavements to be rehabilitated to identify areas where material properties are not uniform. This can cause damage to construction equipment (ARRA 2016).
- Storage of bituminous and cementitious additives: Cement and lime slurry storage needs to have agitators or similar equipment to keep the recycling additives in suspension when held in the slurry feed tank as well as during transport (ARRA 2016).
- Fabric and geosynthetic incorporation into the CIR layer: The contractor should conduct field investigations and prevent the incorporation of shredded materials into CIR materials (ARRA 2016).
- Curing time: In addition to the ambient temperature being above 50°F, 3% of moisture content, or less, allows for faster curing (ARRA 2016).
- Moisture: Add portland cement or lime slurry to the CIR mix to enhance moisture-damage protection (ARRA 2016; Tabaković et al. 2016).
- Drainage system: Strengthen the drainage system of the rehabilitated pavement by selecting the appropriate CIR material prior to the mix design (ARRA 2016).

2.6 Laboratory and field performance of CIR

Several researchers have investigated the laboratory and field performance of CIR mixtures in terms of rutting susceptibility and cracking resistance (Buchanan et al. 2004; Cox and Howard 2015b).This section presents a review of both laboratory and field performance of CIR mixtures in previous studies.

2.6.1 Laboratory performance tests

2.6.1.1 Asphalt pavement analyzer (APA) test

The asphalt pavement analyzer (APA) test is typically conducted in accordance with AASHTO T 340 to determine the rutting potential of CIR mixes (AASHTO 2010). A vertical load of 100 lb is applied to pressurized rubber hoses (i.e., pressure of 100 psi [0.7 Mpa]) placed on top of CIR specimens. The APA test determines whether a CIR mixture subjected to 8,000 passes at 147°F (64°C) is susceptible to rutting (i.e., specimens fail before reaching 8000 passes). Each state specifies the maximum rut depth allowed at 8000 APA passes. For instance, most states specifications do not include a rut-depth threshold for CIR pavements. However, for HMA pavements, rut-depth values should be above 0.2 in. (5 mm) per New Jersey specifications, while in Mississippi, rut-depth values should range between 0.15 in. (4 mm) and 0.24 in. (6 mm) for high traffic (Buchanan et al. 2004; Cox and Howard 2015b).

2.6.1.2 Dynamic modulus testing

The dynamic modulus test is conducted according to AASHTO T 62 to evaluate the stiffness of CIR mixtures under different loading frequencies (e.g., 0.1, 10, and 25 Hz) and at various testing temperatures (e.g., 40°F [4°C], 98°F [37°C], and 129°F [54°C]; AASHTO 1986). The dynamic modulus is determined by dividing the maximum dynamic stress by the maximum axial strain obtained for CIR mixtures at a given loading frequency and testing temperature. The result of the dynamic modulus test is a master curve developed based on the approach of time and temperature correspondence. The master curve for a CIR mixture evaluates the rutting susceptibility (i.e., at high testing temperature and low loading frequency) and cracking resistance (i.e., low testing temperature and high loading frequency) of CIR mixtures (Kim et al. 2009; Diefenderfer et al. 2016).

2.6.1.3 Flow number testing

The flow number (FN) test is conducted in accordance with AASHTO TP 79 (AASHTO 2015). The FN test characterizes the rutting potential of asphalt mixtures subjected to haversine loading. Cumulative deformation is determined as a function of load cycles. In this test, load is generally applied for 0.1 second and then released for 0.9 second to form one cycle. This process is repeated up to 10,000 loading cycles. The results of the FN

test are presented as a cumulative permanent-deformation curve (El-Basyouny et al. 2005; Kim et al. 2009).

2.6.1.4 Resilient modulus testing

The resilient modulus (M_r) test is conducted in accordance with ASTM D7369 (ASTM 2020c). The M_r test evaluates the elastic properties of asphalt mixtures (i.e., CIR mixtures) by measuring stress-strain responses of these mixtures when subjected to a load. The minimum load repetition for the M_r test typically ranges between 50 and 200. The load repetition depends on testing temperature, the CIR mixture's components, and loading frequency. For instance, Kavussi and Modarres (2010) conducted the M_r test on emulsified asphalt CIR mixtures by using 100 load repetitions and a 2 Hz loading frequency.

2.6.1.5 Indirect tensile test

The indirect tensile testing (IDT) test is conducted according to AASHTO T 283 (AASHTO 2018c).The IDT test is typically performed at 25°C with a loading rate of 50 mm/min. When conducted at lower temperatures (i.e., 0°C), the loading rate is reduced to 25 mm/min. In this testing, a cylindrical CIR specimen is subjected to compressive loads, creating a vertical stress (tensile) within the vertical plane, causing the specimen to break in two halves. Studies have shown that the fracture energy obtained from the IDT stress-strain curve can characterize the cracking potential of CIR mixtures (Koh and Roque 2010; Cox and Howard 2015b).

2.6.1.6 Semicircular bend test

The SCB test is conducted on cut and notched CIR specimens in accordance with AASHTO TP 105 (AASHTO 2020e). Similar to the ITS test, the SCB test is performed at 77°F (25°C) or at 32°F (0°C), with loading rates of 2 and 1 in./min (50 and 25 mm/min), respectively. This test characterizes the cracking resistance of CIR mixtures to loading by evaluating the fracture energy of these mixtures. For instance, Charmot et al. (2017) evaluated the cracking behavior of CIR mixtures prepared with varying contents of emulsion and cement at low temperature 32°F (0°C) to optimize these mixtures (e.g., determining the optimum binder-to-water ratio that corresponds to the maximum SCB fracture energy).

2.6.2 Laboratory Performance Evaluation

2.6.2.1 Properties of CIR mixtures

Apeagyei and Diefenderfer (2013) conducted the M_r test on CIR cores collected from different locations on Highway I-81 7 to 12 weeks after construction. The M_r test was conducted at three temperatures (39°F [4°C], 68°F [20°C], and 100°F [38°C]) and one loading frequency (10 Hz). The M_r results indicated a temperature-dependent behavior of CIR mixtures: as the temperature increases, M_r values decrease, indicating that CIR specimens become less stiff at high temperatures. Apeagyei and Diefenderfer (2013) reported that the resilient modulus test was used successfully to determine the mechanistic stiffness of CIR mixtures and, therefore, can be used in optimizing CIR mixtures. In a different study, Kavussi and Modarres (2010) conducted M_r tests on CIR mixtures prepared with emulsified asphalt and cement and allowed to cure for different times (7, 28, and 120 days) at room temperature. Results showed that the M_r values of CIR specimens significantly increased with an increase in both curing time and cement content. In addition, the testing temperature of CIR specimens impacted M_r values. Each increase in testing temperature caused the M_r values of CIR specimens to decrease (Kavussi and Modarres 2010).

Kim and Lee (2012) conducted a dynamic modulus test, in accordance with AASHTO T 342, on CIR emulsion mixes at three different temperatures (40°F [4°C], 70°F [21°C], and 100°F [37°C]) and six different frequencies (0.1, 0.5, 1, 5, 10, and 25 Hz; AASHTO 2019). Kim and Lee (2012) reported that, similar to FN testing, CIR cationic mixtures (i.e., CSS-1h) presented higher dynamic modulus values than CIR anionic mixes (i.e., HFMS-2P). Kim and Lee (2012) also stated that $|E^*|$ of CIR emulsion mixtures was affected by neither temperature nor loading frequency. Thus, they recommended the dynamic complex modulus to evaluate the stiffness of CIR mixtures at high and low temperatures (Kim and Lee 2012).

2.6.2.2 Rutting performance of CIR mixtures

Cox and Howard (2015b) conducted APA testing, according to typical Mississippi specs for asphalt mixtures, on CIR specimens with different properties (i.e., at 147°F [64°C]) for 8,000 cycles with a 100 lbf (0.45 kN) load applied by pressurized rubber hoses of 100 psi (0.69 Mpa). Results showed that CIR specimens prepared with cement had higher rutting re-

sistance than those mixtures prepared with emulsion only. Therefore, adding cement (i.e., 1%) to CIR mixtures would improve the resistance of emulsified asphalt CIR mixtures to rutting. Cox and Howard 2015b recommended the APA test for evaluating rutting susceptibility of CIR-rehabilitated pavements.

In addition to the APA test, previous studies conducted the FN test on CIR mixtures with different properties (i.e., binder type, content, and curing process) to assess CIR rutting resistance (Kim and Lee 2012, Rodezno et al. 2015). Kim and Lee (2012) conducted an FN test on CIR mixtures prepared with emulsions (CSS-1h and HFMS-2P) to evaluate rutting susceptibility of asphalt emulsion CIR mixtures. The FN test consisted of applying a 20 psi (140 kPa) loading stress on CIR emulsion mixtures at 104°F (40°C) up to 20,000 passes until 5% of the cumulative permanent strain was achieved. The results of the FN test conducted by Kim and Lee (2012) showed that CSS-1h emulsion CIR specimens presented higher FN values than those of HFMS-2P emulsion CIR specimens. In addition, an increase in emulsion content from 0.5% to 1.5% caused CIR specimens to fail. Therefore, Kim and Lee (2012) recommended the FN test to select optimum binder content (typically emulsions) when designing CIR mixtures.

2.6.2.3 Cracking performance of CIR mixtures

The IDT testing is conducted at 77°F (25°C) with a load rate of 50 mm/min in accordance with AASHTO T 283 (AASHTO 2018c). Different studies showed that the fracture energy obtained from the IDT stress-strain curve can characterize the cracking behavior and the cracking potential of CIR mixtures (Koh and Roque 2010; Cox and Howard 2015b). Recently, Lee et al. (2016) developed a volumetric-based CIR mix design procedure using the SGC. In this study, CIR specimens were prepared using RAP obtained from different geographic locations and emulsified asphalt. The CIR mixtures were compacted to densities similar to those measured in the field. The ITS and creep compliance of CIR specimens were determined using the IDT test. This study also focused on testing a full-scale CIR test section located in Arizona. Lee et al. (2016) reported that the IDT results were satisfactory; and therefore, they recommended this test for cracking characterization of CIR mixtures.

Charmot et al. (2017) evaluated the cracking behavior of CIR mixtures prepared with varying contents of emulsion and cement, at low temperature (0°C). Results of SCB low-temperature fracture tests showed that

there is a strong correlation between fracture energy and emulsion contents (positive trend) and fracture energy and cement content (negative trend). In addition, the SCB fracture energy was efficient in predicting CIR cracking performance and determining optimum contents of emulsion and cement. Therefore, Charmot et al. (2017) reported that the SCB test, conducted at low temperatures, was successfully used to evaluate CIR cracking performance and to select optimum contents for bituminous and cementitious additives.

In summary, previous studies conducted by several researchers showed that performance tests such as APA, dynamic complex modulus, and FN tests successfully characterized the rutting performance of emulsified and foamed asphalt CIR mixture (Kavussi and Modarres 2010; Kim et al. 2011; Kim and Lee 2012; Apeagyei and Diefenderfer 2013; Cox and Howard 2015b). These tests were able to capture the impact of varying the binder content and testing temperature on the strength of CIR mixtures. Both ITS and SCB tests were efficient in characterizing cracking performance of CIR mixtures. Researchers found that fracture energy and tensile strength presented a strong correlation with the content of bituminous and cementitious additives (Koh and Roque 2010; Cox and Howard 2015b; Charmot et al. 2017). In addition, the ITS test was generally conducted when developing a mix design for CIR mixtures to determine optimum binder contents of these mixtures. Based on these findings, ITS and SCB tests seem reasonable to evaluate cracking resistance of CIR mixtures.

2.6.3 Field Performance Evaluation

A laboratory experimental program for CIR mixtures helps establish a job mix formula to use when implementing CIR in the field. CIR pavements are generally monitored with respect to functional and structural performances after the completion of construction. The functional performance of pavements is often evaluated using the International Roughness Index (IRI) (percentage of cracks and rut depth) while the structural performance is measured using nondestructive methods (i.e., falling weight deflectometer [FWD]; Harun et al. 2010; VanFrank 2015; Buss et al. 2017). What follows is a discussion of CIR pavements' performance evaluation.

2.6.3.1 General pavement surveys

Buss et al. (2017) aimed to investigate all the factors that can affect long-term performance of CIR-rehabilitated pavements to estimate the viability

and effectiveness of the CIR technique on pavements with different levels of deterioration. The Pavement Management Information System of Iowa DOT provided pavement performance data of approximately 100 CIR projects on different pavements around Iowa. Buss et al. (2017) carried out statistical analysis to investigate the different types of pavement distresses likely occurring on CIR-rehabilitated pavements. The study by Buss et al. (2017) focused on the following distresses:

Transverse cracks: A previous study by Huang (2004) revealed that the variation of temperature (from hot summer to very cold winter) is one of the reasons transverse cracking forms in asphalt pavements. In general, three types of transverse cracking appear on asphalt pavements' surfaces, depending on the width of cracks (Miller and Bellinger 2003):

- Low transverse cracks: when the mean width of a crack is less than 6 mm
- Medium transverse cracks: when the mean width of a crack is between 6 mm and 19 mm
- High transverse cracks: when a mean width of a crack is more than 19 mm wide

Buss et al. (2017) reported that, 1 year after construction, there were no visible transverse cracks in any of the CIR pavements. Low to medium transverse cracks were observed in several CIR pavements 12 years after construction.

Longitudinal cracks: This type of crack is generally found under one of the following levels of severity (Miller and Bellinger 2003):

- Low-severity longitudinal cracks: when the mean width of a crack is equal to or less than 6 mm
- Moderate-severity longitudinal cracks: when the mean width of a crack is between 6 mm and 19 mm
- High-severity longitudinal cracks: when a mean width of a crack is equal to or more than 19 mm wide

Buss et al. (2017) investigated longitudinal cracks present in two locations of the CIR-rehabilitated pavement: outside the wheel path and inside the wheel path. Analysis conducted on Iowa CIR-rehabilitated pavements showed that only low-severity cracks were present outside the wheel path. Eight years after construction, low-severity cracks appeared outside the

wheel path and tended to increase in the following years while a significant number of medium to high-severity longitudinal cracks were found in the wheel path (Buss et al. 2017).

Fatigue cracks: Also known as alligator cracks, this pavement distress is generated when pavements are subjected to heavy load (Huang 2004). CIR-rehabilitated pavements in Iowa showed a considerable decrease in alligator cracking rates compared to pavement constructed with conventional methods. Alligator cracks started to appear as low-severity cracking 9 years after CIR construction (Buss et al. 2017).

Rutting: This type of pavement distress is created in the wheel path as a longitudinal depression on the pavement surface (Huang 2004). Prior to constructing CIR pavement, rutting was observed in constant rates. After construction, the rutting rate was insignificant until the twelfth year when rutting progressively increased to the original rutting depth (same condition as before constructing CIR) (Buss et al. 2017). Buss et al. (2017) concluded that CIR technology significantly improved rutting in most CIR-rehabilitated pavements for 10 years after construction.

2.6.3.2 CIR pavement functional performance

In general, the IRI indicates the ride quality of roadways. Harun et al. (2010) conducted a study to evaluate the ride quality of different Malaysian roadways constructed via CIR technology. Sixty months after construction, IRI testing was performed on several locations of the CIR-rehabilitated roadways. Harun et al. (2010) obtained the IRI results by using the guidelines for evaluating the performance of CIR-rehabilitated pavements. They found that the IRI values ranged from 2.5 m/km to 3.5 m/km, indicating a poor ride quality of the tested roadways. In another study, Diefenderfer and Bowers (2017) analyzed a CIR pavement section on I-81, constructed in 2011 by Virginia DOT. The pavement section was produced using foamed asphalt and portland cement. In 2016, this CIR pavement section had carried almost 10 million equivalent single-axle load, also known as ESALs. Diefenderfer and Bowers (2017) reported that the average rut depth was around 2.54 mm and 0.7 m/km for the ride quality, which was regarded as an “excellent” ride quality, according to Virginia DOT.

2.6.3.3 Pavement structural performance

The structural performance of CIR-rehabilitated pavements is generally evaluated with deflection data measured by FWD. The outcomes of this test assist in determining the structural condition of CIR-rehabilitated pavements. In addition, the elastic modulus of CIR pavements can also be determined using FWD to evaluate resistance to deformation under traffic load (Harun et al. 2010). Da Silva et al. (2013) conducted a set of FWD tests on CIR test sections during rainy and dry seasons for 2 years (2009 and 2010) to study both seasonal and traffic effects. Da Silva et al. (2013) observed a significant difference in deflections between rainy and dry seasons (around 20%). With regard to traffic effects, deflections also increased by 15% per year, then continued increasing during rainy seasons and the following dry season (da Silva et al. 2013).

2.6.3.4 Marshall stability testing (strength and durability testing)

Cohen et al. (1989) constructed a trial CIR section of full-scale pavement in Israel type HFMS-1 (high floating anionic emulsion) emulsion and subjected it to low-volume traffic. The CIR mix was designed in the lab according to the modified Marshall mix design procedure but was modified to meet climate conditions in Israel (140°F [60°C]). The CIR mix consisted of 70% RAP, 20% virgin aggregates, 10% quarry sand, and HFMS-1. Twelve months after the construction of the CIR section, strength tests (Marshall stability test) at 140°F (60°C) and durability tests were performed, in accordance with ASTM D1559, on cores obtained from the cold recycled section (ASTM 1998). Cohen et al. (1989) reported that the CIR layer showed satisfactory performance by attaining an acceptable resistance to deformation, cracking, and rutting after 1 year of service. Furthermore, the results of durability tests showed a high durability potential and a high resistance of the CIR layer to the damaging effects of water and high and low temperature (Cohen et al. 1989).

2.7 Summary

Overall, CIR has been used successfully to treat deteriorated asphalt pavements in less time, more cost-efficiently, and without causing harm to the environment, compared to conventional asphalt pavement rehabilitation techniques. In addition, previous studies on CIR mixtures often considered the assessment of strength and cracking parameters, such as ITS, SCB fracture energy, and fracture index, when selecting optimum contents of

binding agents, recycling additives, and water of CIR mixtures. Mix design methods generally disregarded the rutting performance of CIR mixtures (Dong and Charmot 2018). The information provided in the literature review leads to the following conclusions.

The use of the CIR method was generally limited to low- and medium-trafficked pavements, reporting no case of heavily trafficked pavements (i.e., airfields). For instance, some agencies restricted the use of CIR technique on pavements with traffic no greater than 4,000 ADT (Tario 2010).

Virgin aggregate were added to CIR mixtures to improve the strength of these mixtures and to reduce the creep of RAP (Bleakley and Cosentino 2013). Note that both RAP gradation and extracted aggregate gradation were two of the main properties for determining whether virgin aggregates were needed (Kandhal and Mallick 1997; Bennet and Maher 2005; Alam et al. 2010; Bleakley and Cosentino 2013).

Several methods for designing CIR mixtures are currently available. Modified Marshall and modified Hveem mix designs are the most common (ARRA 2016). Other mix design methods were developed by different DOTs (i.e., Pennsylvania and New Jersey), agencies (i.e., Wirtgen and the Asphalt Institute), and DoD (i.e., UFGS).

The type and amount of bituminous additives as well as RAP properties (i.e., size, gradation, and existing binder properties) are important factors affecting the long-term performance of CIR-rehabilitated pavements.

In summary, there is a need to extend the use of CIR technology to rehabilitate not only low- to medium-trafficked pavements but also heavily trafficked pavements such as airfields. Because the performance of the CIR layer at the postconstruction stage depends on traffic level (low, medium, or heavy), a required preliminary study of materials should include a comparison between the structural requirements for heavy traffic and the structural properties achieved by the CIR technique. Thus, considering both cracking and rutting performance measures when selecting optimum binder contents is important. Therefore, this report presents a BMD approach for optimizing the performance of CIR mixtures.

3 Description of Cold In-Place Recycling (CIR) Materials Used

CIR mixtures are made of pavement millings, also known as RAP; asphalt binder (i.e., foamed asphalt or emulsified asphalt); recycling additives (i.e., lime slurry or portland cement); and water. This study used RAP millings to prepare CIR mixtures without the addition of virgin aggregates. The study used two bituminous additives: CSS-1h emulsified asphalt and neat PG 64-22 foamed asphalt. Portland cement was added to CIR mixtures to increase their strength. Water was added to CIR mixtures to enhance the process of coating RAP with portland cement and to facilitate the compaction process of these mixtures. Prior to mixing, the team identified the characteristics of RAP, bituminous additives, and cementitious additives. This chapter discusses the materials acquired for this study and presents the characteristics for each.

3.1 Reclaimed asphalt pavement

To collect RAP needed for preparing CIR mixtures, a portion of an HMA pavement section located at Rowan University Accelerated Pavement Testing Facility (RUAPTF) was reclaimed using a milling machine typical of CIR projects. The rehabilitated pavement was tested in full-scale accelerated pavement testing (Figure 5). A number of tests were performed on dry RAP to characterize the gradation, the maximum specific gravity, and the existing binder content of the RAP millings. The following subsections provide additional details about the properties of RAP millings collected as part of this study.

Figure 5. RAP obtained from RUAPTF

3.1.1 Sieve analysis

Dry sieve analysis was conducted in accordance with AASHTO T 27 to determine the gradation of collected RAP (AASHTO 2020b). A meaningful quantity of CIR millings (approximately 992 lb [450 kg]) was sieved using a large sieve shaker to obtain a more representative gradation of the collected RAP. Figure 6 shows the general gradation of the obtained RAP. As the figure shows, the gradation of RAP millings was dominated by materials finer than sieve no. 4 (i.e., 65% of RAP passing sieve no. 4).

Figure 6. Gradation of RAP materials.

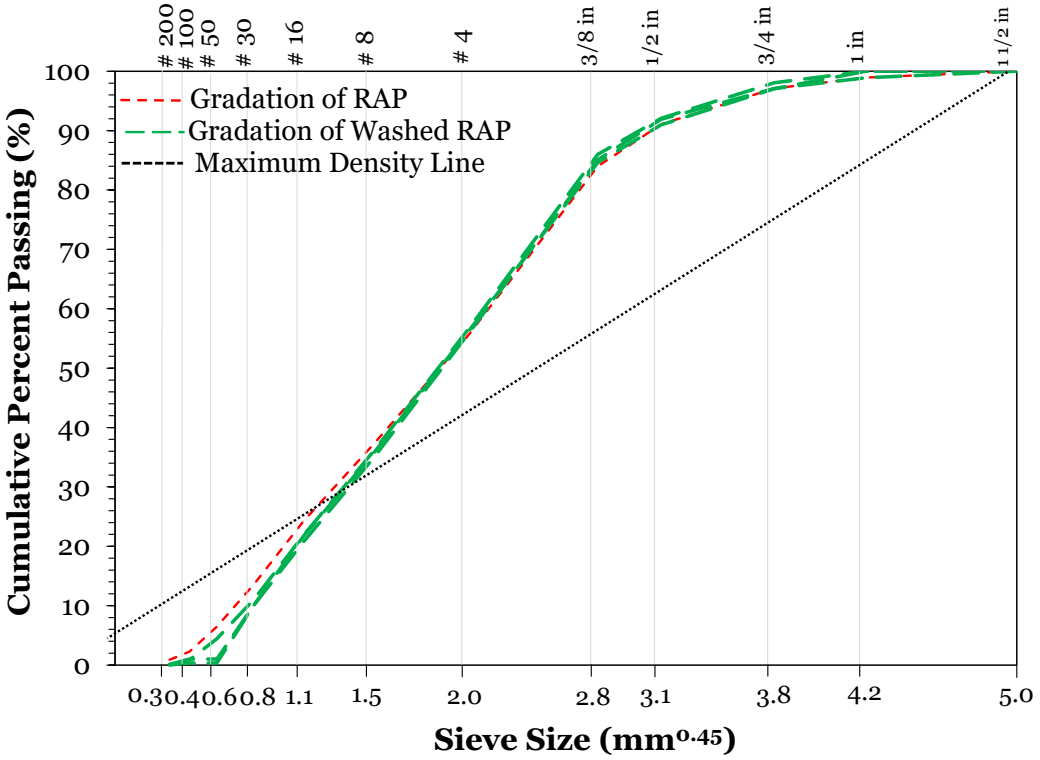

The team performed washed sieve analysis on three similar RAP replicates in accordance with AASHTO T 11 (AASHTO 2020a). The results, summarized in Figure 6, showed that the RAP millings collected for this study contained an average of 2.4% of particles passing sieve no. 200, which is a good indicator of the permeability of the RAP (drainage). This information is very important to know since the CIR mixture will be the base layer of the pavement. All the CIR mixtures prepared as part of this study are considered to have good permeability.

3.1.2 Maximum specific gravity

The maximum theoretical specific gravity (G_{mm}) of collected RAP was determined using the CoreLok device (Figure 7) in accordance with ASTM D6857 (ASTM 2018a; Cox and Howard 2017). Three replicates of RAP batched to the general gradation (Figure 6) were allowed to dry overnight in an oven at 80°C (176°F) to ensure that RAP millings were completely dry. Table 5 presents the results of G_{mm}.

Figure 7. CoreLok device.

Table 5. Maximum specific gravity results of RAP.

Sample ID	G_{mm}	Average G_{mm}	Standard Deviation
RAP-1	2.525	2.527	0.002
RAP-2	2.529		
RAP-3	2.528		

3.1.3 Existing binder content

Extraction and recovery of the RAP asphalt binder was performed in accordance with AASHTO T 319 (AASHTO 2008). Prior to initiating the extraction of the binder, three samples of RAP millings were blended to the general gradation and dried in an oven at 80°C (176°F) overnight. The results of the aged asphalt binder content, presented in Table 6, showed that the estimated average RAP binder content was approximately 5.5%.

Table 6. Aged binder content of RAP.

Samples	RAP Weight before (g)	RAP Weight after (g)	Weigh of Aged Binder (g)	Binder Content (%)	Average (%)
RAP-1	1881.6	1771.8	63.3	5.65	5.5%
RAP-2	1870.6	1761.45	55.5	5.66	
RAP-3	1788.1	1692.36	60.2	5.22	

3.2 Bituminous additives

One of this study's objectives was to evaluate the impact of different bituminous additives on the laboratory performance of CIR mixtures. Two bituminous additives, commonly used for CIR, were selected for this study based on literature findings. These binders were CSS-1h emulsified asphalt and neat PG 64-22 foamed asphalt.

3.2.1 Emulsified asphalt

This study used a slow-setting cationic asphalt emulsion (CSS-1h). A contractor in New Jersey manufactured this emulsion and supplied it in small quantities periodically. The obtained emulsion was stored in 1 gal. (4 L) plastic containers at room temperature to prevent the emulsion from breaking (Figure 8). Before every use, these containers were gently agitated to prevent settlement and separation of the emulsion. Table 7 presents the main properties of the CSS-1h emulsion.

Figure 8. Bottles of CSS-1h emulsion.

Table 7. Properties of CSS-1h emulsified asphalt.

Properties	Results
Sieve (%)	0.00
25 °C Saybolt Furol viscosity	22.0 seconds
25 °C, penetration	29 (0.1 mm)/(2.9 mm)
pH	5
Residue	63.15%

3.2.2 Foamed asphalt

This study used a neat PG 64-22 asphalt binder to produce foamed asphalt. The contractor supplied asphalt binder in 5 gal. (19 L) buckets. A Wirtgen WLB 2S asphalt foaming machine (laboratory scale) was used to produce foamed asphalt (Figure 9). Prior to preparing foamed asphalt CIR mixtures, the asphalt foaming process was evaluated at different water contents of foamed asphalt (2%–3.5%, with increments of 0.5%). The optimum water content (OWC) of foamed asphalt was that at which foamed asphalt exhibited maximum values for the half-life and the expansion ratio. Table 8 presents the properties of neat PG 64-22 foamed asphalt determined at three temperatures (155°C, 165°C, and 175°C).

Figure 9. Laboratory-scale foaming machine.

Table 8. Foaming properties test results.

Temperature (°C)	Half-Life (seconds)	Expansion Ratio	OWC (%)
155	8	8	2
165	10.5	10	2.5
175	7.5	9	3

As Table 8 shows, an increase in the binder temperature from 311°F (155°C) to 329°F (165°C) caused a notable increase in the values of expan-

sion ratio and half-life. However, these values were reduced when the temperature was increased from 329°F (165°C) to 347°F (175°C). This showed that at 329°F (165°C), neat PG 64-22 foamed asphalt presented the highest half-life and the best expansion ratio values (peaks as shown in Figure 10): 10 seconds for the half-life and 10.5 for the expansion ratio. Therefore, the study produced foamed asphalt at 329°F (165°C) by using a foaming water content of 2.5% to ensure high-quality foamed asphalt CIR mixtures.

Figure 10. Selecting optimum foaming water content.

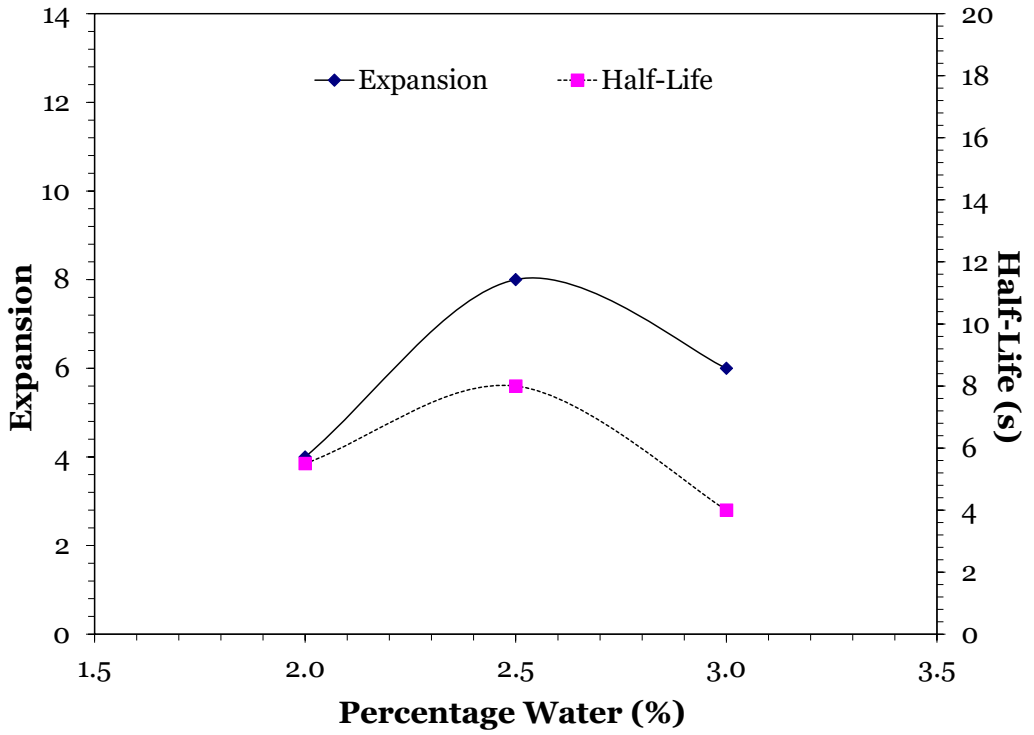

3.3 Additives portland cement and water

Type I portland cement was used to improve the strength of the CIR mixtures. The amount of portland cement added to the CIR mixtures was 1.0% of the total mix weight of these mixtures. The dosage of cement was selected after the recommendations from Cox and Howard (2015a). In addition, 3.0% of water (of total mix weight of CIR mixtures) was added to facilitate the mixing process. No virgin aggregates were used in this study.

4 Balanced Mix Design Approach for Cold In-Place Recycling Mixtures

Current CIR mix design methods focus on selecting CIR optimum binder and water contents based mostly on strength tests (e.g., maximum tensile strength and Marshal stability) and cracking performance tests (e.g., raveling and critical cracking temperature tests). Currently established CIR design methods often do not account for rutting performance of CIR mixtures when selecting optimum binder contents. To address this gap, this study established a laboratory experimental program to evaluate rutting susceptibility and cracking resistance of emulsified and foamed asphalt CIR mixtures compacted with different gyration levels and subjected to different curing processes. The goal of performance testing was to develop a CIR mix design method that balanced rutting and cracking when selecting optimum binder contents of CIR mixtures. The following subsections describe the developed CIR BMD method and discuss the performance evaluation program used as part of this study.

4.1 Description of the BMD method

This section presents a systematic approach for designing CIR mixes. The method aimed to balance rutting and cracking performance when selecting the optimum binder content. The developed design method consisted of five steps (Figure 11).

Figure 11. BMD design approach of CIR mixtures

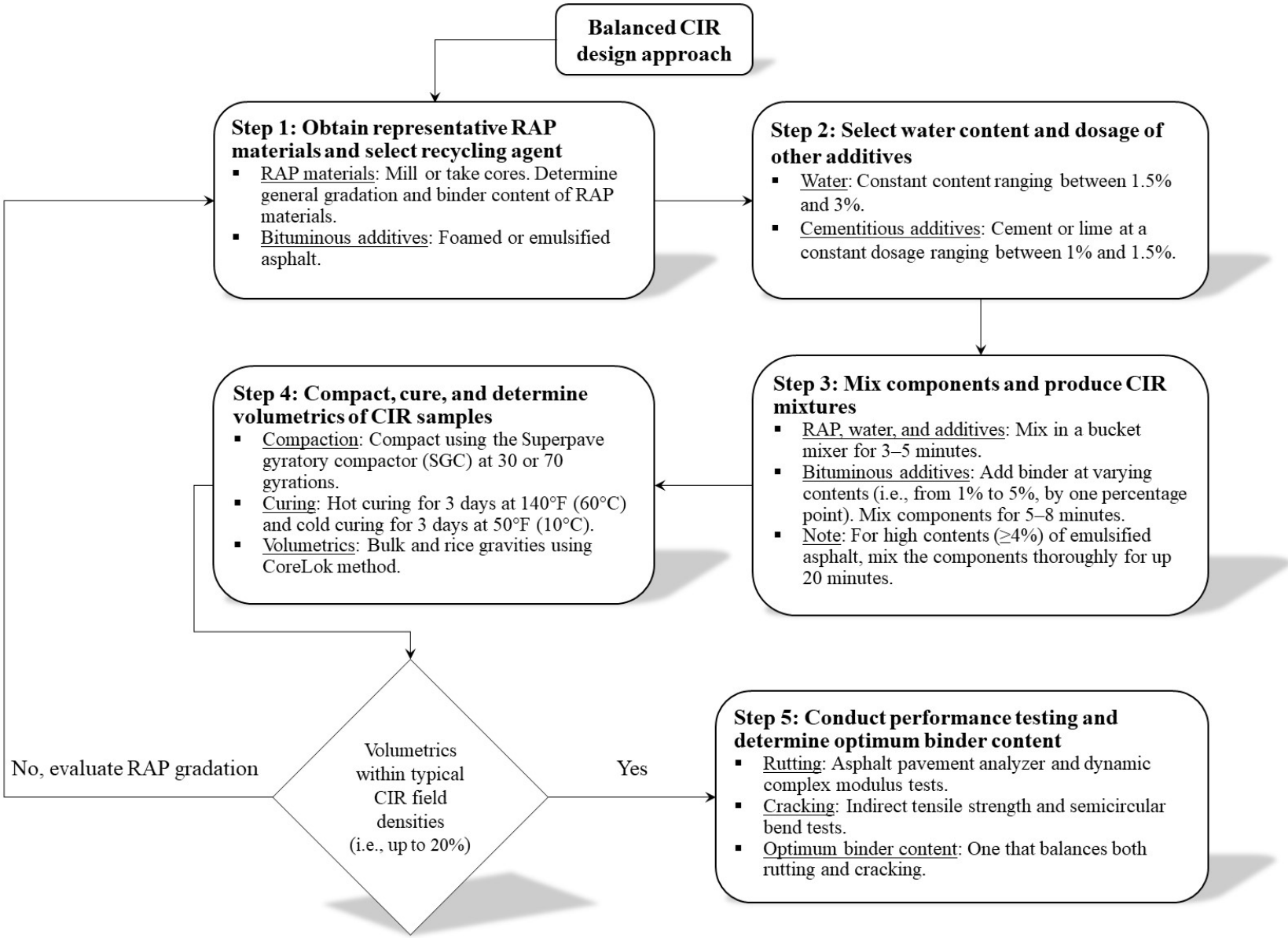

4.1.1 Step 1: Obtain representative RAP materials and select bituminous additives

First, the research team obtained representative RAP materials from the pavement structure to be rehabilitated. RAP millings for laboratory production of CIR mixtures were obtained through milling a portion of the pavement section to be rehabilitated. Gradation and binder content were then determined for the RAP millings. In addition, the team selected the types of bituminous additives, which are emulsified asphalt and foamed asphalt.

4.1.2 Step 2: Select CIR water content and dosages for other stabilizing additives

The process of producing CIR mixtures in the field involved mixing processed RAP millings with bituminous additives, water, and other cementitious additives (such as portland cement or lime). To simulate this process and facilitate compaction in the laboratory, water was added into the mix. In the literature, the amount of water added into the CIR mix varied from 1.5% to 3%. As part of this step, the research team determined the type and quantity of additives to be used for stabilizing such mixes in the field. Portland cement and lime are the most commonly used chemical additives for stabilizing CIR mixtures. For this study, a constant water content of 3% and a constant dosage of 1% (of total mix weight) of portland cement were added to the CIR mixtures because the focus was on the BMD (Scholz et al. 1991; Cox and Howard 2015b; Kim and Lee 2011; Lee et al. 2016).

4.1.3 Step 3: Mix components and produce CIR mixtures

To produce CIR mixtures, batches of dry RAP millings were mixed with water at the selected water content (Step 2) and stabilizing agent (cement or lime) by using a bucket mixer for 3–5 minutes. The CIR bituminous additives (foamed or emulsified asphalt) was then added at varying dosage rates to the mix and allowed to mix for 5–8 minutes. The RAP materials were graded according to the gradation determined in Step 1 (i.e., similar to the gradation determined for the representative RAP samples).

In this study, five binder contents ranging from 1% to 5% of the total mix weight, in increments of 1 percentage point, were used to demonstrate the proposed design approach. For the production of foamed asphalt, a laboratory foaming machine was used to inject cold water (i.e., 2.5%) into hot liquid asphalt (i.e., 329°F [165°C]) and produce foamed asphalt.

4.1.4 Step 4: Compact, cure, and determine volumetrics of CIR samples

CIR samples were then compacted at one of two levels of compaction (i.e., 30 gyration and 70 gyrations) by using an SGC to produce test specimens for performance testing (Figure 12). In this study, the selection of the level of compaction depended on the level of traffic on the roadway to be rehabilitated (i.e., 30 for low to medium traffic levels and 70 gyrations for heavy traffic; Ali et al. 2012). In general, asphalt pavements are classified into three main categories depending on the traffic level (Li et al. 2018): (1) low-trafficked pavements with cumulative ESALs lower than 1.5 million per lane, (2) medium-trafficked pavements with cumulative ESALs ranging between 1.5 and 12 million per lane, and (3) heavily trafficked pavements with cumulative ESALs higher than 12 million per lane. In this study, the purpose of compacting the CIR specimens with a higher number of gyrations (i.e., 70 gyrations) was to evaluate the potential of using CIR for heavily trafficked pavements (Rushing et al. 2012).

The compacted samples were then allowed to cure at hot conditions, that is placing the specimens in an oven for 3 days at 140°F (60°C). Cold curing at 50°F (10°C) for 3 days was also used to better represent the environmental conditions during placement in the field. In addition, three loose CIR samples were used for determining the maximum theoretical (Rice) specific gravity by using CoreLok (ASTM D6857 [ASTM 2018a]).

Figure 12. Superpave Gyratory Compactor.

4.1.5 Step 5: Density measurements of CIR mixtures

Once cured, air voids were determined for all compacted samples by using the CoreLok method (AASHTO T 331 [AASHTO 2013] and ASTM D6857 [ASTM 2018]; Figure 13). If the air-void levels of the specimens were not representative of typical field CIR densities (i.e., up to 20% air voids, depending on binder content), the compacted samples were discarded. In this case, the research team conducted additional testing to adjust the gradation of the RAP millings (Step 1). Mineral filler (<0.003 mil [0.075 µm]) or corrective virgin aggregates could be added if the RAP gradation, after evaluating the gradation of RAP by using more samples, was similar to the original gradation determined at the beginning of the design process. This process was continued until the compacted CIR specimens' air voids were representative of typical field densities for CIR pavement layers.

Figure 13. Density measurements using CoreLok.

(a) Rice specific gravity (ASTM D6857 [ASTM 2018a])

(b) Bulk specific gravity (AASHTO T 331 [AASHTO 2013])

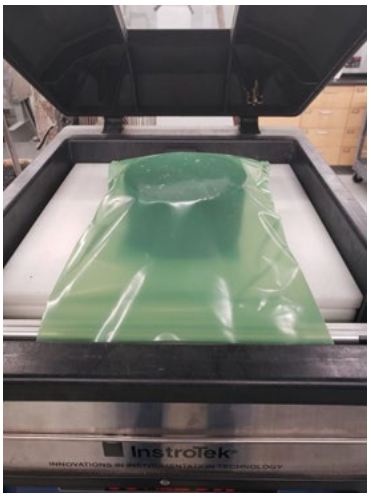

4.1.6 Step 6: Conduct performance testing and determine optimum binder content

In this step, performance testing was selected and conducted to characterize the rutting and cracking susceptibility of CIR mixtures. In this study, rutting was quantified using the APA (AASHTO T 340) and the dynamic complex modulus (AASHTO T 342) while cracking was quantified Semicircular Bend Fracture Energy (SCB-FE; AASHTO TP 105 [AASHTO 2010, 2019, 2020e]). In addition, the strength of CIR mixes was measured using the IDT test in accordance with AASHTO T 283 (AASHTO 2018c).

On completion of all performance tests and regression analysis, the optimum binder content of the CIR mix was selected using criteria that balanced rutting and cracking performance. Figure 14 presents an example of a binder-content range that balances rutting and cracking performance. Figure 14*a* shows that, when the binder content determined by maximizing cracking resistance (i.e., at peak cracking measure) is lower than that obtained for maximizing rutting performance, the optimum binder content is the one maximizing the cracking resistance. This is because the rutting threshold was met at lower binder contents. Figure 14*b* presents a second case where the binder content based on cracking performance is higher than that obtained for optimal rutting performance. In this second case, the area between both binder contents (shaded area) was considered as the optimum binder-content range. The midpoint of this range was selected as the optimum binder content, balancing rutting and cracking performances.

Figure 14. Example of how to select an optimum binder content by using CIR rutting and cracking performance measures.

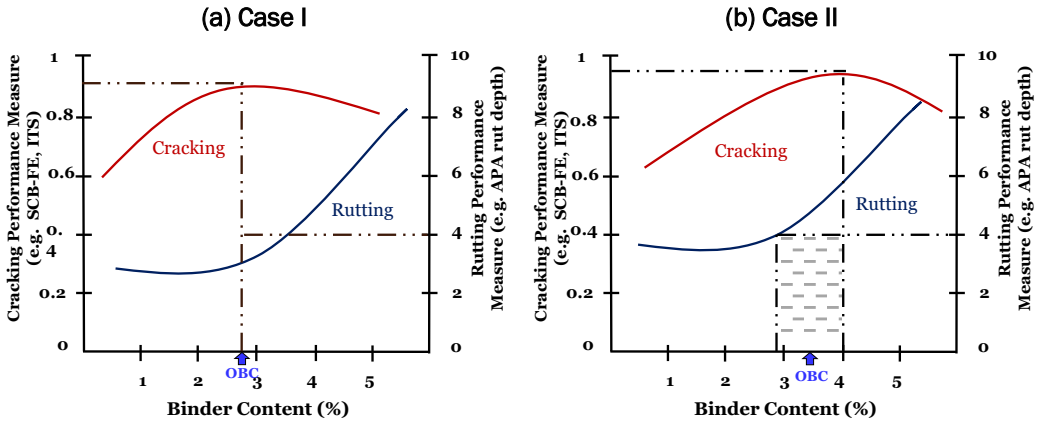

4.2 CIR test methods

The purpose of conducting performance tests was to utilize performance measures (rutting and cracking) to select optimum binder contents. In this study, APA rut depth and the dynamic complex modulus ($|E^*|$) were selected to quantify rutting in accordance with AASHTO T 340 and AASHTO T 342, respectively, while ITS and SCB-FE were used to quantify the strength and the cracking resistance in accordance with ASTM D6931 and AASHTO TP 105, respectively (AASHTO 2010, 2019, 2020e; ASTM 2017). Other tests can be used provided that binder content is a strong predictor of test measures.

4.2.1 Asphalt pavement analyzer

The APA is a wheel-tracking device typically used for evaluating the rutting potential of asphalt mixtures (Figure 15). This test was conducted in accordance with AASHTO T 340 (AASHTO 2010). It involves applying a 100 lb (45 kg) force on a steel wheel on top of a pressurized hose (100 psi [0.69 Mpa]), which then transfers the load to the test specimens. The wheel moves back and forth on top of the hose, and each movement from one side of the specimen to the other is considered one loading cycle. This study used the APA to determine rut-depth values of all four CIR mixtures discussed above. The test was conducted at 147°F (64°C) with specimens allowed to condition for a minimum of 6 hours at that temperature before testing. A total of six APA replicates (i.e., six SGC-compacted specimens) were tested (see chapter 5 for the average rut depth). All CIR samples were compacted to a height of 3 in. (75 mm), and the test was terminated after 8,000 loading cycles.

Figure 15. Asphalt pavement analyzer test.

4.2.2 Dynamic complex modulus

The dynamic complex modulus test is used to evaluate the performance of asphalt mixtures over a spectrum of temperatures and loading frequencies (Figure 16). As a result, this test provides a general overview of an asphalt mixture stiffness under a range of traffic speeds (i.e., frequencies) and environmental conditions (i.e., temperatures; AASHTO T 342 [AASHTO 2019]). At high temperatures and low loading frequencies, rutting is the predominant failure mode of asphalt mixtures (including CIR mixtures). In this study, $|E^*|$ was measured at standard temperatures of 39°F (4°C), 70°F (21°C), 99°F (37°C), and 129°F (54°C) while also applying loading at frequencies of 0.1, 0.5, 1, 5, 10, and 25 Hz. The dynamic modulus values obtained for high temperatures (37°C and 54°C for this study) and at low

frequencies (10 Hz) were selected to determine the rutting potential of CIR mixtures. This study used the frequency of 10 Hz was when interpreting $|E^*|$ results as it represents a common speed at which traffic travels (Ali et al. 2012). All samples were first compacted to a height of 7 in. (180 mm), allowed to cure, and then cored and cut to obtain cylindrical specimens having a diameter of 4 in. (100 mm) and a height of 6 in. (150 mm.). Three replicates were tested for each mix.

Figure 16. Dynamic complex modulus test.

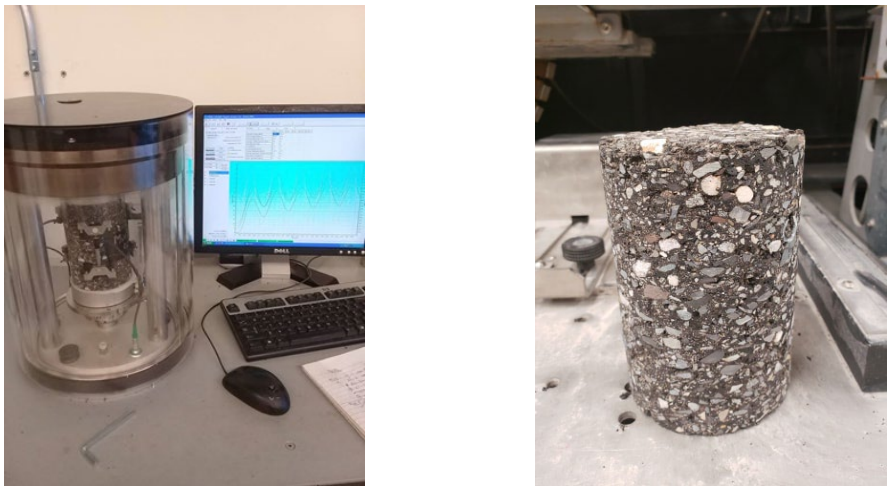

4.2.3 Indirect tensile strength

ITS is a measure of an asphalt mixtures' tensile strength (Figure 17). This test involves diametrically loading asphalt specimens at a rate of 2 in./min (50 mm/min) at room temperature or higher or 0.5 in./min (12.5 mm/min) at 32°F (0°C) and lower and determining the stress at which a specimen breaks (using peak load). Higher ITS values are desirable as they indicate that the tested asphalt mixture is stronger than lower ITS values. For this study, samples of all four CIR mixtures (previous section) were compacted to a height of 2.5 in. (63 mm) and tested at 32°F (0°C) to determine ITS. Three replicates were tested for each mix.

Figure 17. ITS test.

4.2.4 Semicircular bend

The SCB is another test used for characterizing the cracking susceptibility of asphalt mixtures (Figure 18). Similar to the procedure of the IDT test, the notched semicircular specimens are loaded diametrically using a loading rate of 50 mm/min. Using the recorded load versus displacement SCB curve, the fracture energy is computed as the area under that curve. The fracture energy is an indicator of an asphalt mixture's ability to resist cracking; the higher the fracture energy, the more resistant the mix. In this study, SCB specimens were notched to simulate a crack in the test specimen using a 0.5 in. (12.5 mm) long and 0.04 in. (1 mm) wide notch. Testing was conducted at 32°F (0°C), and three replicates per mix were tested according to AASHTO TP 105 (2020e). A testing temperature of 32°F (0°C) was selected for both ITS and SCB because it represents a more conservative temperature at which cracking will be more pronounced. This also falls in line with Charmot et al. (2017).

Figure 18. Semicircular bend test.

5 Results, Analysis, and Discussion

This chapter presents the challenges of the developed BMD approach by demonstrating and analyzing performance-testing results obtained for a total of eight CIR mixes. Specifically, chapter 5 discusses the most appropriate performance tests of those considered in this study to use when designing CIR mixes. In addition, this chapter discusses various cases that might be encountered when using this BMD approach and how to select an optimum bituminous additives content for each case.

5.1 Overview of CIR mixes and factors considered

To evaluate the practicality and applicability of the developed BMD for CIR mixtures, several performance tests (chapter 4) were conducted on CIR mixes prepared at different binder contents (ranging from 1% to 5% with 1% increments). Table 9 presents all eight CIR mixes considered in this study along with the nomenclature used for each CIR mix based on its design factors. For instance, if a mixture was prepared using emulsion, compacted at 30 gyrations, and allowed to cure in an oven at 140°F (60°C) for 3 days, the mixture will be designated as CIR-E30H, where "E" stands for emulsion, "30" stands for 30 gyrations, and "H" stands for hot curing.

As Table 9 shows, the following factors were considered when preparing CIR mixtures:

- Bituminous additives type: Two bituminous additives were considered (for more details, refer to chapter 3). The first was asphalt emulsion (CSS-1h) and the second was foamed asphalt (PG64-22).
- Compaction level: Two compaction levels were considered when preparing CIR samples. The first was 30 gyrations, and the second was 70 gyrations. The 70-gyration compaction effort was selected to represent heavily trafficked airfields or roadways.
- Mix curing: Two curing procedures were implemented in this study to evaluate their impact on material performance. The first curing condition was "hot curing," which involved placing samples in an oven at 140°F (60°C) for 3 days. The second condition was "cold curing" through placing the samples in an oven at 50°F (10°C) for 3 days.

Table 9. CIR mixtures' properties and designations.

Mixture	Bituminous Additives	Gyration Level	Curing Process
CIR-E30H	CSS-1h Emulsion	30 Gyrations	3 days at 140°F (60°C)
CIR-E30C	CSS-1h Emulsion	30 Gyrations	3 days at 140°F (60°C)
CIR-E70H	CSS-1h Emulsion	70 Gyrations	3 days at 140°F (60°C)
CIR-E70C	CSS-1h Emulsion	70 Gyrations	3 days at 140°F (60°C)
CIR-F30H	PG 64-22 Foamed	30 Gyrations	3 days at 50°F (10°C)
CIR-F30C	PG 64-22 Foamed	30 Gyrations	3 days at 50°F (10°C)
CIR-F70H	PG 64-22 Foamed	70 Gyrations	3 days at 50°F (10°C)
CIR-F70C	PG 64-22 Foamed	70 Gyrations	3 days at 50°F (10°C)

Considering these factors and accounting for field curing (testing temperatures discussed in chapter 4) allowed the study to comprehensively evaluate the practicality and applicability of the developed balanced CIR mix design approach. Determining the most suitable performance tests for evaluating rutting and cracking is also possible on this wide range of CIR mixes. In addition, the experimental factors above investigate the impact of bituminous additive type, compaction level, and curing method on the performance of CIR mixtures. The significance of such impacts was assessed using statistical analyses (i.e., Analysis of Variance, ANOVA) and is presented in the upcoming sections of this chapter.

5.2 Analysis of volumetric data (air voids)

Figures 19 and 20 present the air-void levels obtained for emulsified and foamed asphalt CIR samples compacted to different heights, depending on the performance test considered. All compacted samples met the air-void levels specified in the BMD approach (i.e., all were less than 20% air voids). However, initial CIR samples prepared using the washed sieve analysis gradations presented in Figure 6 (chapter 3) had air-void higher than 20%. As this was not representative of typical field CIR air-void levels, the research team sieved and graded 462 kg of RAP millings to determine the general gradation. Using the general gradation, all compacted CIR samples met the 20% maximum air-void level without the need for adding virgin aggregates. However, for practical reasons, designers may add virgin aggregates to adjust the RAP millings gradation and thus ensure meeting the air-void requirements in a short period of time.

In general, Figures 19 and 20 show that an increase in binder content decreases air-void levels (drop by up to 4% for every increase of 1% binder).

In terms of bituminous additive type, emulsified asphalt CIR mixtures presented slightly higher air voids than foamed asphalt (up to 2% difference for the same binder content). Compaction level also impacted CIR volumetrics. That is, CIR mixtures compacted with 70 gyrations were lower by up to 4% air-void level than that of CIR mixtures compacted using 30 gyrations. CIR mixtures subjected to hot curing (3 days at 140°F [60°C]) had lower air-void levels than that of mixtures subjected to cold curing. These volumetric results were expected because the addition of more binder fills more voids within the RAP matrix, causing air voids to drop. In addition, increasing the compaction effort typically leads to lower air voids.

5.3 Identification of proper performance tests for balanced design of CIR mixes

A successful BMD approach conducts performance tests (or measures) that can distinguish between CIR mixes prepared at different binder contents. In other words, if binder content influences the performance of a CIR mix, which is generally the case for asphalt mixtures, laboratory tests must be capable of capturing this impact so a designer can optimize the selection of binder content that maximizes (or balances) performance.

Figure 21 presents the relationships between rutting and cracking performance measures with binder content for the CIR-E30H mix. As Figure 21*a* shows (APA rut depth vs. binder content), increases in binder content resulted in an increase in APA rut-depth values. Using a second-degree polynomial regression curve clearly shows (Figure 21*a*) that the relationship between the APA rut depth and CIR binder content is significant (strong correlation at 99.4% R^2). This indicates that the APA test is capable of capturing the change in CIR mixes' rutting resistance caused by a change in binder content.

Figure 21*b* presents the relationship between $|E^*|$ (second rutting measure) at high temperatures (99°F [37°C] and 129°F [54°C]) and CIR binder content. As Figure 21*b* shows, $|E^*|$ was not able to differentiate between the CIR samples prepared at different binder contents for both test temperatures. This is because change in binder content did not result in a meaningful increase (or decrease) in measured $|E^*|$ values (remaining a constant trend).

Figure 19. Volumetric analyses of emulsified asphalt CIR mixtures.

(a) CIR-E30H

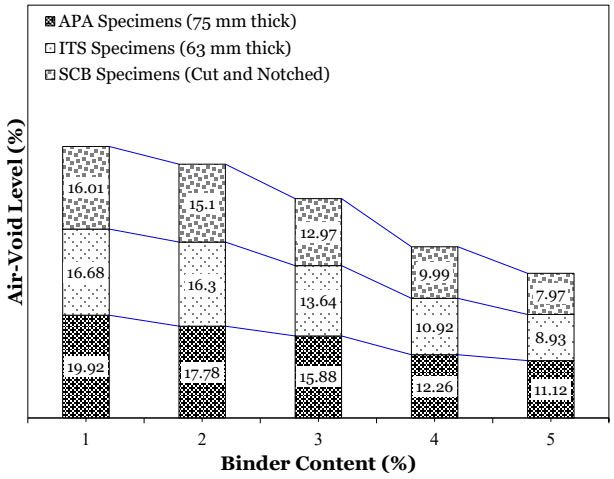

(b) CIR-E70H

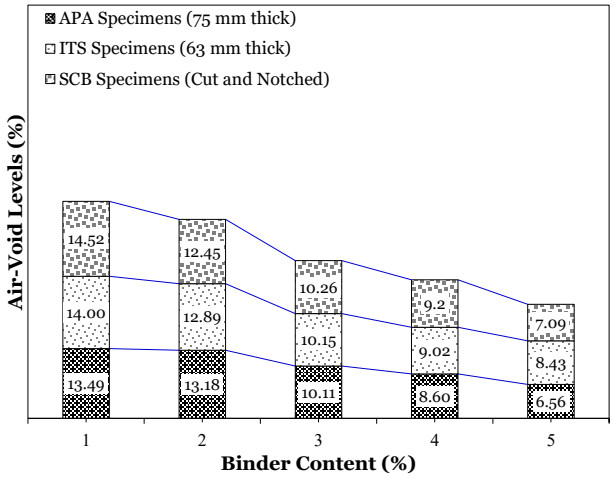

(c) CIR-E30C

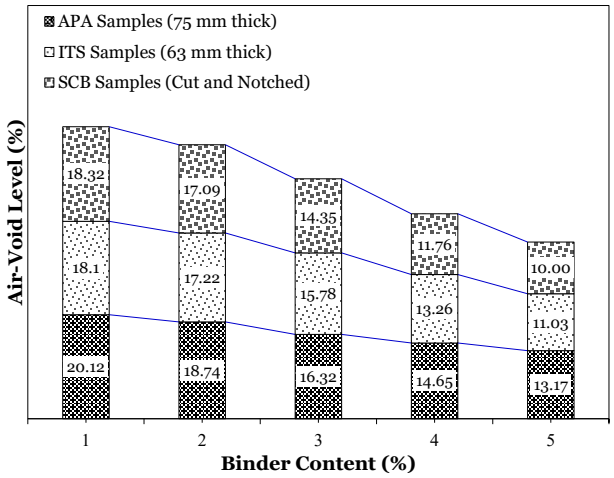

(d) CIR-E70C

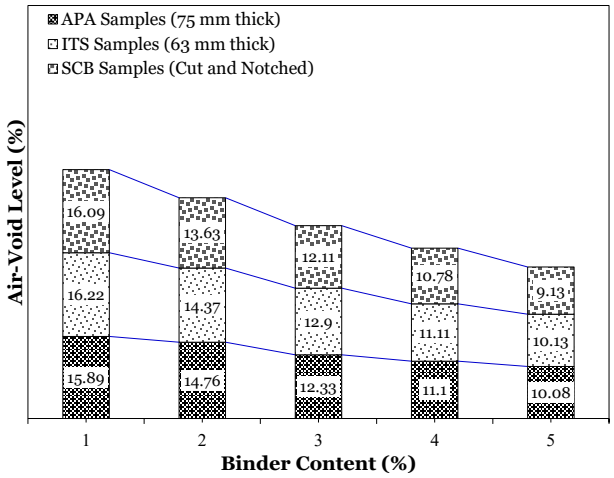

Figure 20. Volumetric analyses of foamed asphalt CIR mixtures.

(a) CIR-F30H

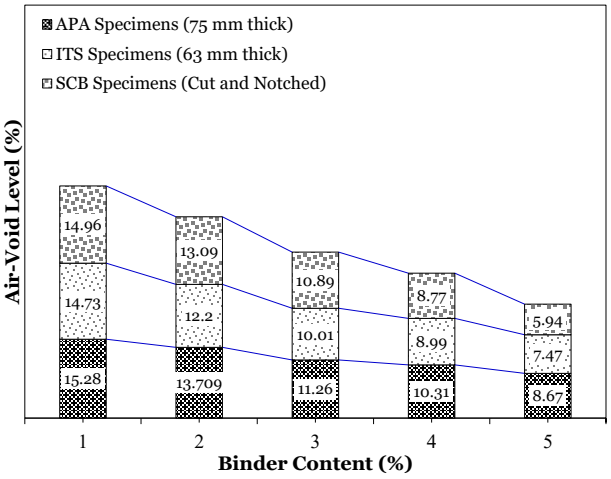

(b) CIR-F70H

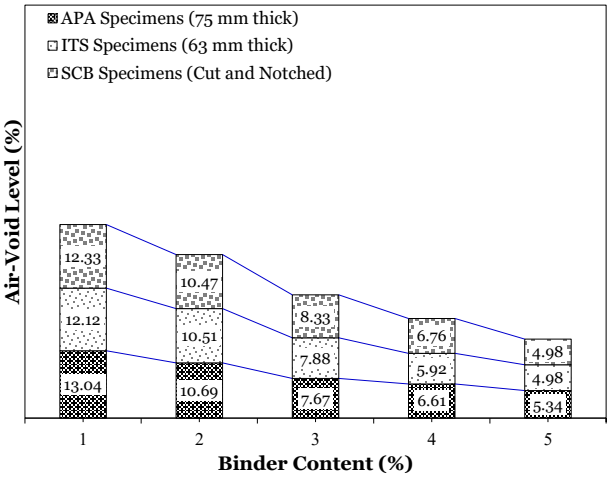

(c) CIR-F30C

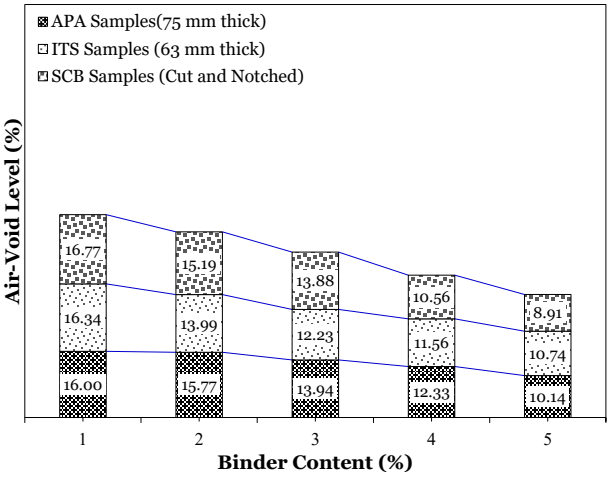

(d) CIR-F70C

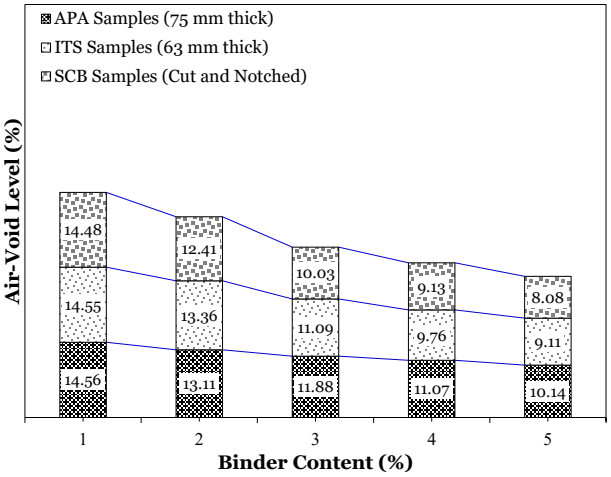

Figure 21. Correlation between performance measures and binder content (CIR-E30H Mix).

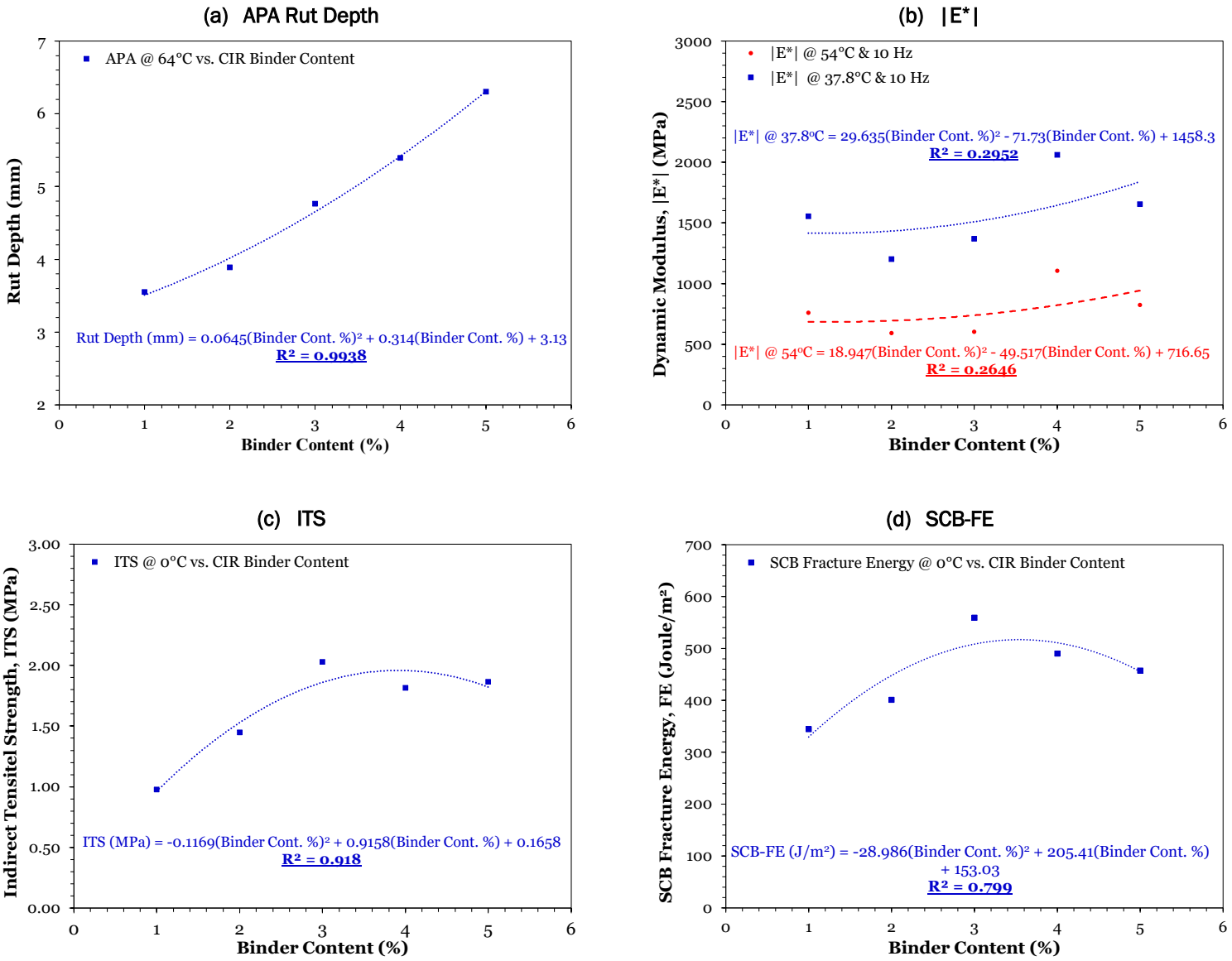

Weak correlations (R^2 of 29.6% at best for 99°F [37°C] results) were also observed for this relationship (second-degree polynomial regression curve), indicating that the CIR mix's dynamic modulus is not a strong predictor of the binder content. Therefore, the dynamic complex modulus test does not appear suitable for the CIR BMD method as it cannot be used for selecting a binder content that maximizes rutting resistance.

With regard to strength and cracking, Figure 21*c* and *d* presents the relationships obtained for the ITS and SCB-FE with binder content, respectively. As illustrated in Figure 21*c*, increase in binder content resulted in an increase in measured ITS values until a peak was reached. After the peak in ITS, the increase in binder content resulted in a decrease in ITS values measured. A similar observation (or trend) was found for SCB-FE measured values (Figure 21*d*). For both the ITS and SCB-FE, strong correlations were obtained for these relationships (ITS vs. Binder content: R^2 = 92%; SCB-FE vs binder content: R^2 = 80%). These results demonstrate that both measures (ITS and SCB-FE) were able to capture the effect of varying binder contents. Both measures also allow for maximizing (and ultimately balancing) strength and cracking resistance of CIR mixtures. Furthermore, it is worth noting that these trends fall in line with previous studies that aimed to select an optimum binder content for CIR mixes (Niazi and Jalili 2009; Brovelli and Crispino 2012; Berthelot et al. 2013; Gao et al. 2014; Bessa et al. 2016; Graziane et al. 2018). Therefore, the study team considered both ITS and SCB-FE measures for developing the BMD design for CIR mixtures.

5.4 Balanced CIR optimum binder content selection

To select a balanced optimum binder content (i.e., one that balances rutting and cracking performance), this study determined the relationships between APA rut depth and both strength and cracking measures (ITS and SCB-FE) as well as binder content for all eight mixes considered. These relationships assist in selecting an optimum binder content by using two main parameters: (1) maximum CIR strength or cracking resistance (peak of ITS or SCB-FE), and (2) *assumed* CIR rut-depth threshold (0.2 in. [5 mm]). Note that the trends observed for the mixes varied and can be grouped into three cases: (1) both cracking and rutting measures are relevant, (2) only cracking measures are relevant, and (3) both rutting and cracking measures show increasing trends (Table 10). It is important to mention that a performance measure has a relevant trend when the binder content increases, the rutting measure (APA rut depth) increases, and the

cracking measure (SCB-FE) and strength measure (ITS) show peaking trends. The following subsections discuss each case.

Table 10. Selection methods of CIR optimum binder contents.

Cases	Trend of Rutting Measure	Trend of Cracking Measure	Optimum Binder Content Selection
I	Increasing	Peaking	Midpoint of the area between rut-depth threshold (5 mm) and SCB-FE and ITS peaks
II	Constant	Peaking	Peak of SCB-FE and ITS
III	Increasing	Increasing	APA Rut depth vs. SCB-FE: APA rut-depth (5 mm) threshold APA Rut depth vs. ITS: Midpoint of the area between rut-depth threshold (5 mm) and ITS peaks

5.4.1 Case I: Both performance measures are relevant

Figure 22 illustrates this case for CIR-E30H mix. As shown, the trends for rutting and cracking performance measures continuously increase (APA rut depth) and "peak" (SCB-FE and ITS), respectively, with the increase in binder content, making both measures relevant for selecting an optimum binder content. Assuming a rut-depth threshold of 0.2 in. (5 mm), the optimum binder content for optimizing rutting performance can be selected as shown in Figure 22 (i.e., 2%). Based on peak SCB-FE (Figure 22*a*) and ITS (Figure 22*b*) values, the optimum binder content for maximizing strength and cracking performance can be selected as 3.2% and 3%, respectively. These selected optimum binder contents established two ranges for binder contents balancing rutting and cracking, depending on whether ITS or SCB-FE was utilized. In this case for CIR-E30H, the average of the midpoint of both ranges (established based on ITS vs. APA and SCB-FE vs. APA) are used as the optimum binder content (i.e., for CIR-E30H, the optimum binder content is 2.7%). It is important to mention that, in some cases, the determined optimum binder content can exceed the rutting threshold (0.2 in.[5 mm]) to achieve more cracking resistance. The rutting threshold, suggested by the research team, can be exceeded by no more than 0.04 in. (1 mm) when selecting balanced optimum binder content.

Figure 22. BMD results for CIR mixtures (case I).

(a) CIR-E30H: APA vs. SCB-FE

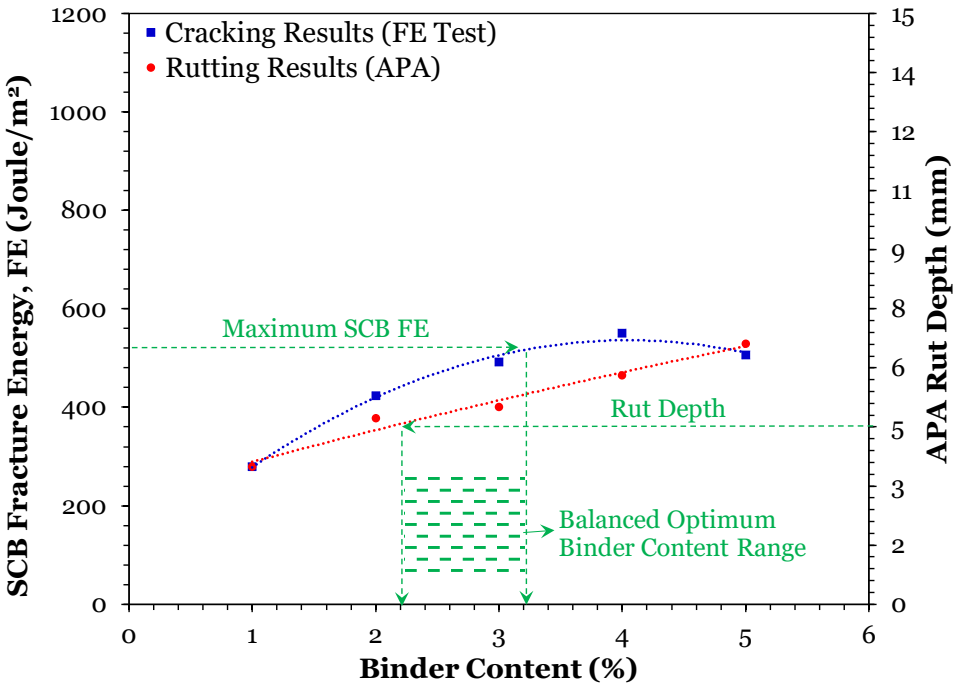

(b) CIR-E30H: APA vs. ITS

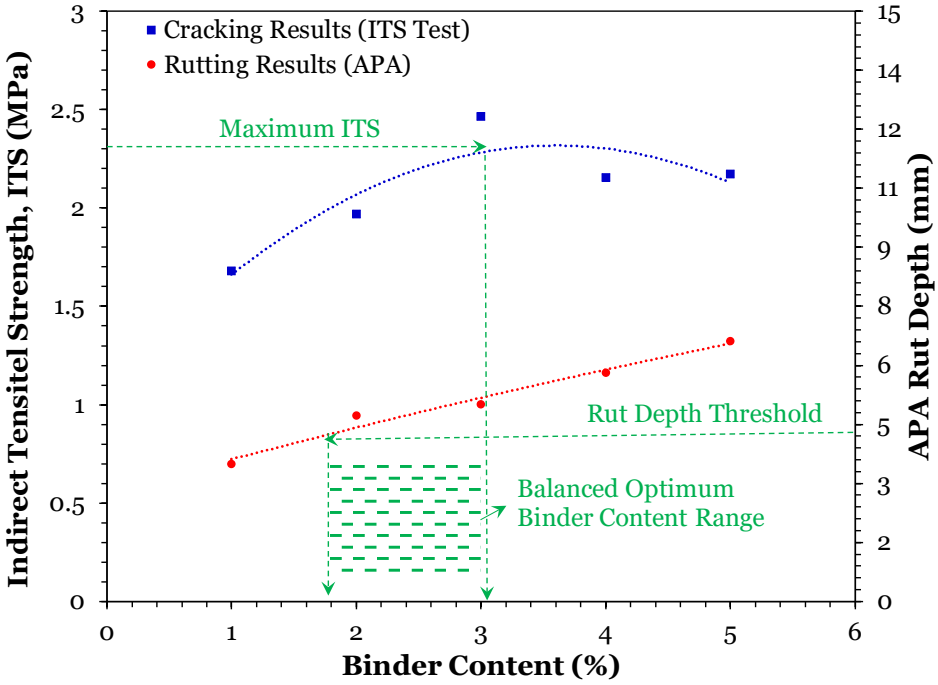

5.4.2 Case II: Only cracking measures are relevant

This case occurs when the rut-depth values measured for a CIR mix are relatively constant when binder content increases while cracking measures are also showing a "peaking trend." Figure 23 presents an example for CIR-E70H mix. For this case, any of the binder contents can be selected for designing CIR mixtures to meet a rutting threshold of 5 mm, making the rutting performance irrelevant when selecting the optimum binder content. Therefore, for this case, the optimum binder content can be selected based on the peak ITS and SCB-FE values and a slight 5% percent reduction in these peak values. The research team suggested this reduction because it will not meaningfully change strength (e.g., for CIR-E70H, peak ITS is 312 psi [2.15 Mpa] while a 5% reduction is at 348 psi [2.04 Mpa]). The binder content resulting in a maximum cracking resistance is 3.5% for CIR-E70H). Note that using this 5% reduction in the cracking performance measure may present a more practical way of selecting optimum binder contents without compromising performance.

Figure 23. BMD results for CIR mixtures (case II).

(a) CIR-E70H: APA vs. ITS

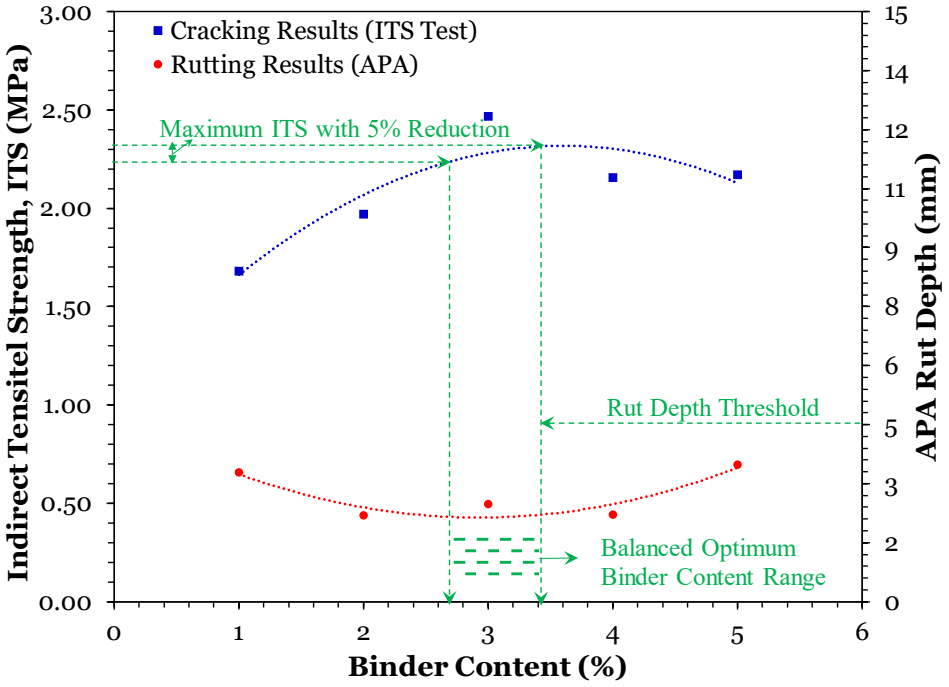

Figure 23 (cont.). BMD results for CIR mixtures (case II).

(b) CIR E70H: APA vs. SCB-FE

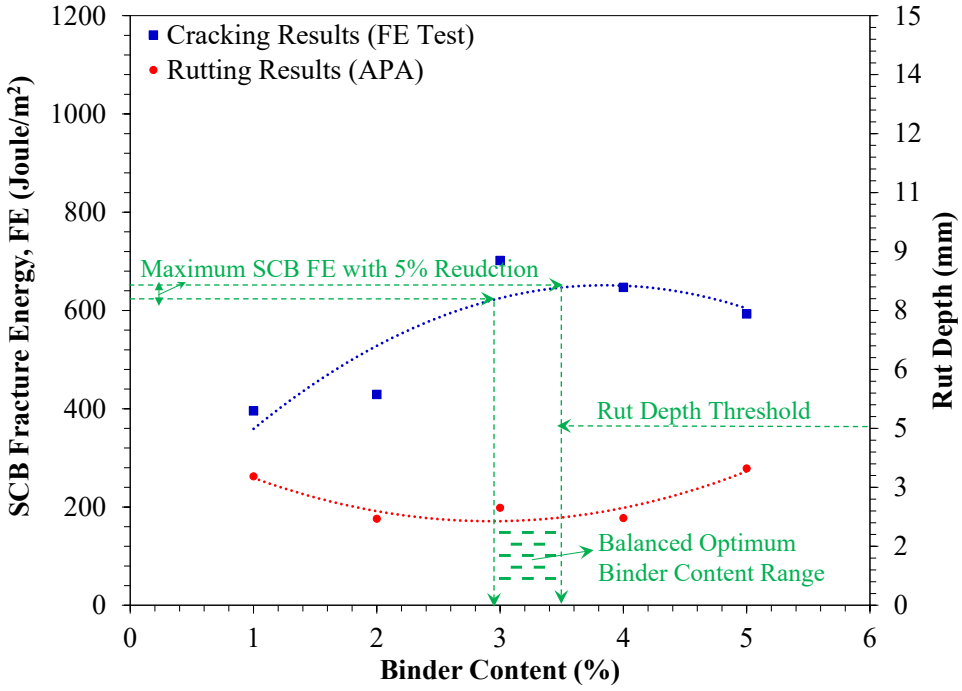

5.4.3 Case III: Both performance measures show increasing trends

In this case (Figure 24), one or both of the SCB-FE and ITS values are showing increasing trends with no clear peak as the binder content of the mix is increased. In this case, and at the assumed rut-depth threshold of 0.2 in.(5 mm), the optimum binder content for maximizing rutting performance is 2.5% (Figure 24) for CIR-E30C. For ITS values, Figure 24*a* does not clearly show a "peaking trend," so the optimum binder content for balancing cracking performance is selected as the average of the midpoint of the optimum binder-content range (established based on SCB-FE vs. APA). However, as shown in Figure 24*b*, the optimum binder content is selected as the one that resulted in the highest SCB-FE values (i.e., 2.6% binder content). For ITS values (Figure 24*a*), the optimum binder content was selected as the one that resulted in the highest ITS values. Based on this, the BMD optimum binder content for CIR-F30H is 2.6% (Figure 24).

Figure 24. BMD results for CIR mixtures (case III).

(a) CIR-F30H: APA vs. ITS

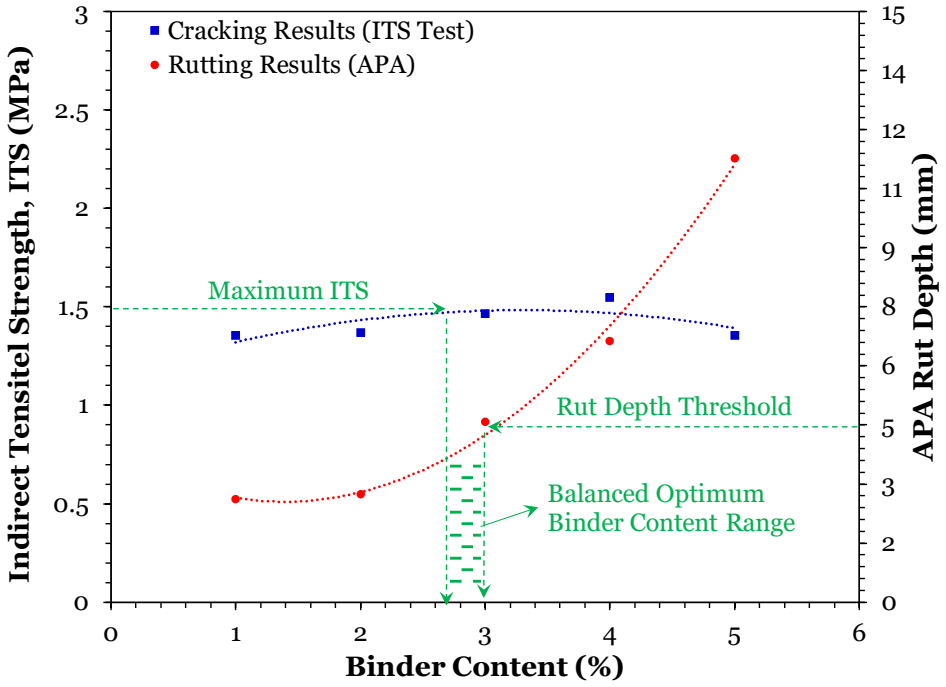

(b) CIR-F30H: APA vs. SCB-FE

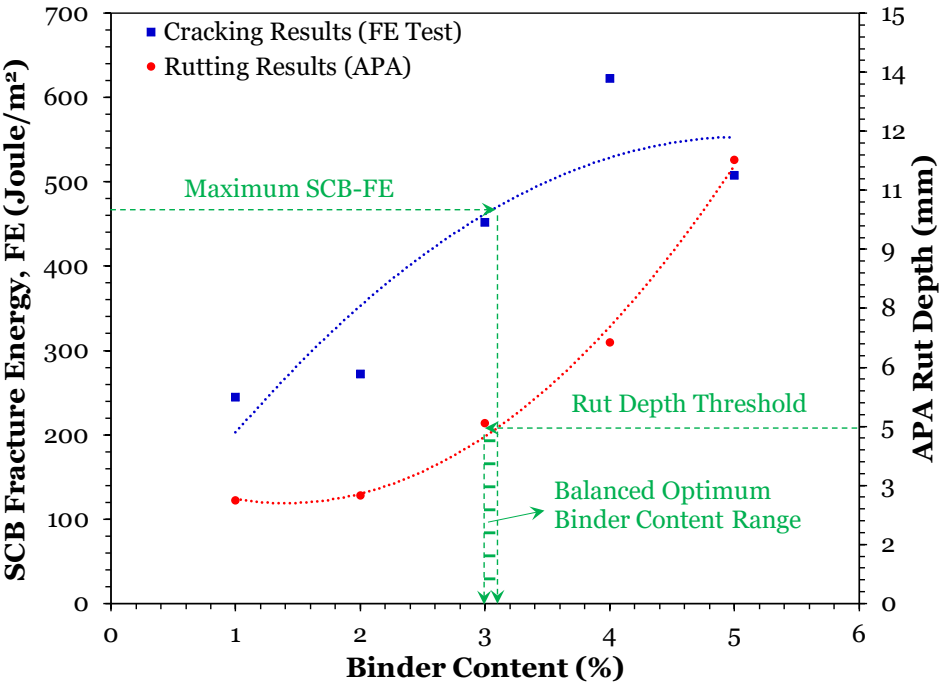

In summary, the results presented in Figures 22 through 24 indicate that CIR mixtures can be successfully designed using the BMD approach developed as part of this study. The BMD method is efficient because it yielded

balanced optimum binder contents, ranging between 2.5% and 3.2%, that are similar to those typically found in the literature (e.g., Kim and Lee 2011). Table 11 summarizes the balanced optimum binder contents for all eight CIR mixtures considered in this study and as determined based on case I, II, or III. The variability of the selected balanced optimum binder contents (Table 11) varied for the eight CIR mixes. The lowest coefficient of variation within the data was 1.3% (CIR-F70C) while the highest coefficient of variation was 19.8% (CIR-F70H), indicating that the variability in the selected optimum binder contents is low.

Table 11. Balanced optimum binder contents for all eight CIR mixtures considered in this study.

Mixture	Optimum Binder Content (%)			Average	Standard Deviation	Coefficient Of Variance (%)	Case
	Sample 1	Sample 2	Sample 3				
CIR-E30H	3.2	2.4	2.5	2.7	0.4	16.1	I
CIR-E70H	3.2	2.9	2.8	2.9	0.1	3.0	II
CIR-F30H	2.7	2.6	2.6	2.6	0.1	2.9	III
CIR-F70H	2.0	2.8	3.0	2.6	0.5	19.8	I
CIR-E30C	2.8	3.0	2.7	2.8	0.1	4.5	III
CIR-E70C	3.2	2.6	3.2	3.0	0.3	11.2	I
CIR-F30C	3.0	2.8	3	2.9	0.1	4.6	III
CIR-F70C	3.2	3.3	3.2	3.2	0.04	1.3	III

5.5 Performance of CIR mixtures at optimum binder content

5.5.1 General performance comparison

Figure 25 presents the overall results for rutting measures (APA rut depth and $|E^*|$ at 129°F [54°C] and 10 Hz) and cracking measures (ITS and SCB-FE at 0°C) at optimum binder contents for all eight CIR mixtures. As Figure 25 shows, both rutting and cracking performance varied for the different CIR mixtures. For instance, APA rut-depth values (Figure 25*a*) ranged between 0.75 in. (1.9 mm; CIR-F70H) and 0.2 in. (5.1 mm; CIR-F30C), indicating a satisfactory rutting performance (APA rut-depth threshold assumed at 0.2 in. [5 mm]). In addition, all CIR mixtures subjected to hot curing presented relatively lower APA rut-depth values than those of CIR mixtures subjected to cold curing (Figure 25*a*).

In terms of $|E^*|$ (Figure 25*b*), all CIR mixtures had similar moduli values at high temperature (129°F [54°C]) and 10 Hz loading frequency. The sigmoidal master curves developed for the eight CIR mixtures at optimum binder contents showed that bituminous additive type, compaction level, and curing process had no to little impact on CIR rutting performance. All CIR mixtures subjected to hot curing presented slightly higher $|E^*|$values than those subjected to cold curing.

For cracking performance (Figure 25*c* and *d*), the tensile strength values (at 32°F [0°C]) of CIR mixtures ranged between 57 psi (0.39 Mpa) (CIR-E30C) and 303 psi (2.09 Mpa) (CIR-E70H), while SCB fracture energy values (at 32°F [0°C]) ranged between 174.8 and 622.3 $J.m^{-2}$. Figure 25*c* shows that CIR mixtures subjected to hot curing exhibited significantly higher tensile strength and SCB fracture energy than those with cold curing. In summary, CIR mixtures prepared with different bituminous additives types, gyration levels, and curing processes did not have similar performances in terms of rutting and cracking. Thus, there is a need to evaluate the impact of each factor (binding agent, compaction level, and curing process) on CIR rutting susceptibility and cracking resistance, which the following sections present.

Figure 25. Performance-testing results for all eight CIR mixtures considered in this study.

(a) APA results

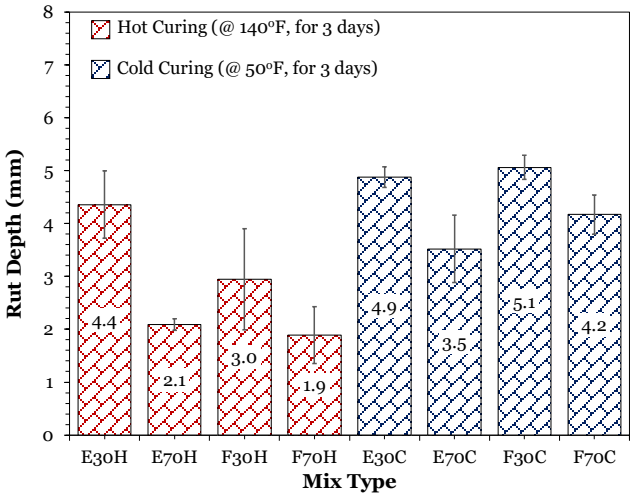

(b) Dynamic complex modulus results

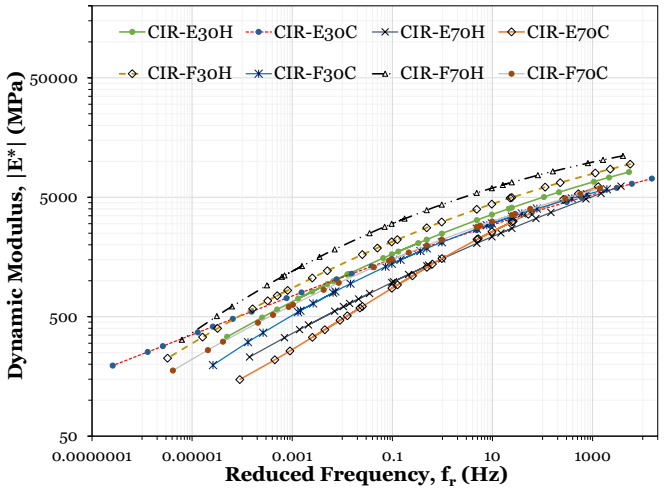

(c) ITS results at 32°F (0°C)

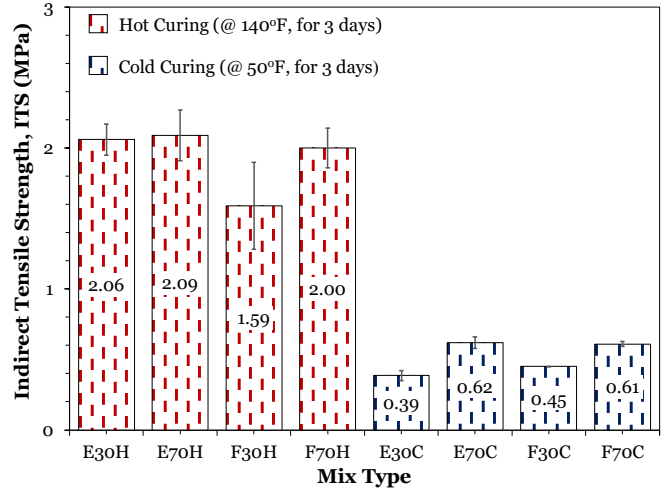

(d) SCB-FE results at 32°F (0°C)

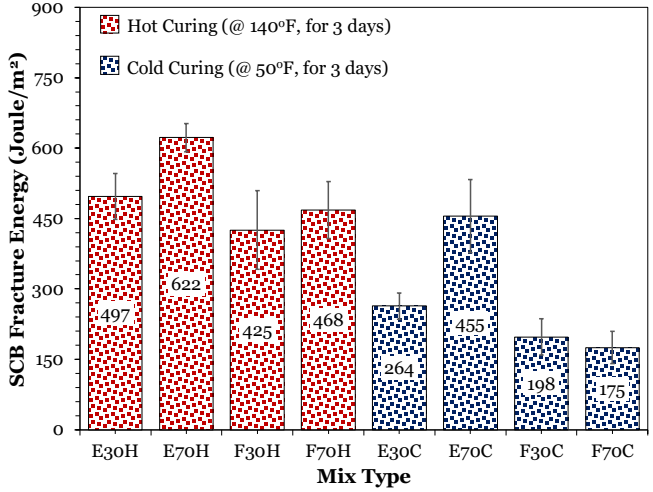

5.5.2 Impact of bituminous additives on performance (rutting and cracking)

Figures 26 and 27 present rutting and cracking performance-testing results, respectively, at optimum binder contents for emulsified and foamed asphalt CIR mixtures. As shown in Figure 26*a* and *b*, both emulsified and foamed asphalt CIR mixtures had similar APA rut-depth values (within 0.04 in. [1 mm]) for the same compaction effort and curing process. In addition, Figure 26*c* and *d* shows that emulsified and foamed asphalt CIR mixtures had similar $|E^*|$ values. These observations indicate that the bituminous additives used in the various CIR mixes did not have a strong impact on their rutting resistance.

Regarding cracking performance, Figure 27 shows ITS and SCB-FE results for all eight CIR mixtures, grouped by curing conditions. As Figure 27*a* and *b* shows, both emulsified and foamed asphalt CIR mixtures had similar ITS values when compacted at the same gyration level and subjected to the same curing process. However, emulsified CIR mixtures presented higher SCB-FE values (approximately 20% more) than those of foamed asphalt mixes. This effect was more pronounced for mixes compacted at 70 gyrations (Figure 27*c* and *d*). These observations indicate that CIR mixtures prepared with CSS-1h emulsified asphalt mixes may be slightly better at resisting cracks than neat PG 64-22 foamed asphalt CIR mixes, provided that both are prepared using the same gyration level and curing process. It is important to note that these results are limited to the materials used in this study and that different results may occur for other binder or emulsion grades and types.

Figure 26. Performance-testing results highlighting the effect of bituminous additive type on CIR rutting performance.

(a) APA rut-depth results after hot curing

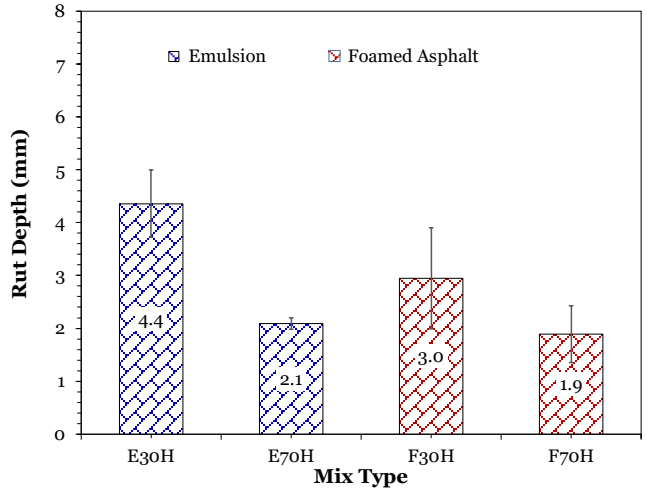

(b) APA rut-depth results after cold curing

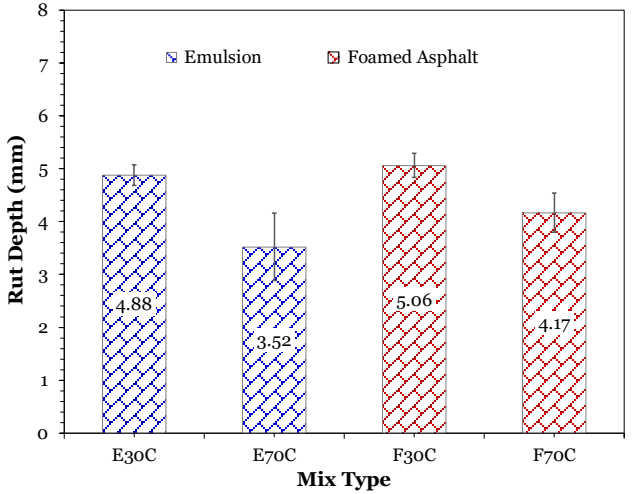

(c) |E*| results after hot curing

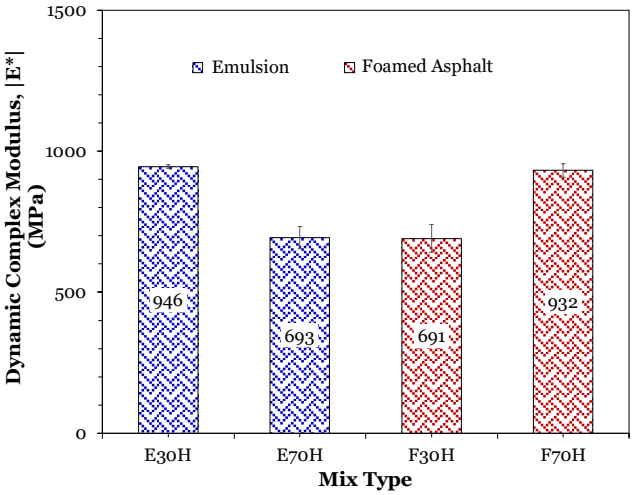

(d) |E*| results after cold curing

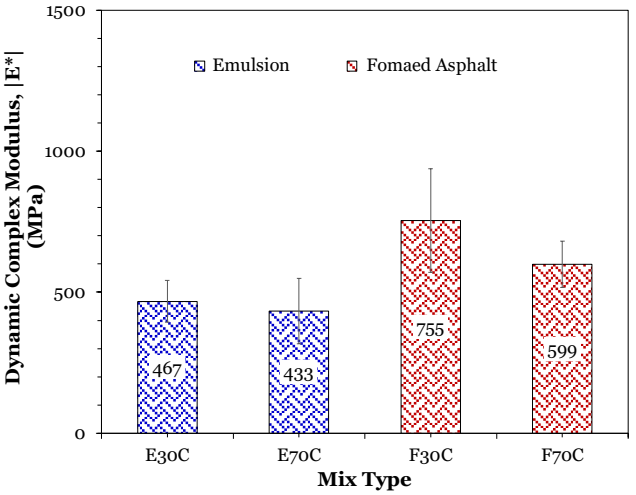

Figure 27. Performance-testing results highlighting the effect of bituminous additive type on CIR cracking performance.

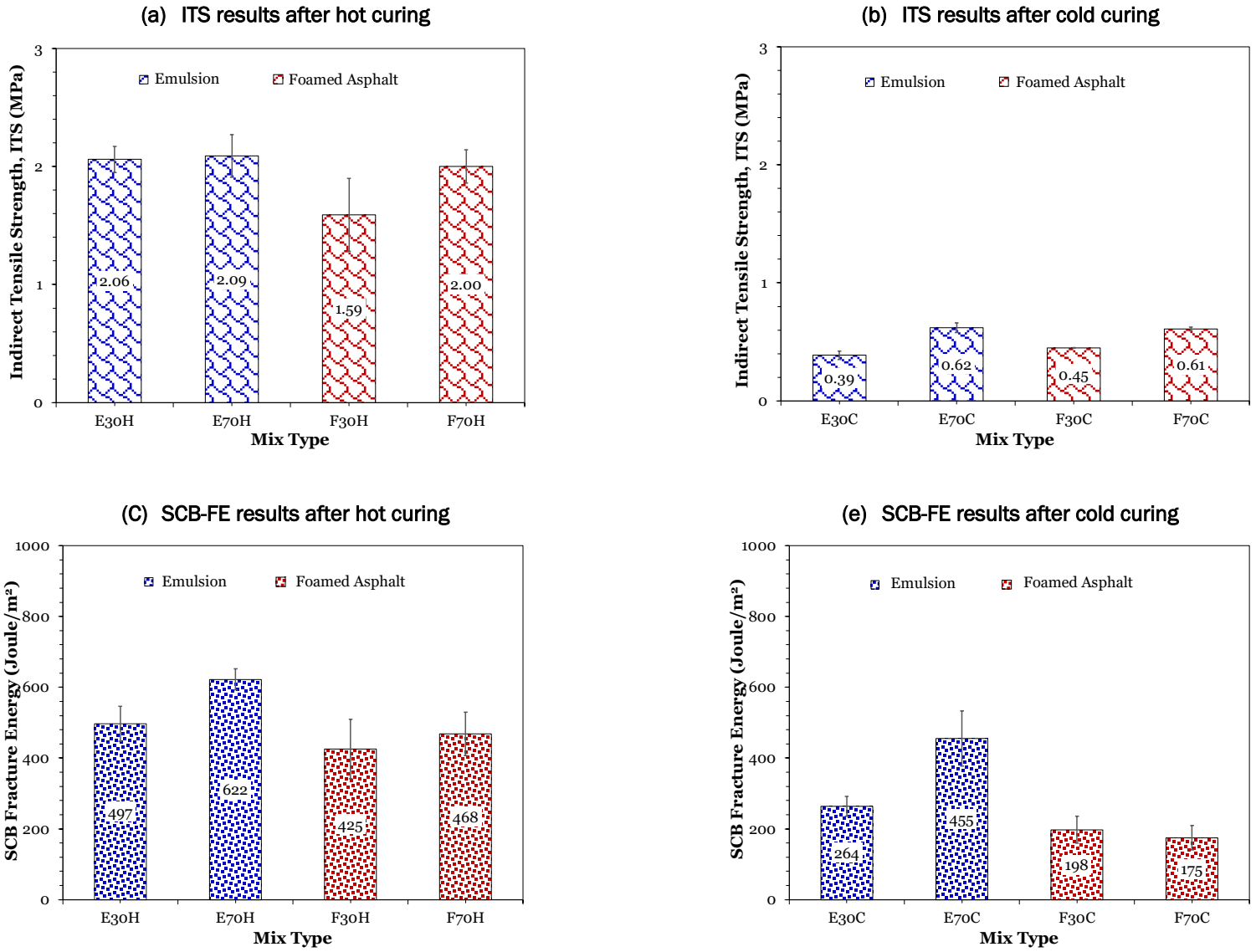

5.5.1 Compaction-level impact on performance (rutting and cracking)

Figures 28 and 29 illustrate the impact of compaction level on CIR rutting and cracking performances when the same bituminous additives and curing process are used in preparing mixes. As shown in Figure 28*a* and *b*, both emulsified and foamed asphalt CIR mixtures compacted at 30 gyrations had higher APA rut-depth values than those of CIR mixtures compacted at 70 gyrations. This observation was expected as higher compaction energy (i.e., 70 gyrations) results in "denser" (or having fewer voids) CIR mixes, which in turn leads to increased rutting resistance. Figure 28*c* and *d* presents $|E^*|$ results for all eight mixes. As the figure shows, mixes compacted at 70 gyrations and cold cured had similar $|E^*|$ value to those compacted at 30 gyrations and cold cured. Hot-cured mixes had mixed $|E^*|$ results (Figure 28*c*). These mixed observations may indicate that $|E^*|$ was not able to capture the impact of compaction effort on CIR mix performance. Thus, only APA results established a clear trend.

Figure 29 presents the results for cracking performance, grouping them by curing process. As Figure 29*a* and *b* shows, both emulsified and foamed asphalt CIR mixtures compacted at 70 gyrations presented slightly higher ITS values than those compacted at 30 gyrations. This indicates that compaction effort did impact cracking performance as measured using the ITS. In contrast, Figure 29*c* and *d* shows that both emulsified and foamed asphalt compacted at 70 gyrations exhibited significantly higher fracture energy than that for CIR mixtures compacted at 30 gyrations. This indicates that using higher compaction effort for CIR mixes, as expected, leads to better cracking resistance. This may also indicate that the ITS results were not able to capture this impact.

Figure 28. Performance-testing results highlighting the effect of compaction level on CIR rutting performance.

(a) APA rut-depth results after hot curing

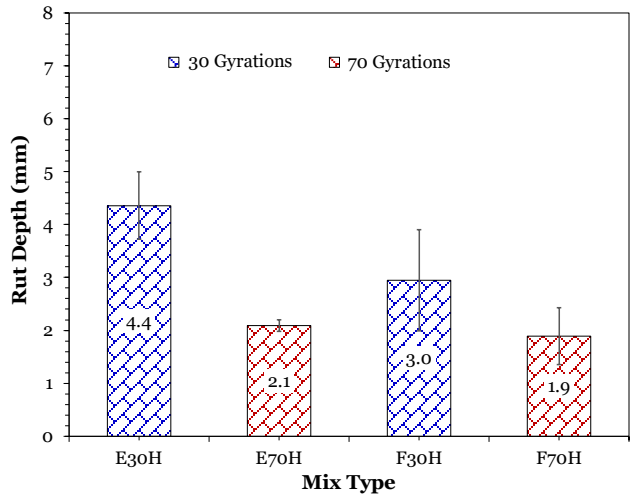

(b) APA rut-depth results after cold curing

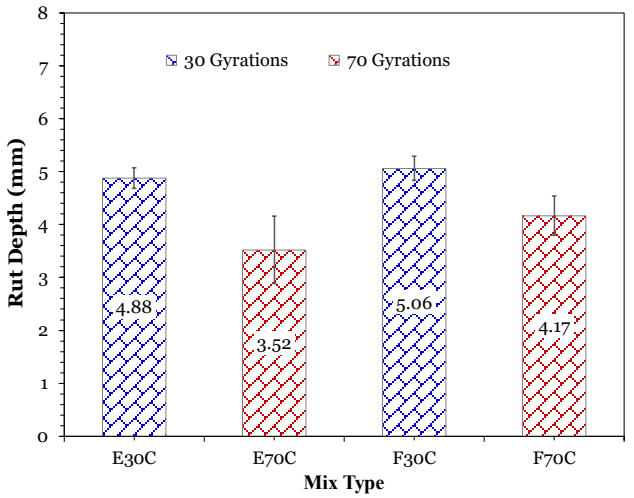

(c) |E*| results after hot curing

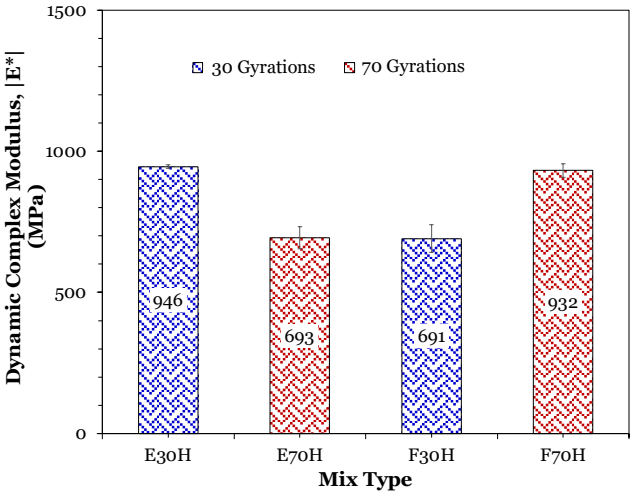

(d) |E*| results after cold curing

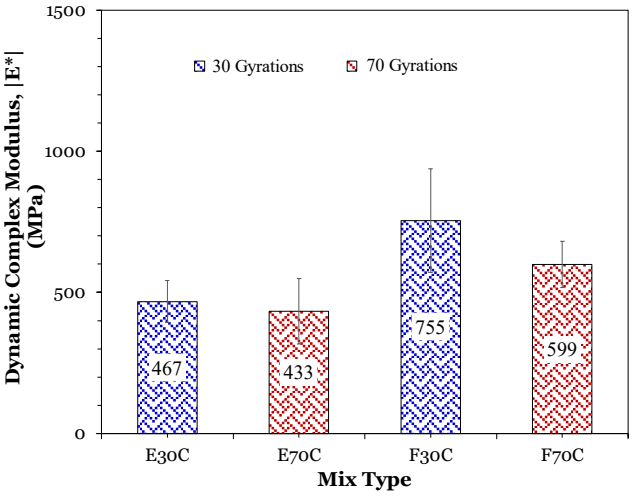

Figure 29. Performance-testing results highlighting the effect of compaction level on CIR cracking performance.

(a) ITS results after hot curing

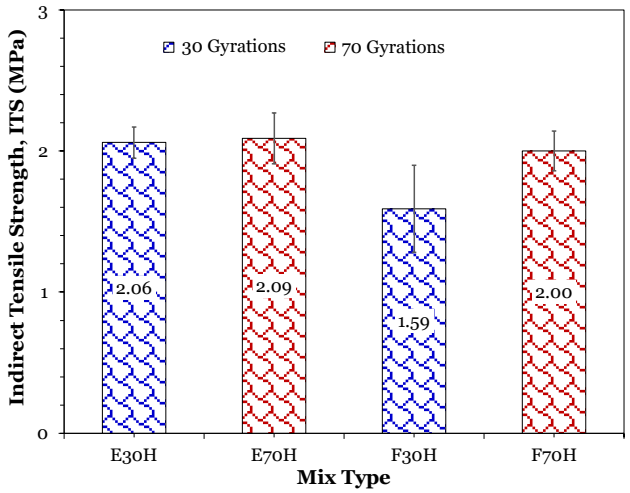

(b) ITS results after cold curing

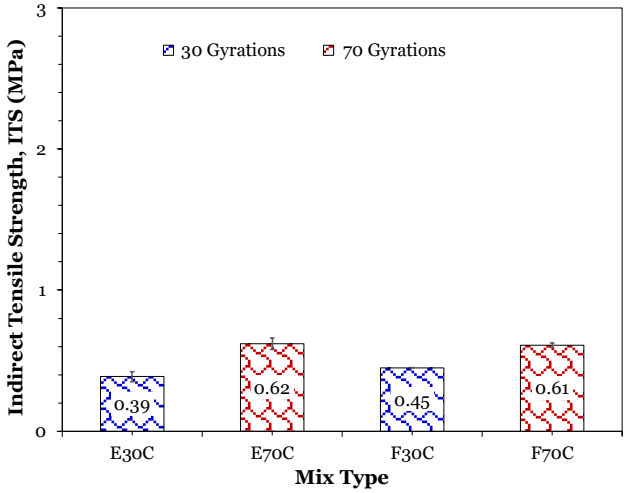

(c) SCB-FE results after hot curing

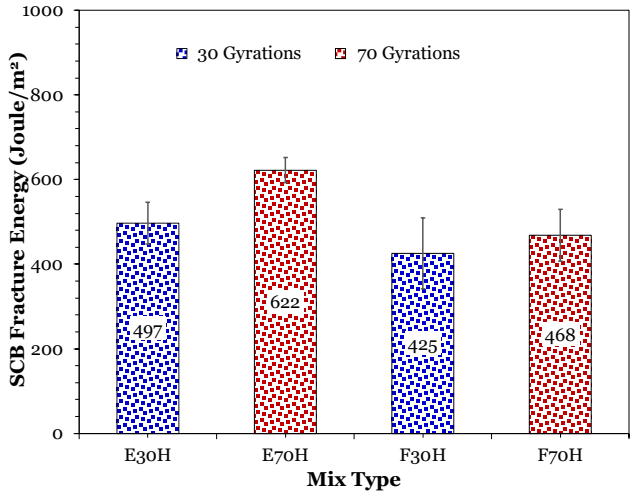

(a) SCB-FE results after cold curing

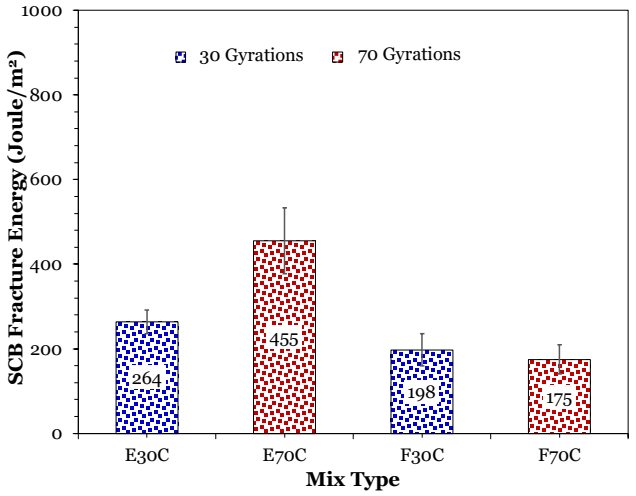

5.5.1 Impact of curing process on performance (rutting and cracking)

Figures 30 and 31 illustrate performance-testing results, highlighting the impact of curing process (i.e., hot vs. cold) on the performance of CIR mixtures, grouped by gyration level. As Figure 30*a* shows, CIR mixtures subjected to hot curing (at 140°F [60°C] for 3 days) had slightly lower rut-depth values than those subjected to cold curing (at 50°F [10°C] for 3 days). When the compaction effort is increased to 70 (Figure 30*b*), the impact of curing process is more pronounced on rutting resistance (approximately 80% lower rutting for hot-cured samples when compared to cold-cured samples). Therefore, curing CIR mixtures at high temperatures (or allowing them to cure for longer time) will lead to better rutting resistant mixtures. Figure 30*c* and *d* presents the $|E^*|$ testing results for all eight CIR mixtures, grouped by compaction effort. As Figure 30*c* illustrates, both emulsified and foamed asphalt CIR mixtures compacted using 30 gyrations had similar $|E^*|$ values at both curing conditions. When compacted at 70 gyrations (Figure 30*d*), hot-cured CIR mixtures had higher $|E^*|$ than those cold cured.

Figure 31 presents cracking test results for all eight CIR mixtures, grouped by gyration level. As Figure 31*a* shows, the ITS values for CIR mixtures subjected to hot curing were higher (by more than 300%) than those mixtures subjected to cold curing. This is regardless of the compaction effort used to prepare the samples. Similarly, hot-cured emulsified and foamed asphalt CIR mixes had higher fracture energy than those cold cured. These results indicate that the curing process affects the cracking performance of CIR mixtures and that hot curing (or allowing the mix to cure for a longer period of time if temperatures are low) leads to superior cracking performance. Overall, these observations were expected because the increase in curing temperature ensures that a CIR mix has gained more strength in a shorter period of time than that cured at a lower temperature for the same period of time.

Figure 30. Performance-testing results highlighting the effect of curing process on CIR rutting performance.

(a) APA rut-depth results at 30 gyrations

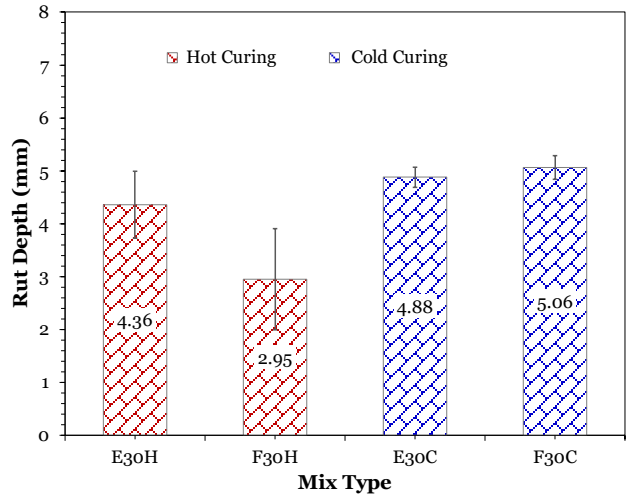

(b) APA rut-depth results at 70 gyrations

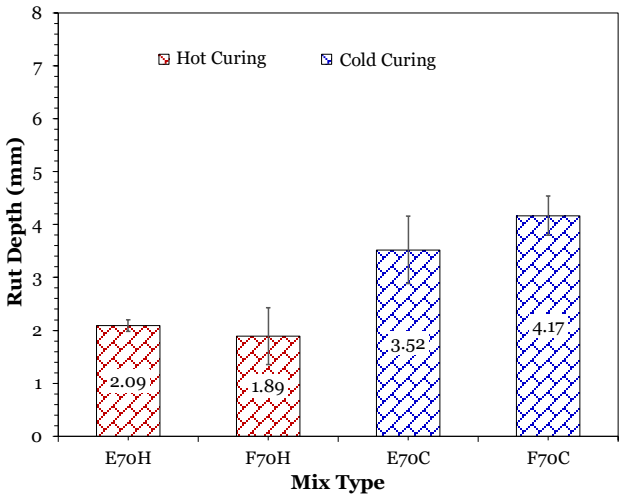

(c) |E*| results at 30 gyrations

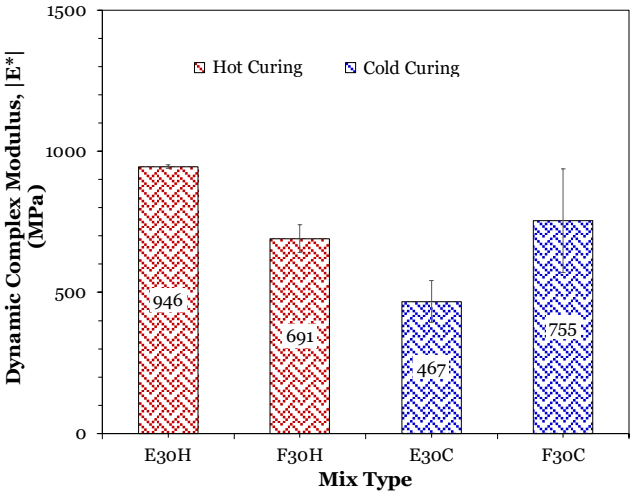

(d) |E*| results at 70 gyrations

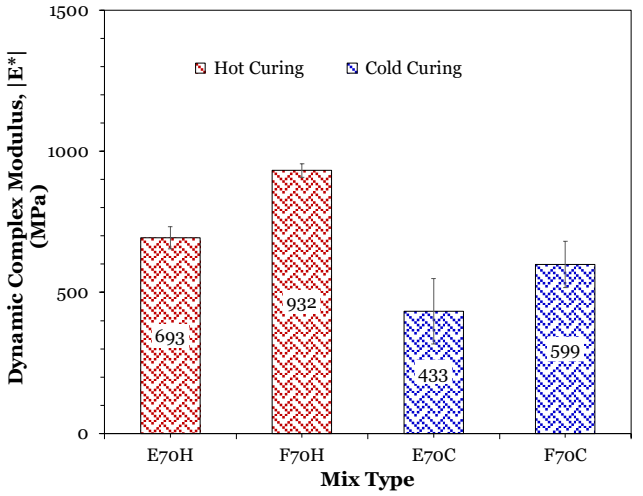

Figure 31. Performance-testing results highlighting the effect of curing process on CIR cracking performance.

(a) ITS results at 30 gyrations

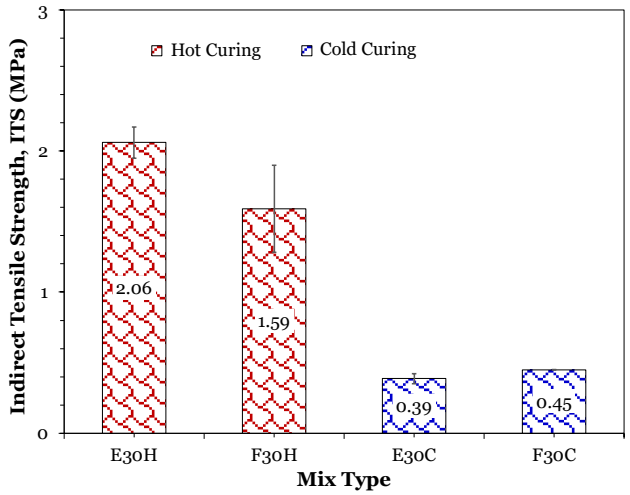

(b) ITS results at 70 gyrations

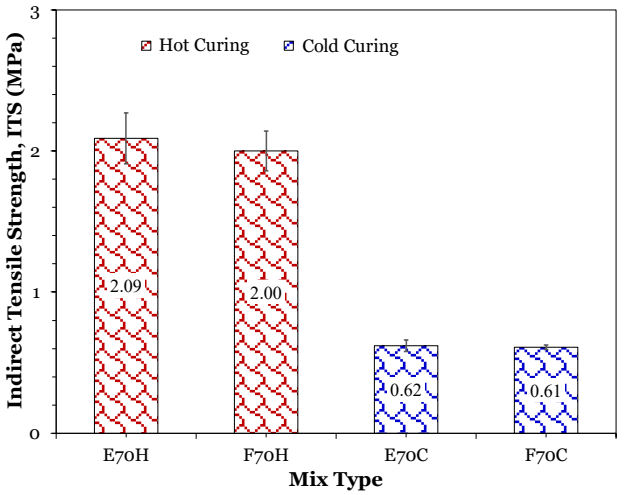

(c) SCB-FE results at 30 gyrations

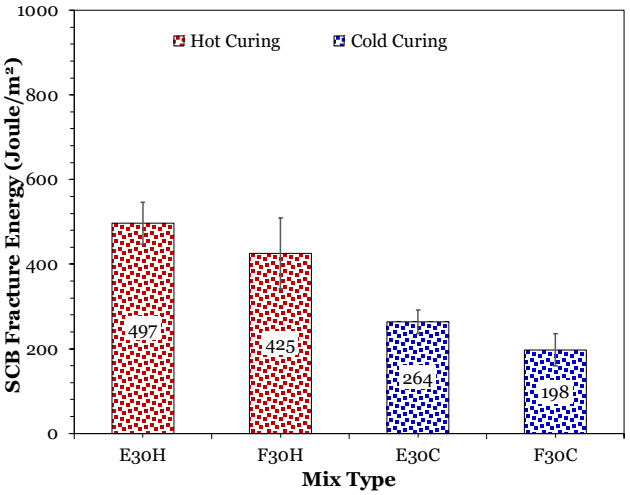

(d) SCB-FE results at 70 gyrations

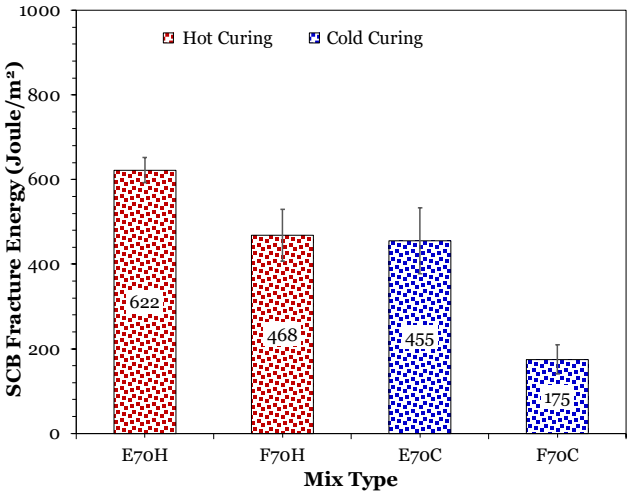

5.6 Statistical analyses

To further compare the difference between all eight CIR mixtures and to evaluate the impact of bituminous additives, compaction effort, and curing process on performance, ANOVA was conducted. Specifically, this study statistically compared the rutting and cracking testing results for all eight mixes to evaluate the effect of binding agent type, compaction level, and curing process on CIR performance. The interaction between these three factors (i.e., binder type, compaction level, and curing process) was also assessed to determine the significance of their impact on performance (i.e., *p*-value is less than 0.05). The following subsections discuss the results of the ANOVA for data from each performance test.

5.6.1 ANOVA results for APA rut-depth measurements

Table 12 presents ANOVA results obtained when comparing the difference in mean between the rut-depth measurements (APA test) for all eight CIR mixtures. None of the interactions between bituminous additives, compaction effort, and curing process were statistically significant. As Table 12 shows, only the compaction effort (number of gyrations applied to compact samples) had a significant impact on the rut-depth measurements (i.e., *p*-value of 0.017). These results also indicate that rut-depth measurements for foamed asphalt CIR mixes were statistically similar to those for emulsified asphalt CIR mixes, provided that both mixes were compacted using the same compaction effort. Curing process did not show a significant impact on APA rut-depth measurements for all eight mixes.

Table 12. ANOVA results comparing APA rut-depth measurements for all eight CIR mixtures.

Source	*F*-Statistic	*p*-Value
Binder	0.449	0.509
Gyration	6.563	0.017
Curing	1.177	0.289
Binder * Gyration	0.814	0.376
Binder * Curing	0.002	0.969
Gyration * Curing	0.131	0.721
Binder * Gyration * Curing	0.250	0.622

5.6.2 ANOVA results for dynamic complex modulus (|E*|) data

Table 13 presents the ANOVA results obtained when comparing the |E*| values measured at 54 C and 10 Hz loading frequency for all eight CIR mixtures considered in this study. As Table 13 shows, only the curing process had a statistically significant impact (i.e., *p*-value of 0.033) on measured |E*| values, further validating the observation that hot curing leads to CIR mixes with higher stiffness and ultimately better rutting resistance. These results (Table 13) also indicate that |E*| measurements for foamed asphalt CIR mixes were statistically similar to those for emulsified asphalt CIR mixes, provided that both mixes were cured using the same curing process (i.e., either hot curing or cold curing). Compaction effort and other interaction effects between factors did not have a significant impact on measured |E*| values.

Table 13. ANOVA comparing |E*| values measured at 54 °C and 10 Hz loading frequency for all eight CIR mixtures.

Source	*F*-Statistic	*p*-Value
Binder	0.900	0.371
Gyration	0.600	0.813
Curing	6.580	0.033
Binder * Gyration	0.330	0.577
Binder * Curing	0.490	0.501
Gyration * Curing	0.690	0.428
Binder * Gyration * Curing	1.437	0.265

5.6.3 ANOVA results for ITS measurements

Table 14 presents the ANOVA results obtained when comparing the ITS values for all eight CIR mixtures. As Table 14 shows, both compaction effort and curing process had a statistically significant impact (i.e., *p*-values of 0.002 and 0.000, respectively) on measured ITS values. These results (Table 14) also indicate that ITS measurements (or cracking resistance) for foamed asphalt CIR mixes were statistically similar to those for emulsified asphalt CIR mixes, provided that mixes were compacted and cured using the same compaction effort and curing process. The results also suggest that curing and compaction effort significantly affect the cracking resistance of CIR mixtures. Bituminous additives and other interaction effects between factors did not have a significant impact on measured |E*| values.

Table 14. ANOVA analysis on ITS measure.

Source	*F*-Statistic	*p*-Value
Binder	0.037	0.849
Gyration	11.660	0.002
Curing	220.54	0.000
Binder * Gyration	0.001	0.981
Binder * Curing	0.596	0.448
Gyration * Curing	1.958	0.175
Binder * Gyration * Curing	0.082	0.777

5.6.4 ANOVA results for semicircular bend fracture energy data

Table 15 presents the ANOVA results for comparing SCB-FE measurements for all eight CIR mixtures. All factors (bituminous additive type, compaction level, and curing process) are statistically significant (i.e., *p*-values of 0.011, 0.027, and 0.000, respectively). These results indicate that bituminous additives, compaction effort, and curing process have a significant impact on the cracking resistance of CIR mixtures. Therefore, these factors should be considered when designing and using CIR mixtures for rehabilitating deteriorated flexible pavements. In addition, the ANOVA results suggest that the SCB-FE test was more capable of differentiating between the cracking performance of CIR mixes than was the ITS. As a result, the SCB-FE test may be more suitable than ITS for conducting BMD of CIR mixes. All other two-way and three-way interactions were insignificant (Table 15).

Table 15. ANOVA analysis on SCB-FE measure.

Source	*F*-Statistic	*p*-Value
Binder	7.620	0.011
Gyration	5.561	0.027
Curing	25.942	0.000
Binder * Gyration	1.284	0.268
Binder * Curing	2.094	0.161
Gyration * Curing	0.001	0.974
Binder * Gyration * Curing	0.775	0.387

6 Construction and Accelerated Testing of Full-Scale CIR Pavement Sections

This chapter discusses three full-scale CIR pavement sections constructed at RUAPTF located at the Center for Research and Education in Advanced Transportation Engineering Systems (CREATEs). The sections were constructed to evaluate field performance under full-scale accelerated pavement loading and to assess the impact of varying binder content on the performance of CIR full-scale pavement sections. Analyses of all full-scale testing results are also presented as part of this chapter.

6.1 Description of constructed CIR sections

This study constructed three full-scale CIR pavement sections in April 2019 at the RUAPTF. The CIR mixes for these sections were selected based on findings from the laboratory BMDs conducted as part of chapter 4. Specifically, one CIR section was constructed using a "CIR4%FAC" CIR mix (i.e., containing 4% bituminous additives content), one section used a "CIR3%FAC" CIR mix (i.e., containing 3% bituminous additives content), and a third section used a "CIR2%FAC" CIR mix (i.e., containing 2% bituminous additives content). All CIR mixes were produced using foamed asphalt binder (foamed neat PG 64-22) and without adding cement. While the intention was to add 1% cement to the CIR mix as in the laboratory design, no cement was added to the mix due to a miscommunication with the contractor. Details of the three mixes are as follows:

A. CIR4%FAC section:
   a. Binder type: neat PG 64-22 foamed asphalt
   b. Target binder content: 4% by total mix weight
   c. Cement content: 0% by total mix weight
   d. Target total added water: 3.1% (3% by mix weight and 2.5% by foamed asphalt weight)
   e. Strength: minimum 145 psi (1 Mpa) ITS

B. CIR3%FAC section:
   a. Binder type: neat PG 64-22 foamed asphalt
   b. Target binder content: 3% by total mix weight
   c. Cement content: 0% by total mix weight
   d. Target total added water: 3.1% (3% by mix weight and 2.5% by foamed asphalt weight)
   e. Strength: minimum 145 psi (1 Mpa) ITS

C. CIR2%FAC section:
   a. Binder type: neat PG 64-22 foamed asphalt
   b. Target binder content: 2% by total mix weight
   c. Cement content: 0% by total mix weight
   d. Target total added water: 3.1% (3% by mix weight and 2.5% by foamed asphalt weight)
   e. Strength: minimum 145 psi (1 Mpa) ITS

Figure 32 presents the location in RUAPTF (Figure 32*a*) and the pavement structure of the CIR pavement sections (Figure 32*b*). The CIR sections were constructed in a 225 ft (68.6 m) long by 12 ft (3.7 m) wide lane at RUAPTF. The structure of the pavement sections is as follows (from the top down):

1. 1 in. (25 mm) of a 4.75 mm nominal maximum aggregate size high-performance thin overlay (HPTO) mix
2. CIR layer (the next paragraph describes this further)
3. A 0.5 in. (12.5 mm) thin layer of the old HMA pavement
4. A 16 in. (406 mm) New Jersey DOT–designated I-3 subbase layer consisting of 4.75 mm nominal maximum aggregate size with a gradation ranging between 100% and 30% passing
5. A 12 in. (304 mm) layer of compacted soil
6. Natural soil

Each test section was 60 ft (18.3 m) long by 12 ft (3.7 m) wide with two approximately 20 ft (6.1 m) transition areas between the sections. A paving contractor (from New York State) constructed all sections by using a single-unit CIR train by first milling approximately 4 in. (0.1 m) of the existing surface HMA layer (Figure 32*b*). Then, millings were mixed with water and foamed asphalt (at the desired dosage) to produce CIR mixes, which were then dumped over into a paver. Finally, the CIR layer for each section was placed and compacted using vibratory and roller compactors. To facilitate continuous operations of the milling and mixing machine without interruptions, foamed asphalt binder was used as the only CIR bituminous additive. This eliminated the need to stop operations for switching binder tanks and cleaning the equipment. This was also necessary since the length of the lane was "short" relative to typical distances used to reach the target bituminous additives contents for CIR mixes during actual field CIR construction. The transition areas between the sections were necessary for the contractor to reduce the binder content of the CIR mix from 4% to 3%

and from 3% to 2%. As noted earlier, no portland cement or virgin aggregates were added when constructing each of the three sections. However, this study evaluates the minimum performance of CIR pavements designed when cementitious additives are not added (e.g., portland cement and lime slurry).

Figure 32. Location and pavement structure of all three CIR sections.

(a) Locations of CIR sections

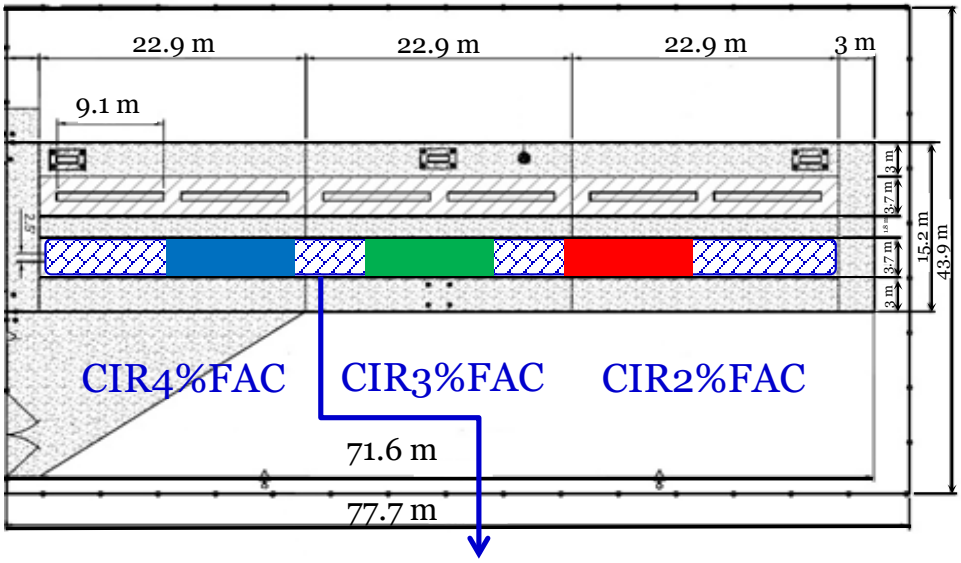

RUAPTF Lane in which CIR sections were constructed
68.6 m long

(b) Pavement structures

During construction of the sections (after the paver placed the CIR mixes and before roller compaction), the CREATEs team installed pavement sensors in each section. As Figure 33 shows, two pressure cells, four asphalt strain gauges, and three thermocouples were placed at the bottom of each CIR layer. The strain gauges were installed in both longitudinal (in direction of loading) and transverse directions. All sensors survived the construction phase except for one pressure cell located in the CIR2%FAC CIR section. Once all instruments were placed and the CIR sections were compacted, the mixes were allowed to cure for 2 weeks, after which a 1 in. (25 mm) thick layer of a standard New Jersey HMA mix was placed, also known as HPTO.

Figure 33. Locations and types of pavement sensors placed in the full-scale CIR sections constructed at CREATEs.

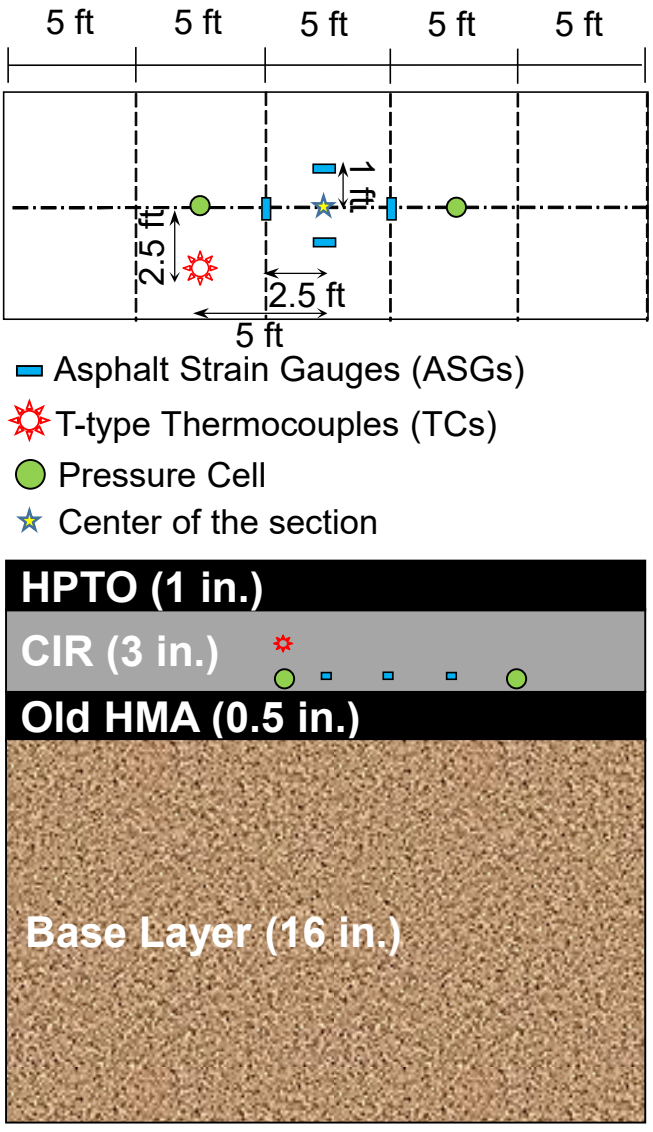

It is important to also mention that, for quality control purposes, CREATEs' team collected loose CIR mix samples during construction and cores from different locations in each test section(2 ft [0.6 m] from HVS wheel path) after construction. These materials were tested to determine the actual properties of the mixes used for constructing the CIR sections and to evaluate the differences in their laboratory performance. The following sections provide additional details.

6.2 Measured field densities and actual layer thicknesses

A nuclear density gauge was utilized after compaction of the CIR layers to measure as-constructed density (Table 16). Densities were measured at four randomly selected locations in each section. As Table 16 shows, densities for all sections ranged from a minimum of 96.3 lb/ft^3 (1,542 kg/m^3) to a maximum of 120.7 lb/ft^3 (1,930 kg/m^3). The average densities for each section, however, were similar (i.e., within 5.2 lb/ft^3 [83 kg/m^3]). While this is not similar to compaction trends observed in the lab (i.e., mixes with higher binder content had higher bulk densities), the similar average field densities for all three sections is mainly attributed to the inherent difference between lab and field compaction procedures.

After completing construction of the CIR sections (i.e., placement and compaction of a 1 in. [25 mm] thick HPTO layer), cores were taken from all three sections (outside of the load trafficking area) to determine the actual thicknesses of the CIR and HPTO layers. As shown in Table 16, the average thicknesses of the CIR layers for the CIR4%FAC, CIR3%FAC, and CIR2%FAC sections were approximately 2.9 in. (47 mm), 2.7 in. (69 mm), and 2.8 in.(71 mm), respectively. With a target CIR layer thickness of 3 in. (75 mm), the sections were constructed at a maximum of 0.3 in. (8 mm; CIR4%FAC section) less than the target thickness. As a result, the CIR layer thickness and overall pavement structure of each section is considered to be similar for field performance comparison reasons. Therefore, the only difference between the sections is the binder content.

Table 16. Field density measurements for all three CIR sections.

Section	Avg. Density (lb/ft³)	Section Avg. Density (lb/ft³)	Averaged CIR Layer Thickness (in.)
CIR2%FAC	115.1	113.33	2.83
	108.6		
	115.2		
	114.4		
CIR3%FAC	120.7	108.13	2.71
	113.9		
	96.3		
	101.6		
CIR4%FAC	111.4	112.93	2.88
	111.8		
	118.0		
	110.5		

6.3 Properties of field-produced CIR mixes

It is important to quantify the properties of the CIR mixes produced and placed for each of the three field CIR sections to make proper conclusions. For this reason, properties of the field-produced CIR mixes were determined. In particular, compactability (volumetric and air voids of compacted samples), water content, bituminous additives content, strength (using the ITS test), and rutting performance (using the APA test) were evaluated. The following subsections present the testing results.

6.3.1 Water and binder contents of field-produced CIR mixtures

Loose CIR mix samples collected from each full-scale section were tested to determine the amount of water used in producing the CIR mixes. For this reason, loose mix samples, on the day of constructing the three full-scale sections, were weighed in pans and placed in an oven to dry overnight until reaching a constant mass. The average estimated moisture content was approximately 4%. Note that all laboratory mixes were produced at 3% moisture content. The difference in water content may slightly affect performance due to its potential impact on the air voids of the samples (discussed in the previous subsection) and the longer time needed to cure the field mixes.

In addition to testing the water content of the CIR mixes, another important factor was to determine the actual binder content of the field CIR

mixes. As a result, the research team conducted binder extraction and recovery, according to AASHTO T 111 and T 319, to determine the binder content of the three CIR mixes (AASHTO 2011, 2008). Table 17 presents the mineral matter and binder content percentages in each of the mixes. As the table shows, although the binder contents were at most 0.35% lower than targeted binder contents, the average difference in binder contents between the sections was still around 1%. This indicates that the sections were successfully constructed as the binder contents used were within acceptable field construction ranges (i.e., within ±0.5% of target binder contents).

Table 17. Extraction and recovery analysis.

CIR Sections	Mineral Matter (%)	Binder Content (%)	Target Binder Content (%)
CIR2%FAC	0.54	1.81	2.00
CIR3%FAC	0.65	2.65	3.00
CIR4%FAC	0.57	3.76	4.00

6.3.2 Compactability and volumetric properties

Loose mix samples collected during the construction of the CIR sections were compacted using an SGC to prepare samples for ITS and APA performance testing. The samples were compacted using 30 gyrations and were allowed to cure for 3 days at 140°F (60°C). Separately, the obtained cores from each section were cut from both sides to the thickness required for APA and ITS tests, 3 in. (75 mm) and 2.5 in. (63 mm), respectively. Bulk specific gravity (G_{mb}) was determined using the CoreLok device (AASHTO T 331 [AASHTO 2013]). Loose CIR mix samples were also tested to determine their maximum theoretical specific gravity (G_{mm}) by using the CoreLok device (ASTM D6857 [ASTM 2018a]). Figure 34 presents the air voids of both field-produced mixes and cores for ITS and APA test specimens. As the figure shows, the ITS and APA field cores presented lower air-void levels than those of the field-produced, lab-compacted CIR specimens (within +4% max difference). In addition, as expected, air voids decreased with the increase in binder content for both CIR specimens. This drop in air voids could be due to (1) trimming cores from both sides and (2) compacting CIR mixtures during construction is different from the one in the lab.

Figure 34. Comparison of field cores and plant-produced, lab-compacted CIR mixes

(a) Air-void level determined for APA samples

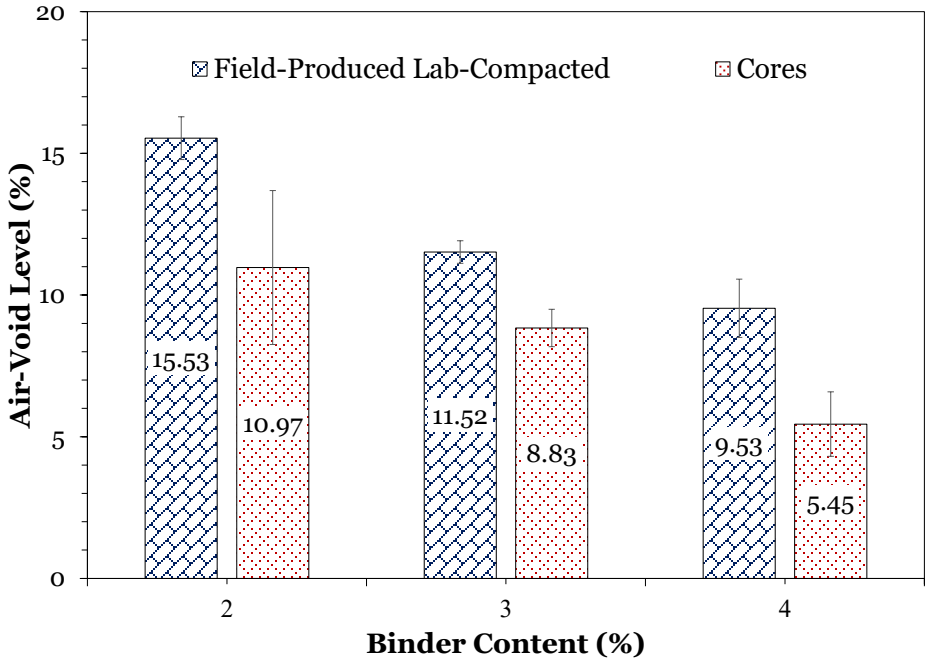

(b) Air-void level determined for ITS samples

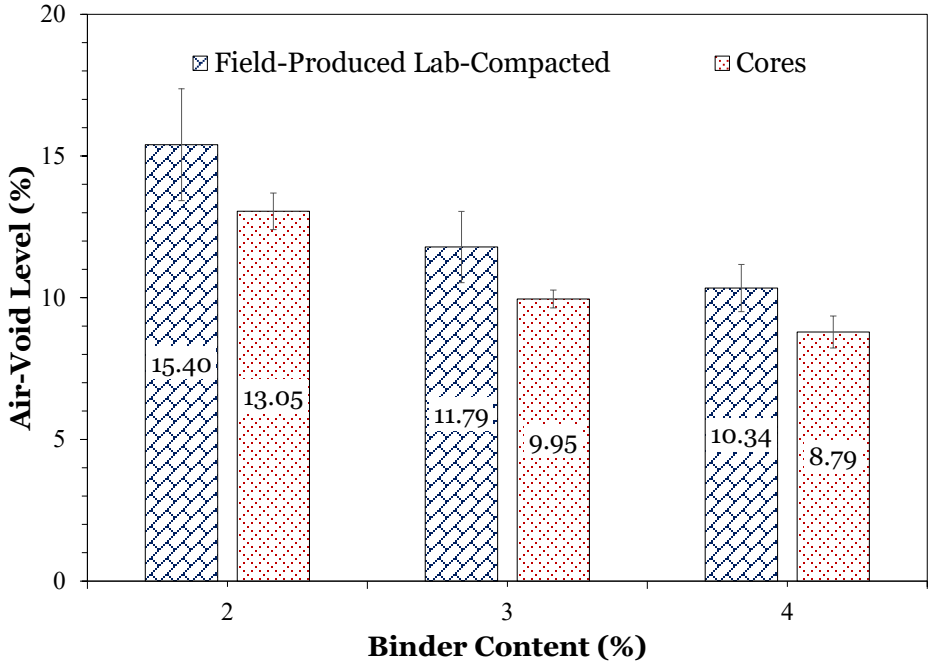

6.3.3 Performance of plant-produced, lab-compacted mixes

APA and IDT tests were conducted on the field cores and the plant-produced, lab-compacted CIR mixtures. Figure 35 shows that ITS values for both field cores and plant-produced, lab-compacted specimens increased with the increase of binder content. This observation falls in line with BMD results discussed in Chapter 4. Conversely, the average ITS values for the plant-produced, lab-compacted specimens were considerably higher than the ones of field cores (by more than 73 psi [0.5 Mpa]). This difference in ITS values could be due to the coring and trimming of CIR specimens, which in return may affect aggregate interlock of the CIR layer, thus, reducing its strength.

Alternately, Table 18 shows that all field-produced, lab-compacted APA samples for all three CIR mixes failed the APA test (i.e., reached more than 0.56 in. [14 mm] before 8,000 cycles). The cycles to failure were different for the different mixes (i.e., at different binder contents). Nonetheless, the number of cycles to failure showed a distinction between the rutting resistances of the field-produced CIR mixes. However, the CIR cores obtained from all the sections passed the APA test and exhibited better rutting resistance than that of field-produced, lab-compacted mixes. This difference in rutting performance between field-produced, lab-compacted samples and CIR cores could be due to the difference in air-void levels. Table 18 also shows that the CIR2%FAC mix (i.e., one with 2% binder content) failed after 6,800 cycles for field-produced compacted mixes and presented lower APA rut depth for CIR2%FAC cores, indicating that it was the most rut-resistant mix. The CIR3%FAC mix was in the middle, as expected, while the CIR4%FAC mix had the highest rutting susceptibility for both field-produced, lab-compacted mixes and CIR4%FAC cores. Despite that all the mixes presented higher rutting susceptibility compared to the balanced CIR mixes (chapter 5), which is probably due to the absence of cement, the resistance of these mixtures to rutting is still different. This means that the BMD approach can be used successfully to optimize the rutting resistances of field-produced CIR mixes.

Figure 35. ITS results for field-produced, lab-compacted CIR mixes and cores obtained from each section.

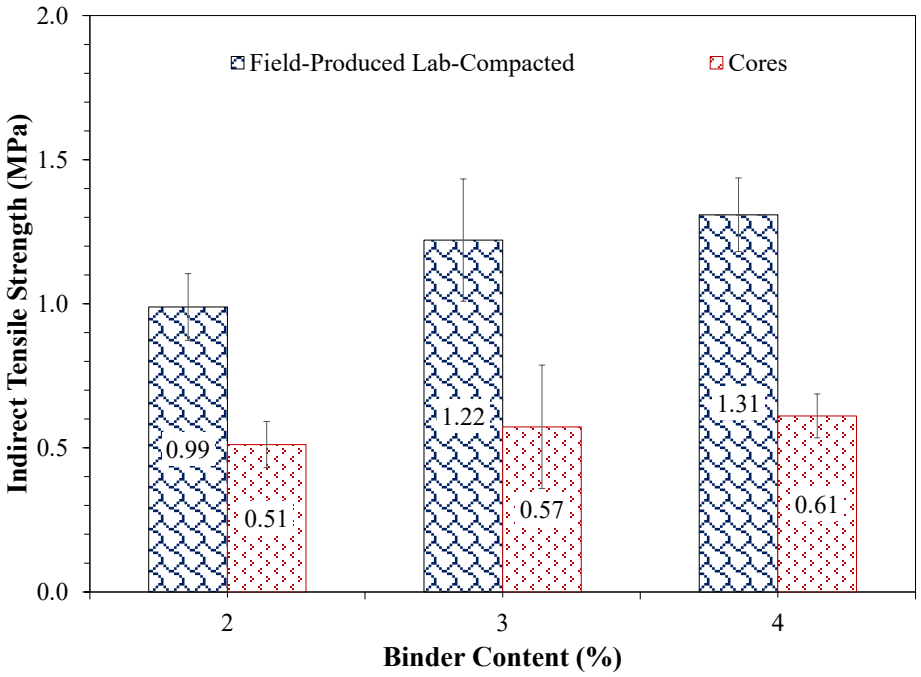

Table 18. APA cycles to failure for field-produced, lab-compacted CIR samples.

CIR Section	APA Rut Depth (mm)	
	Field-Produced, Lab-Compacted	Field Cores
CIR2%FAC	Failed at 6800	12.85
CIR3%FAC	Failed at 4100	13.35
CIR4%FAC	Failed at 2000	13.71

6.4 Testing program of full-scale CIR pavement sections

A testing program was prepared to evaluate the field performance of the three CIR sections constructed as part of this study. The program involved applying full-scale accelerated loading on each of the sections by using the HVS. Testing of the sections by using a heavy weight deflectometer (HWD) and laser profiler was also conducted to evaluate the integrity of the pavement structures and to quantify permanent deformation (rutting), respectively, due to the application of accelerated loading. In addition, the testing program involved collecting mechanistic responses (i.e., compressive stresses and tensile strains at the bottom of the CIR layer of each section) by using the embedded asphalt strain gauges and pressure cells. The following subsections provide additional details about each of the tests conducted.

6.4.1 Full-scale accelerated loading

An HVS was utilized to apply full-scale accelerated loading on each of the CIR sections constructed as part of this study. Loading was applied according to the following program:

- Loading mode: The HVS's wheel carriage applied a bidirectional loading on top of a pavement section without lifting the wheel, with a wheel wander of 8 in. (200 mm).
- Tire configuration: The first 150,000 loading passes were applied using a dual truck tire (115 psi [0.8 Mpa] tire pressure) placed on a single axle while the remaining loading until failure was applied using a single aircraft tire (Douglas DC-8 tire with 196 psi [1.4 Mpa] tire pressure).
- Loading magnitude: The loading magnitude applied using the truck-tire configurations was 9,000 lb (40 kN) whereas 22,500 lb (100 kN) were applied using the aircraft tire configurations.
- Air Temperature: The air temperature around each test section during the application of loading was maintained around 50°F (10°C).
- Failure Criteria: the application of accelerated loading was discontinued when the rut depth, measured using a laser profiler, reached 1 in. (25 mm) for any of the three CIR sections.

6.4.2 Structural integrity testing using a heavy weight deflectometer

An HWD was used to evaluate the impact of accelerated loading on moduli (or structural integrity; Figure 36*a*). For this reason, CREATEs' team conducted HWD testing before the application of accelerated loading and after completion of truck-tire and aircraft-tire loading phases. Testing was conducted at three locations within the HVS loaded area as shown in Figure 36*b*. Deflections were recorded and used to backcalculate the layer moduli values for each of the CIR sections. The impact of accelerated loading was then evaluated and contrasted for all of the three CIR sections.

Figure 36. Heavy weight deflectometer (HWD) and testing locations.

(a) HWD

(b) Location and direction of HWD testing

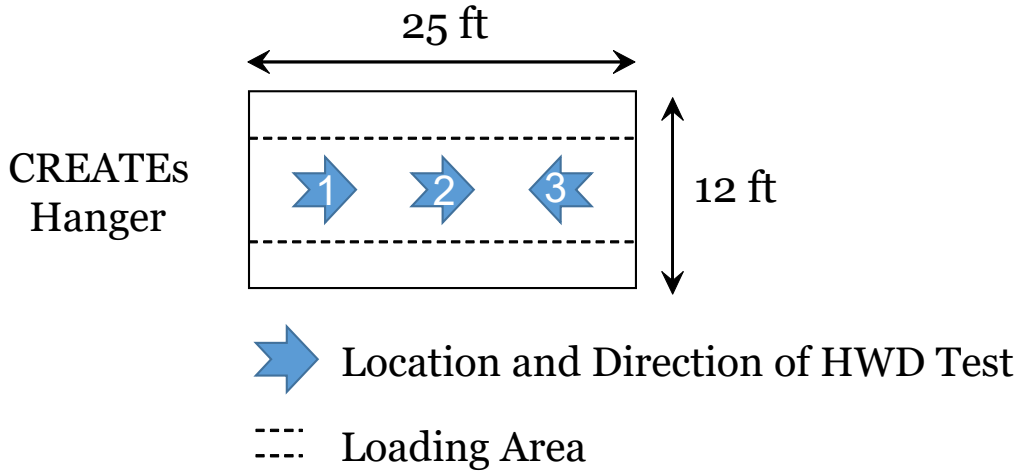

6.4.3 Quantification of rut depth and permanent deformation by using a laser profiler

The permanent deformation observed at the surface of the CIR sections was assessed using a laser profiler to determine the extent of rutting in each section due to the application of HVS loading. For this reason, sur-

face pavement profiles of each CIR section were measured every day, during the application of HVS loading, at three different locations (spaced 6 ft [1.8 m] away from the middle of a section as shown in Figure 37). The loading pass at which the HVS was stopped for taking the laser profile measurements was also recorded, allowing for the evaluation of rutting progression as full-scale loading was applied.

Figure 37b illustrates the approach used to compute the permanent deformation and rut depth at each pass. As the figure shows, the difference between the maximum measured depth (peak) and a flat reference line (determined based on profile depth measurements taken before the application of HVS loading, that is at zero loading cycles) is defined as the measured total rut depth after any particular number of loading passes applied. Comparing the total rut depth after truck and aircraft loading sequences facilitates evaluating the rutting performance of the various CIR sections as well as its sensitivity to the change of CIR mix binder content.

Figure 37. Location for measuring the transverse depth profiles and definition of rut-depth measurements.

(a) Locations of laser profiler testing

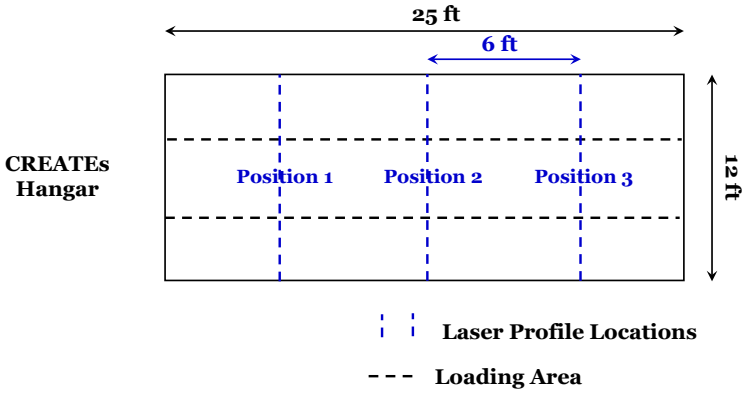

(b) Rut-depth definition

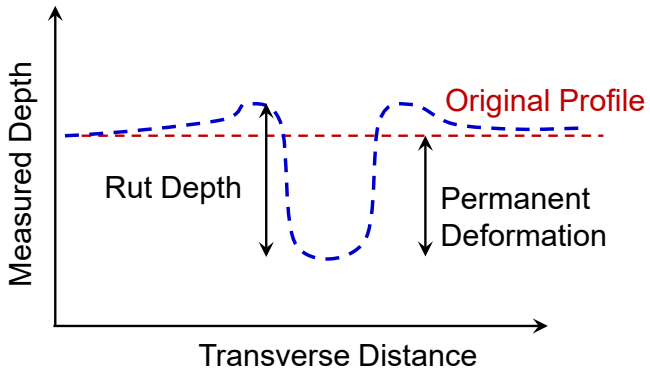

6.4.4 Mechanistic responses recorded from pavement instruments

The mechanistic responses (i.e., compressive stresses and tensile strains) were recorded during the application of HVS full-scale loading from the asphalt strain gauges and pressure cells. Temperature variations were also recorded using type T thermocouples. All measurements from the pavement sensors were collected at a frequency of 1,613 data points per pass from each sensor. Therefore, each sensor provided 6,000 data points in a period of 3.72 s of data recording. Note that data were collected after the application of 10 loading cycles (i.e., 20 bidirectional loading passes on top of a CIR section).

Figure 38 presents the locations and labels of the asphalt strain gauges and pressure cells. As the figure shows, a total of four asphalt strain gauges were placed in each section (two in the direction of loading, ASG1 and ASG2, and two in the transverse direction, ASG3 and ASG4). The tensile strains recorded from each of these sensors for each section were compared to assess the cracking resistance of each section. Similarly, two pressure cells were embedded in each CIR section (Figure 38) with measured peak compressive stresses compared to evaluate the rutting potential of each section. The temperature variations in each section were analyzed to evaluate the impact of temperature on mechanistic responses.

Figure 38. Plan view of instrumented CIR sections.

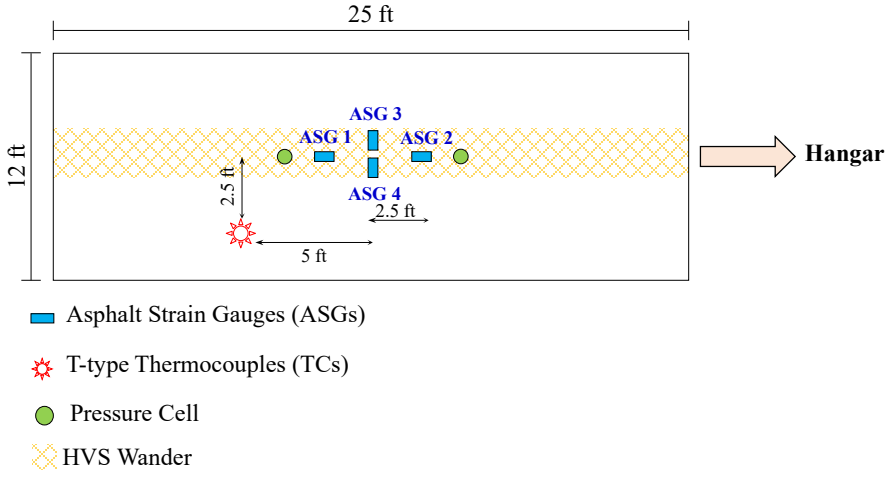

6.5 Discussion of full-scale testing results

6.5.1 Heavy weight deflectometer (HWD) results

Figure 39 presents the deflection basins obtained from HWD testing for all CIR sections before and after the application of HVS truck loading (i.e., 145,000 passes of 9,000 lb (40 kN) truck load) and aircraft loading (i.e., 50,000 passes of 22,500 lb (100 kN) aircraft load). Note that the maximum deflections were normalized to a plate load of 9,000 lb (40 kN) and a test temperature of 68°F (154°C)before and after HVS loading. This was necessary to ensure valid comparisons between the sections and to account for the impact of ambient temperatures during the time of testing (before and after testing was conducted, approximately 1–2 months apart).

As Figure 39*a*, *d*, and *g* shows, recorded deflections for the lower layers (geophones spaced 24 in. [610 mm] and more away from loading) of the CIR sections (below CIR layer) were relatively similar before and after the application of HVS truck loading. This was expected as the materials for all these lower layers in the CIR sections were similar (existing pavement section). This observation also suggests that the application of full-scale truck loading (40 kN; Figure 39*b*, *e*, and *h*) and full-scale aircraft loading (100 kN; Figure 39*c*, *f*, and *i*) using the HVS did not impact the integrity of these layers. For the case of the upper layers of the CIR sections, the deflection recorded (i.e., for geophones placed close to the load but not more than 10 in. away) were different for the different sections. For instance, the deflections directly under the HWD load (geophone located at location 0) and before the application of HVS loading for the CIR4%FAC section (Figure 39*g*) were higher than (by approximately 30 mil [0.8 mm] on average) the deflections at the same location for the other two sections. Similarly, Figure 39*d* shows that the deflections for the CIR3%FAC section were higher than the CIR2%FAC section (Figure 39*a*) for the CIR and HPTO layers of these sections. These observations suggest that before the application of HVS loading, the sections had different structural integrity with the weakest section being the CIR4%FAC section (i.e., the one that had highest deflections).

Figure 39*b*, *e*, and *h* shows that after application of truck loading, deflections in the upper layers (i.e., HPTO and CIR) for all three sections were reduced. The extent of reduction in deflections for the CIR4%FAC section (Figure 39*g* and *h*) was the highest (around 12 mil [0.3 mm] reduction in deflections in position 2), while both CIR2%FAC and CIR3%FAC sections presented similar reduction in deflections (up to 7 mil [0.18 mm] recorded

in position 2 of both sections). After the application of aircraft full-scale loading (Figure 39*c*, *f*, and *i*), little to no reduction in deflections was observed in the upper layers for all the three CIR sections. The CIR4%FAC section presented the highest reduction in deflection after applying aircraft accelerated loading (reduced by about 3 mil [0.08 mm] at both positions 1 and 3), while both CIR2%FAC and CIR3%FAC sections presented similar reduction in deflections (less than 2 mil [0.05 mm]). These results from both truck and aircraft full-scale testing suggest that all the CIR sections presented relatively similar deflection values before and after the application of accelerated truck and aircraft loading.

In addition to the recorded deflection data, the research team backcalculated layer moduli values for the different layers in each CIR section (Tables 19–21). The analyses were conducted on layers with the following seeded values:

- HPTO overlay (1 in. [25 mm], 947,000 psi [6,530 Mpa])
- A composite layer combining two layers: (1) the old HMA (0.5 in. [12.5 mm]) and (2) the CIR. The thickness of the CIR layer and the seeded moduli values varied depending on the CIR section:
  - CIR2%FAC section (2.83 in. [72 mm], 693,670 psi [4,783 Mpa])
  - CIR3%FAC section (2.71 in., 671,234 psi [4,628 Mpa])
  - CIR4%FAC section (2.88 in. [73 mm], 635,265 psi [4,380 Mpa])
- I-3 granular base (16 in. [406 mm], 15,000 psi [103 Mpa])
- Compacted soil (12 in. [304 mm], 10,000 psi [69 Mpa])
- Natural soil (semi-infinite, 10,000 psi [69 Mpa])

It is important to mention that both moduli for the HPTO and CIR layers were determined in the lab by using $|E^*|$ at 10 Hz and 70°F [21°C]. In addition, the modulus of the HPTO overlay was fixed during the backcalculation analysis to better capture the impact of accelerated loading on the stiffness of CIR layer at different asphalt contents (Tables 19–21).

As shown in Tables 19–21, the estimated CIR moduli of each section increased after performing HVS full-scale testing. In fact, after the application of accelerated truck loading, the stiffness of the CIR layer at the three positions of all the CIR sections increased by (a) 50,000 psi (325 Mpa) on average for the CIR2%FAC section, (b) 30,000 psi (207 Mpa) on average for the CIR3%FAC section, and (c) 20,000 psi (138 Mpa) on average for the CIR4%FAC section. Conversely, the estimated moduli of the lower layers did not show a significant change during HVS testing (change by

roughly 5,000 psi [35 Mpa]). After the application of accelerated aircraft loading, the backcalculated moduli of the CIR layer of all test sections increased considerably: (a) by 90,000 psi (620 Mpa) on average for the CIR2%FAC section, (b) by 118,000 psi (814 Mpa) on average for the CIR3%FAC section, and (c) by 270,000 psi (1,862 Mpa) on average for the CIR4%FAC section. Similar to the observations made from deflection basins, this suggests that compaction (or densification) of the upper layers of the CIR sections occurred due to repeated truck and aircraft loading at different positions for each CIR section.

Tables 19–21 show that the CIR3%FAC section had a higher CIR layer modulus (on average) than the other two CIR sections. This was the case before and after the application of accelerated truck loading. This was expected and is a direct result of the lower deflections measured for the CIR3%FAC section when compared to those recorded for the CIR4%FAC and CIR2%FAC sections, specifically in both positions 1 and 2. After the application of aircraft loading, the backcalculated moduli values of the CIR layer for the CIR4%FAC were higher than those of the CIR3%FAC section, which in turn presented higher estimated moduli than those of the CIR2%FAC section. These observations suggest that rate of the densification and compaction of the CIR layer due to repeated truck and aircraft loading seems to increase with the increase of the asphalt binder content of the CIR layer.

Alternately, Table 22 presents the estimated moduli for all the layers forming each CIR section, including the HPTO overlay, after applying the accelerated aircraft loading. The analyses of HWD deflections would help in understanding whether the manifested distresses (i.e., transverse cracks) originated from the CIR layer or from the HPTO layer. As Table 22 shows, the CIR2%FAC section presented estimated moduli of the HPTO layer lower than those of both CIR3%FAC and CIR4%FAC sections. In addition, the CIR layer estimated modulus for the CIR4%FAC section was higher (by more than 200,000 psi [1,380 Mpa] in position 1 and 2) than that of the CIR3%FAC section. This suggested that the CIR4%FAC could be the best performing section when subjected to accelerated truck and aircraft loading. In fact, these observations were evidenced by performing a visual inspection for the three CIR sections, which indeed showed that the CIR2%FAC section, as well as the CIR3%FAC section, presented longitudinal cracks at the surface close to the HVS wheel path, particularly near position 2 (Figure 40).

Figure 39. Deflection basins from HWD testing for all CIR sections before and after the application of accelerated truck and aircraft loading.

(a) CIR2%FAC before HVS loading

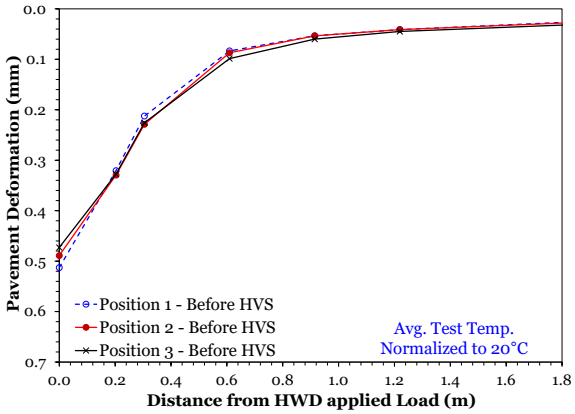

(b) CIR2%FAC after truck loading

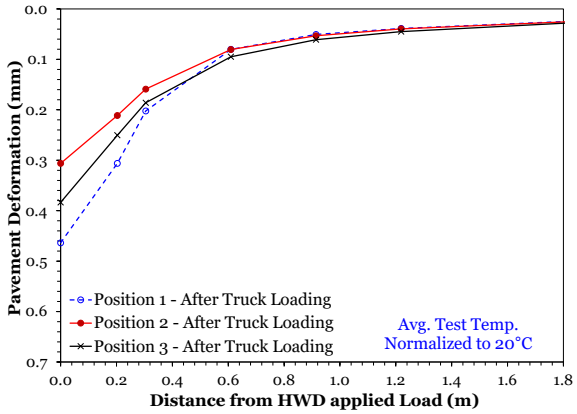

(c) ICIR2%FAC after aircraft loading

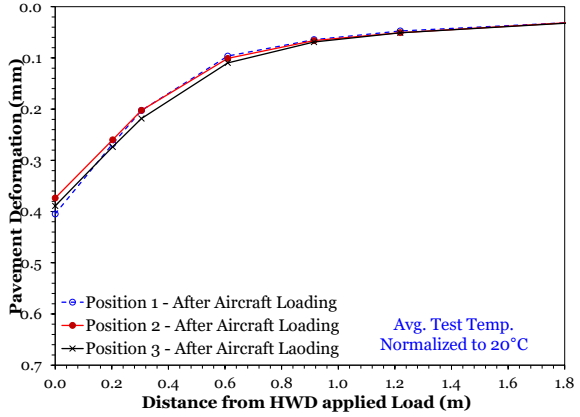

(d) CIR3%FAC before truck loading

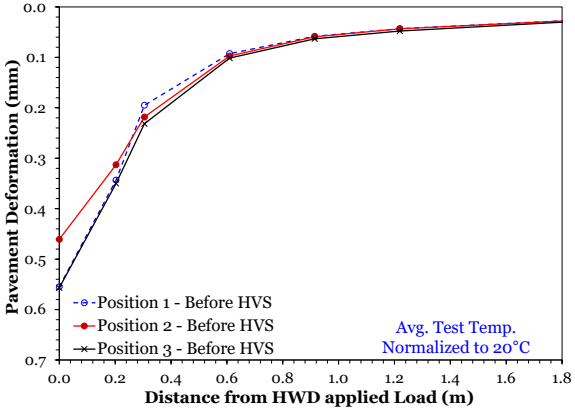

(e) ICIR3%FAC after truck loading

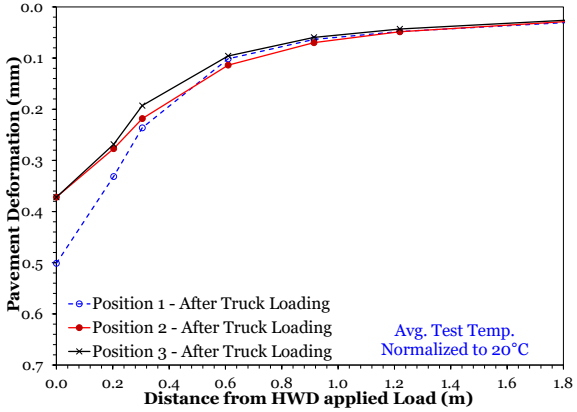

(f) CIR3%FAC after aircraft loading

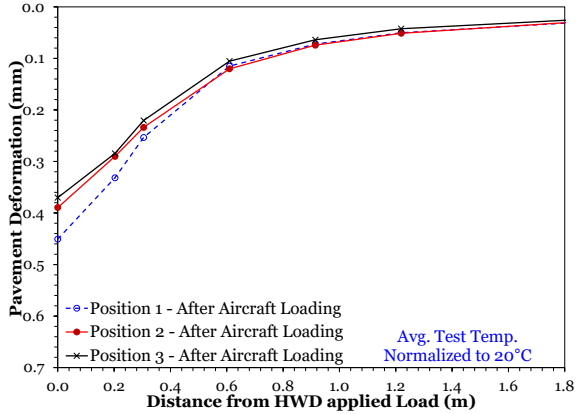

Figure 39 (cont.). Deflection basins from HWD testing for all CIR sections before and after the application of accelerated truck and aircraft loading.

(g) CIR4%FAC before HVS loading

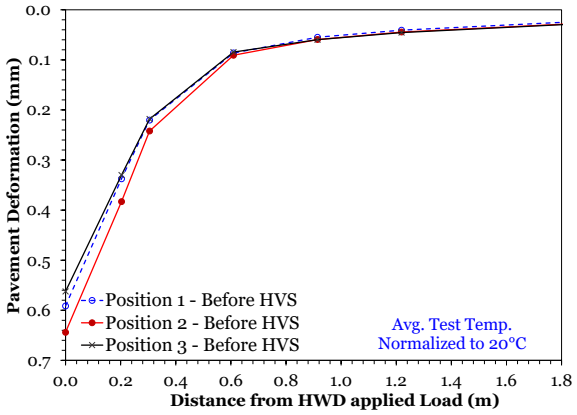

(h) CIR4%FAC after truck loading

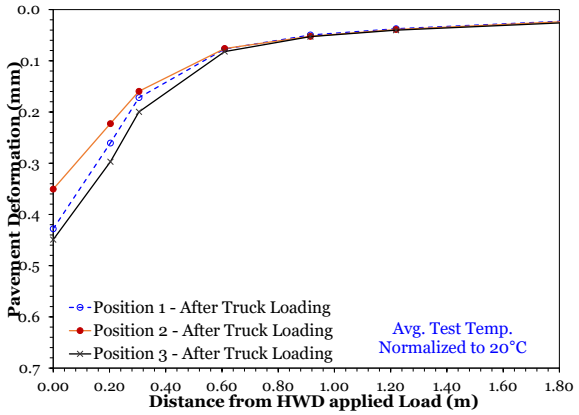

(i) CIR4%FAC after aircraft loading

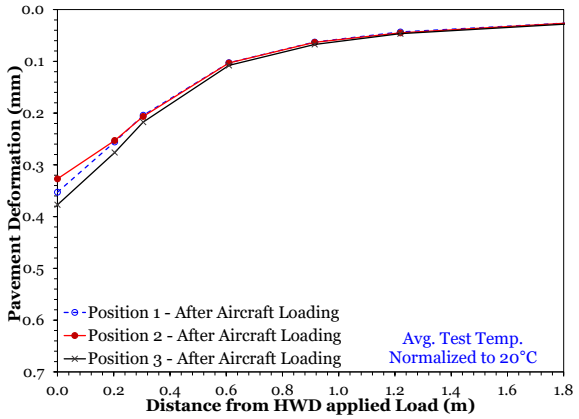

Table 19. Layer moduli values backcalculated for CIR2%FAC sections before and after full-scale accelerated loading.

Pavement Layer	Thickness (in.)	Seed Values (psi)	Est. Mod. Before HVS			Est. Mod. After Truck Loading			Est. Mod. After Aircraft Loading		
			Position 1	Position 2	Position 3	Position 1	Position 2	Position 3	Position 1	Position 2	Position 3
HPTO	1	947,000	947,000	947,000	947,000	947,000	947,000	947,000	947,000	947,000	947,000
CIR	2.83	693,670	35,004	69,597	43,414	63,006	107,573	70,715	162,573	171,887	225,003
HMA	0.5										
I-3 base	16	15,000	19,159	23,106	25,954	21,309	26,255	25,802	24,105	21,843	21,014
Compacted Soil	12	10,000	26,459	27,804	23,635	29,553	27,002	27,837	24,080	27,544	21,097
Natural soil	Semi-infinite	10,000	28,720	29,839	26,102	32,185	32,900	28,746	27,910	25,516	27,305

Table 20. Layer moduli values backcalculated for CIR3%FAC sections before and after full-scale accelerated loading.

Pavement Layer	Thickness (in.)	Seed Values (psi)	Est. Mod. Before HVS			Est. Mod. After Truck Loading			Est. Mod. After Aircraft Loading		
			Position 1	Position 2	Position 3	Position 1	Position 2	Position 3	Position 1	Position 2	Position 3
HPTO	1	947,000	947,000	947,000	947,000	947,000	947,000	947,000	947,000	947,000	947,000
CIR	2.71	671,234	66,258	57,315	46,945	93,124	116,772	102,567	162,263	223,216	282,315
HMA	0.5										
I-3 base	16	15,000	23,154	21,640	25,428	23,154	23,038	26,948	19,007	21,059	22,633
Compacted Soil	12	10,000	22,381	25,088	27,969	22,381	24,280	21,414	26,125	22,988	21,811
Natural soil	Semi-infinite	10,000	29,023	24,889	27,969	29,023	29,777	32,120	24,779	25,668	31,890

Figure 40. Visual inspection results for the three CIR sections after HVS-accelerated loading (longitudinal shots).

(a) CIR3%FAC section

(b) CIR4%FAC section

(c) ICIR2%FAC section

Table 21. Layer moduli values backcalculated for CIR4%FAC sections before and after full-scale accelerated loading.

Pavement Layer	Thickness (in.)	Seed Values (psi)	Est. Mod. Before HVS			Est. Mod. After Truck Loading			Est. Mod. After Aircraft Loading		
			Position 1	Position 2	Position 3	Position 1	Position 2	Position 3	Position 1	Position 2	Position 3
HPTO	1	947,000	947,000	947,000	947,000	947,000	947,000	947,000	947,000	947,000	947,000
CIR	2.88	635,265	35,067	41,045	34,621	43,086	62,343	55,850	305,729	433,927	230,029
HMA	0.5										
I-3 base	16	15,000	20,697	20,414	24,657	25,126	24,935	23,373	25,772	26,128	23,594
Soil Layer	10,000	10,000	30,437	28,561	26,544	30,130	34,459	31,124	30,213	31,380	25,669
Natural soil	Semi-infinite	10,000	30,115	29,141	27,495	35,826	33,036	30,464	31,703	29,108	30,167

Table 22. Layer moduli values backcalculated for CIR sections after the application of accelerated aircraft loading.

Pavement Layer	Seed Values (psi)	Est. Mod. Before HVS			Est. Mod. After Truck Loading			Est. Mod. After Aircraft Loading		
		Position 1	Position 2	Position 3	Position 1	Position 2	Position 3	Position 1	Position 2	Position 3
HPTO	947,000	195,068	176,157	343,510	346,253	498,488	589,750	483,798	505,016	451,390
CIR	635,265	241,929	452,680	818,213	263,041	258,841	259,855	505,059	678,951	328,576
HMA										
I-3 base	15,000	23,866	25,879	21,656	16,495	19,760	25,756	18,764	27,171	21,376
Soil Layer	10,000	26,694	24,904	20,862	28,190	22,550	27,109	27,212	23,765	23,661
Natural soil	Semi-infinite	27,789	26,004	24,493	25,067	24,066	23,653	29,085	29,267	26,821

6.5.2 Permanent deformation and rutting

Figure 41 presents the transverse profiles for all three CIR sections as HVS loading progressed. As Figure 41*a–c* shows, the average maximum rutting observed for the CIR2%FAC section is approximately 0.23 in. (5.78 mm) with an average value of permanent deformation of 0.28 in. (7.18 mm) after the application of 150,000 HVS truck loading passes. Figure 41*d–f* shows that the CIR3%FAC section had an average maximum rutting of 0.33 in. (or 8.34 mm.) with rut-depth values of 0.34 in. (8.61 mm) on average. Figure 41*g–I* shows that the average maximum rutting, as well as the average rut depth, observed for the CIR4%FAC section was approximately 0.29 in. (or 7.3 mm).

These results show that both CIR3%FAC and CIR4%FAC sections presented relatively similar rutting performance (i.e., difference in average rutting is 0.04 in. [1 mm]). However, the rutting resistance for the CIR2%FAC section is slightly better than that of the CIR4%FAC and CIR3%FAC sections (i.e., average rutting is less by 0.11 in. [2.8 mm] than that of the CIR3%FAC section and less by 0.07 in. [1.78 mm] than that of the CIR4%FAC section). In addition, both accumulated rut-depth and permanent-deformation values were similar for all the CIR sections. This may indicate that the accelerated truck loading (i.e., 9,000 lb (40 kN) for 150,000 passes) did not cause a significant shear flow on the surface of the CIR sections. It is also important to mention that both accumulated rut-depth and permanent-deformation values are less than the rutting threshold for asphalt highways, which is 0.5 in. (12.5 mm). Despite these three sections having about 1% difference in the binder content of the CIR mixes, the similar rutting performance for the CIR3%FAC and CIR4%FAC sections with a slightly better rutting resistance for the CIR2%FAC section is likely due to the similar field densities recorded for these sections. Therefore, the binder content of the CIR layer mix may not have been a critical factor defining the rutting performance of CIR layers in the field at truck loading magnitudes (i.e., 9,000 lb [40 kN] in this case).

After the application of aircraft loading, as illustrated in Figure 42, the permanent deformation measured for each CIR section significantly increased and passed the failure criteria of 1 in. (25 mm) before completing 11,000 HVS passes. In fact, the CIR2%FAC section unexpectedly presented the highest rut-depth values as Figure 42*a–c* shows (average maximum rutting of 1.59 in. [40.4 mm]). As shown in Figure 42*d–I*, both CIR3%FAC and CIR4%FAC sections presented relatively similar rutting performance after applying aircraft loading (approximately 1.39 in. [35.2 mm] for the

CIR3%FAC section and 1.30 in. [33.1 mm] for the CIR4%FAC section). This suggests that there may be a minimum binder threshold where the material behaves more like an unbound layer rather than a bound CIR layer (e.g., CIR2%FAC section) under accelerated aircraft loading. In addition, the average rut depth measured for the three CIR sections presented a significant increase compared to the ones measured during accelerated truck loading. In fact, the average rut-depth values were 2.01 in. (51.3 mm) for the CIR2%FAC section, 1.85 in. (47.1 mm) for the CIR3%FAC section, and 1.78 in. (45.3 mm) for the CIR4%FAC section. This suggests that the accelerated aircraft loading (i.e., 100 kN) may cause large shear forces on the pavement surface. Indeed, these results show that both accumulated permanent-deformation and rut-depth values are not within the rutting threshold for airfields, which is 1 in. (25 mm). Figure 43 compares the surface depression (rut) obtained after application of truck- and aircraft-accelerated loading on CIR sections.

To validate the measurements of the laser profiler, the research team performed a forensic investigation at the three locations of the CIR sections where the rut measurements were taken (Figure 37*a*). This investigation consisted of cutting 6 in. (152 mm) deep and 10 in. (254 mm) wide pavement trenches at each location to better determine the actual rutting performance of the CIR layer (below the 1 in. [25 mm] HPTO). Figure 44 illustrates an example of a trench taken from location 1 of the CIR3%FAC section. It is important to note that the rut-depth measurements of the overlay and the CIR layers were taken in place and not from the trenches. Table 23 presents the forensic investigation results for the three CIR sections at three locations after the application of accelerated aircraft loading. As Table 23 shows, the permanent deformation measured for the overlay after the application of aircraft loading is relatively similar for the three CIR sections (about 0.35 in. [9 mm] on average). However, the CIR layer of the three CIR sections exhibited considerably more rutting than the HPTO overlay (by more than 100%). In fact, the CIR layer of the CIR2%FAC section presented higher rutting values (0.9 in. [23.4 mm]), followed by that of the CIR3%FAC section (0.75 in. [19.1 mm] on average) and that of the CIR4%FAC section (0.7 in. [17.5 mm] on average). Conversely, the old HMA layer of the three CIR sections exhibited less rutting than the upper layers (less than 0.3 in. [8 mm]). Based on the forensic investigation results, the CIR layer contributes more than 50% of the total measured permanent deformation for all the CIR sections. In addition, as observed by the laser profiler results, the permanent deformation measured at CIR2%FAC for the CIR layer was the highest among all the sections.

Figure 41. Transverse depth profiles for all CIR Sections after the application of truck full-scale accelerated loading.

(a) CIR2%FAC Position 1

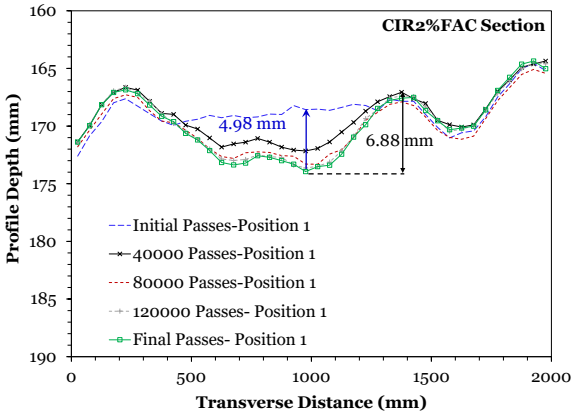

(b) CIR2%FAC Position 2

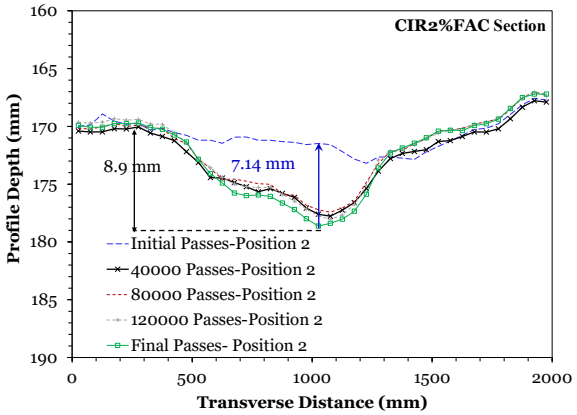

(c) ICIR2%FAC Position 3

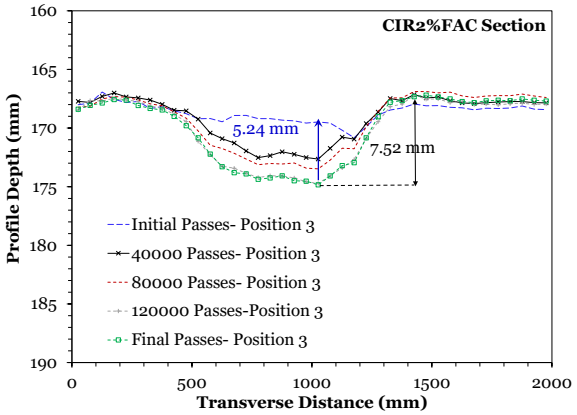

(d) CIR3%FAC Position 1

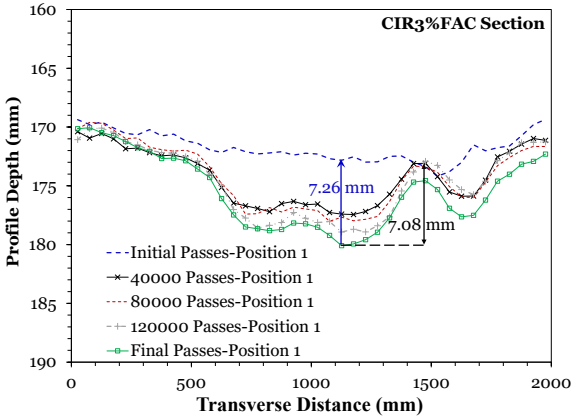

(e) ICIR3%FAC Position 2

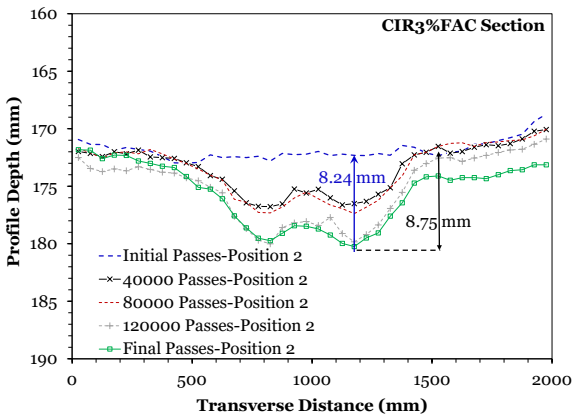

(f) CIR3%FAC Position 3

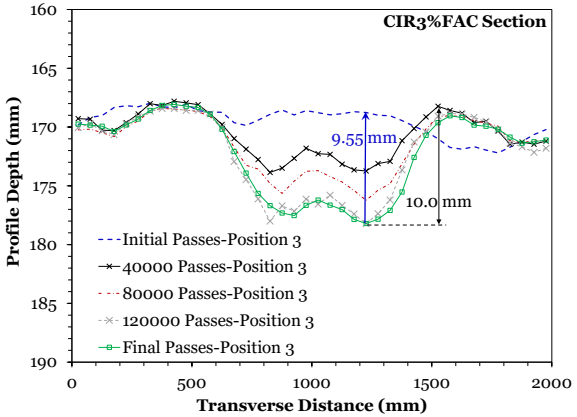

Figure 41 (cont.). Transverse depth profiles for all CIR sections after the application of truck full-scale accelerated loading.

(g) CIR4%FAC Position 1

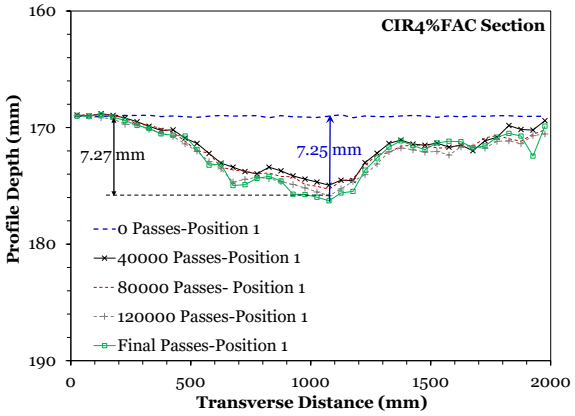

(h) CIR4%FAC Position 2

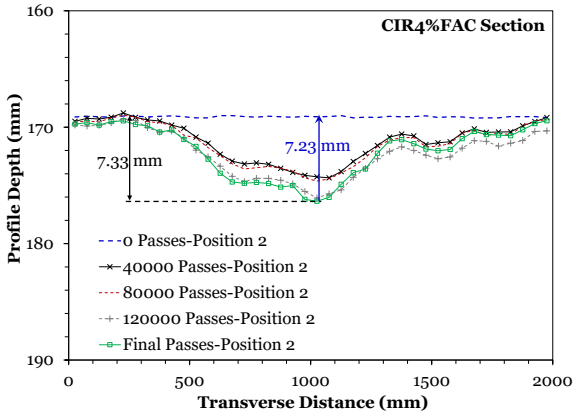

(i) CIR4%FAC Position 3

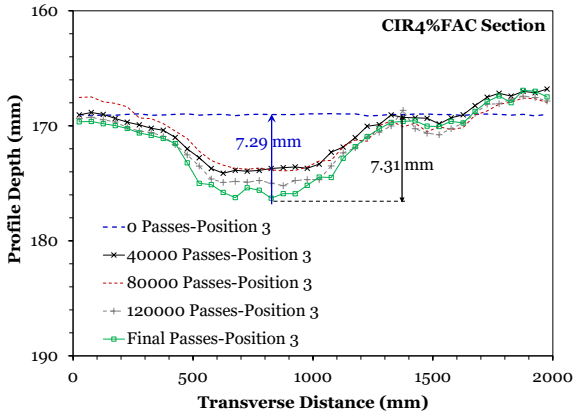

Figure 42. Transverse depth profiles for all CIR sections after the application of aircraft full-scale accelerated loading.

(a) CIR2%FAC Position 1

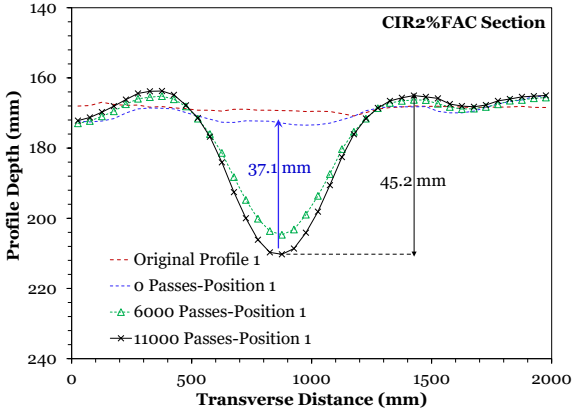

(b) CIR2%FAC Position 2

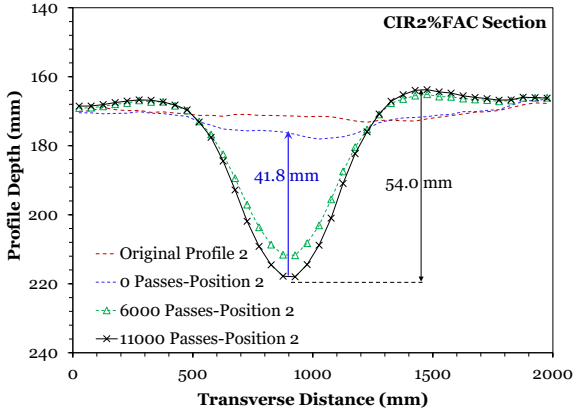

(c) ICIR2%FAC Position 3

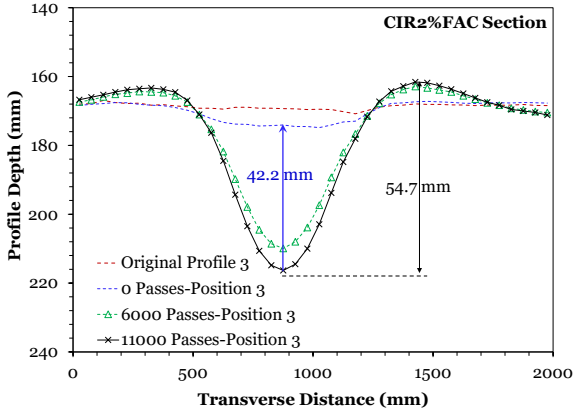

Figure 42 (cont.). Transverse depth profiles for all CIR Sections after the application of aircraft full-scale accelerated loading.

(d) CIR3%FAC Position 1

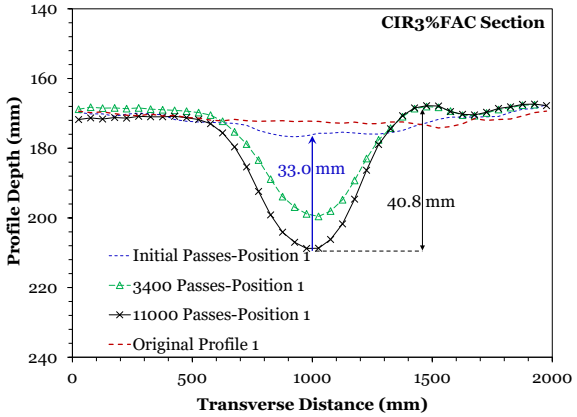

(e) ICIR3%FAC Position 2

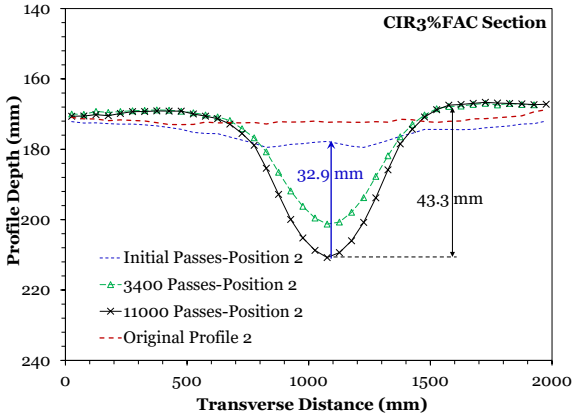

(f) CIR3%FAC Position 3

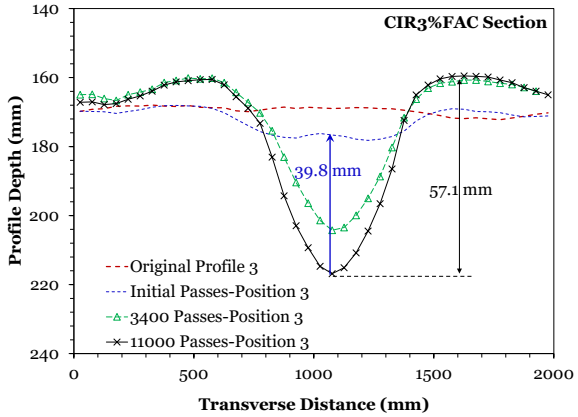

(g) CIR4%FAC Position 1

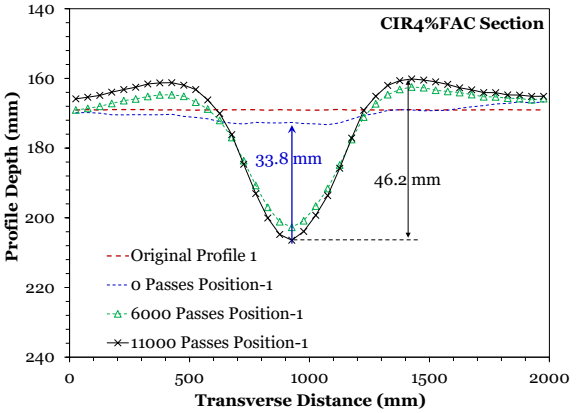

(h) CIR4%FAC Position 2

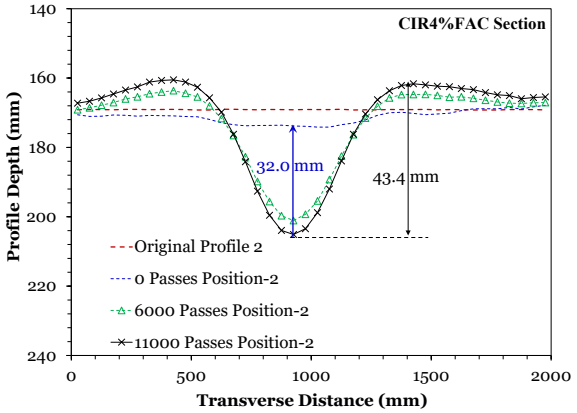

(i) CIR4%FAC Position 3

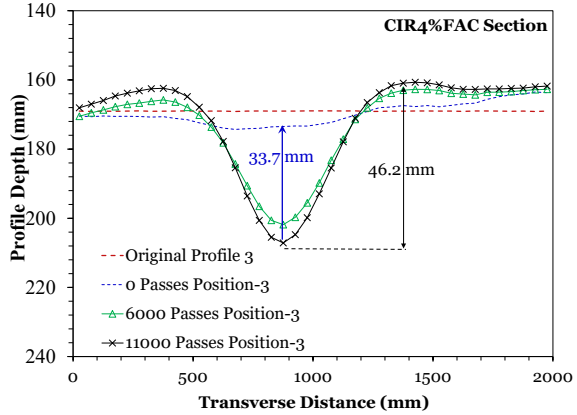

Figure 43. Comparison of rut depth after truck and aircraft full-scale loading.

(a) Rut after truck loading (b) Rut after aircraft loading

Figure 44. Example of pavement trench cut at position 1 in CIR3%FAC section.

Table 23. Forensic investigation of trenches obtained from each CIR section.

CIR Section	Rut Depth (mm)								
	CIR2%FAC			CIR3%FAC			CIR4%FAC		
	Pos1	Pos2	Pos3	Pos1	Pos2	Pos3	Pos1	Pos2	Pos3
Overlay (1 in.)	8.76	8.85	8.82	9.39	11.4	9.15	10.4	10.6	8.89
CIR layer (3 in.)	21.3	23.6	25.2	17.3	22.1	17.8	14.7	17.5	20.3
Old HMA (0.5 in.)	7.11	6.50	6.50	2.54	0.7	6.35	6.09	7.87	6.09
Total Rut Depth	37.1	39.0	40.5	29.2	34.2	33.3	31.2	35.9	35.3

6.5.3 Analysis of mechanistic responses

6.5.3.1 Tensile and compressive strains from asphalt strain gauges

Four asphalt strain gauges (ASGs) were placed in each of the CIR sections. Gauges ASG1 and ASG2 were placed at the bottom of the CIR layer in the longitudinal (or loading) direction while ASG3 and ASG4 were placed in the transverse direction (perpendicular to loading). To analyze the data from the strain gauge, the peak tensile and peak compressive strains were quantified from each strain pulse.

Figure 45 shows example strain pulses as obtained from all strain gauges (ASG1 through ASG4). As illustrated in this figure, the peak tensile strain is defined as the distance between a reference line and the maximum positive peak (above the reference line). Similarly, the peak compressive strain (Figure 45) is defined as the distance between a line and the maximum negative peak (below the reference line). The figure also shows that longitudinal strain gauges provide a different strain pulse (shape and magnitude) than the transverse strain gauges. The research team believes that the orientation of the gauge and the location of the wheel path are the reason for these different pulse shapes and magnitudes, respectively.

Figure 46 presents the peak tensile and compressive strains as obtained from longitudinal gauges ASG1 and ASG2 and transverse gauges ASG3 and ASG4 for all CIR sections. As Figure 46*a* shows, the peak tensile strains seem to remain constant (for the tracked wheel path) for all three CIR sections as truck loading (i.e., 40 kN) progresses. A similar trend is also shown for the peak compressive strains (Figure 46*b*). In addition, Figure 46*a* and *b* shows that the peak tensile and compressive strains for the CIR3%FAC section were lower by about 30 με than the CIR4%FAC section and about 20 με lower than the CIR2%FAC section. This may indicate that all CIR sections are experiencing similar strains at the bottom of the CIR layer when subject to accelerated truck loading. This in turn might indicate that the three CIR sections have similar cracking resistance, despite the 1% difference in binder content.

Figure 45. Example strain pulses as obtained from the transverse and longitudinal asphalt strain gauges (ASGs) at 20,000 loading passes.

(a) Asphalt Strain Gauge 1 (longitudinal direction)

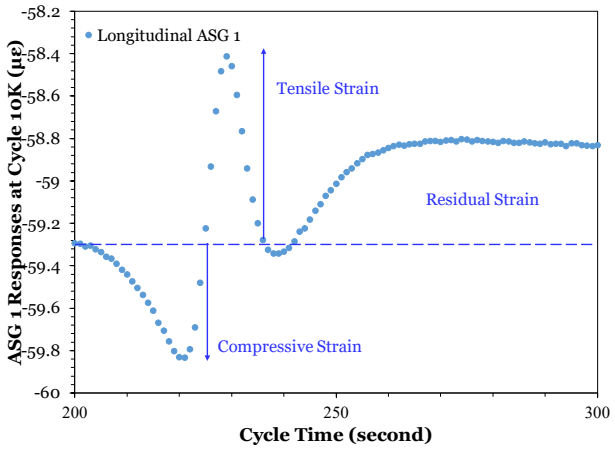

(b) Asphalt Strain Gauge 2 (longitudinal direction)

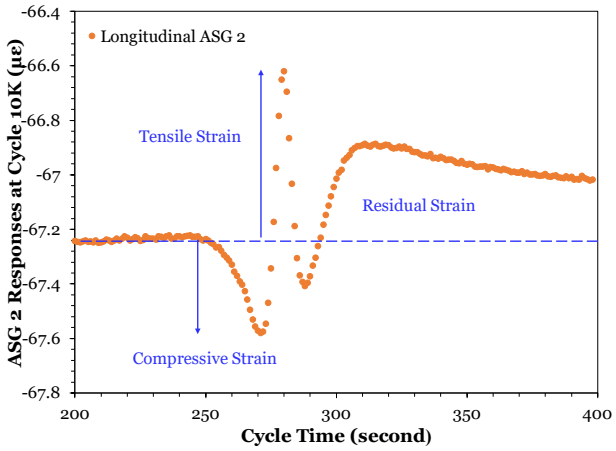

(c) Asphalt Strain Gauge 3 (transverse direction)

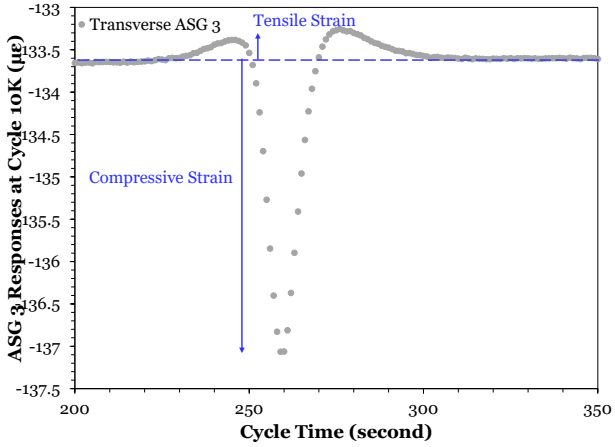

(d) Asphalt Strain Gauge 4 (transverse direction)

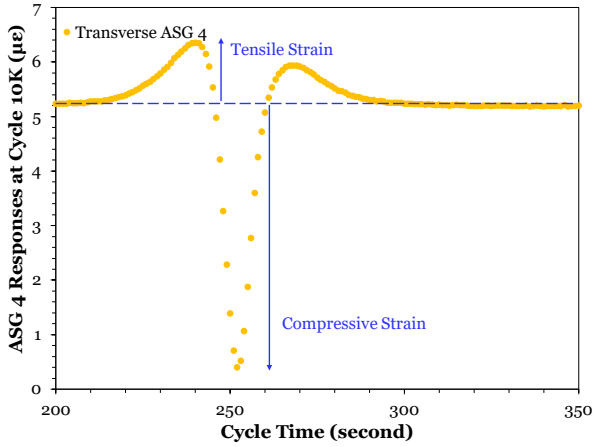

Figure 46*c* and *d* presents the peak tensile and compressive strains as obtained from ASG 3 and ASG 4, which were installed in a transverse direction to the HVS wheel path, for all CIR test sections. As Figure 46*c* shows, similar to ASG 1 and 2 responses, the tensile strains recorded by both ASG 3 and ASG 4 seemed to remain constant as the HVS loading progressed. Additionally, Figure 46*c* and *d* shows that both peak tensile and compressive strains for the CIR4%FAC section were higher than both CIR3%FAC and CIR2%FAC sections (by about 100 με for tension and by about 80 με for compression). This suggests that CIR3%FAC and CIR2%FAC sections might exhibit a slightly better cracking resistance than that of the CIR4%FAC section when subjected to accelerated truck loading.

Figure 47 presents the peak tensile and compressive strains as obtained from longitudinal gauges ASG1 and ASG2 and transverse gauges ASG3 and ASG4 for all CIR sections. It important to note that the stain gauge ASG 2 embedded in the CIR3%FAC section broke prior to applying the aircraft-accelerated loading; thus, the peak tensile and compressive strain data for this section were obtained from only ASG1, ASG3, and ASG4. As Figure 47 shows, all tensile and compressive strain peaks significantly increased (by up to more than 1,000 με) compared to the values obtained during the truck full-scale loading. The HVS testing was terminated at 11,000 passes as previously mentioned in section 6.4.2. Similar to the results obtained during the truck full-scale loading, the peak tensile and compressive strains remained relatively constant for the three CIR section. In addition, the CIR4%FAC section presented higher peak tensile strain values than those obtained for the CIR2%FAC (higher by approximately 400 με) and CIR3%FAC (higher by approximately 600 με) sections, as shown in Figure 47. Based on these observations, the binder content seems to impact the cracking performance of the CIR full-scale sections when subjected to accelerated loading of heavy traffic (i.e., 100 kN), where the CIR3%FAC section presented better cracking resistance. Despite these observations, it is important to note that these peak tensile and compressive strain values should be interpreted cautiously because visual inspection results (Figure 40) showed little to no cracking in the CIR4%FAC section while other sections had cracks. Other factors may influence the cracking resistance of a pavement sections in addition to recorded tensile strains.

Figure 46. Peak tensile and compressive strains after the application of truck full-scale accelerated loading.

(a) Peak tensile strains from ASG 1 and ASG 2

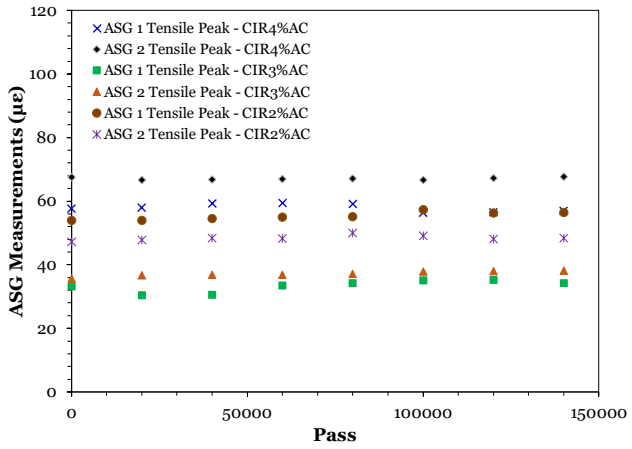

(b) Peak compressive strains from ASG 1 and ASG 2

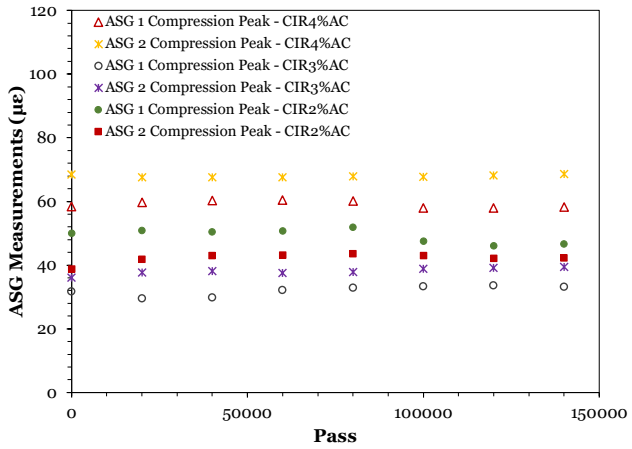

(c) Peak tensile strains from ASG 3 and ASG 4

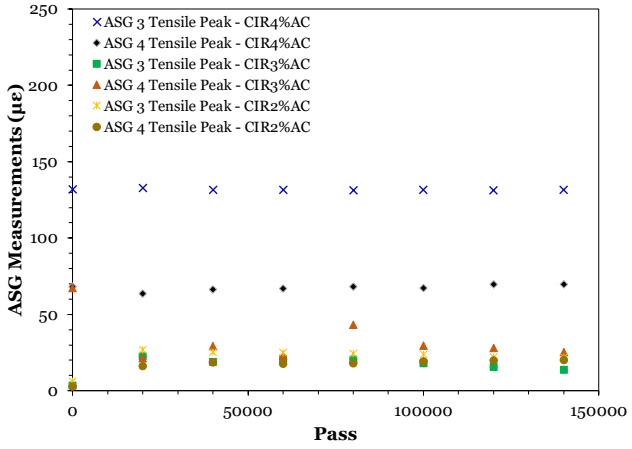

(d) Peak compressive strains from ASG 3 and ASG 4

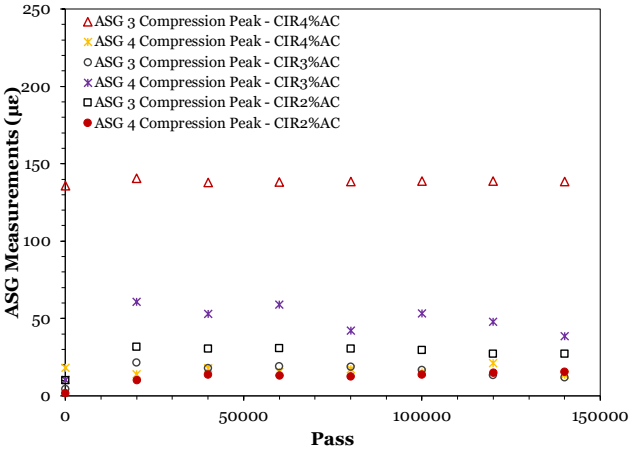

Figure 47. Peak tensile and compressive strains after the application of aircraft full-scale accelerated loading.

(a) Peak tensile strains from ASG 1 and ASG 2

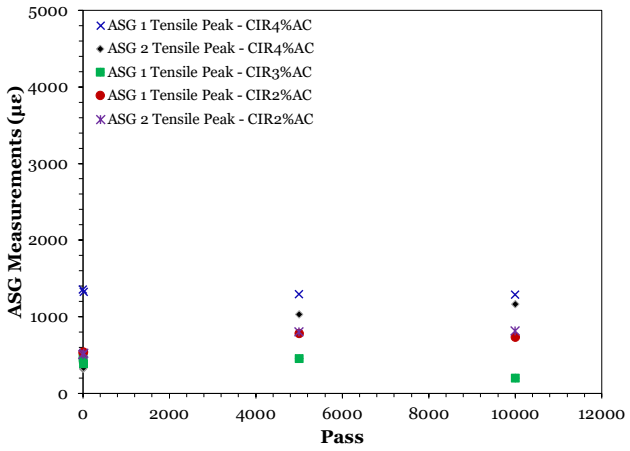

(b) Peak compressive strains from ASG 1 and ASG 2

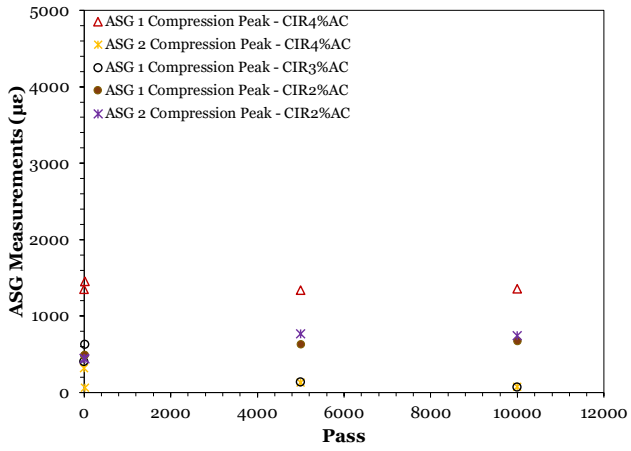

(c) Peak tensile strains from ASG 3 and ASG 4

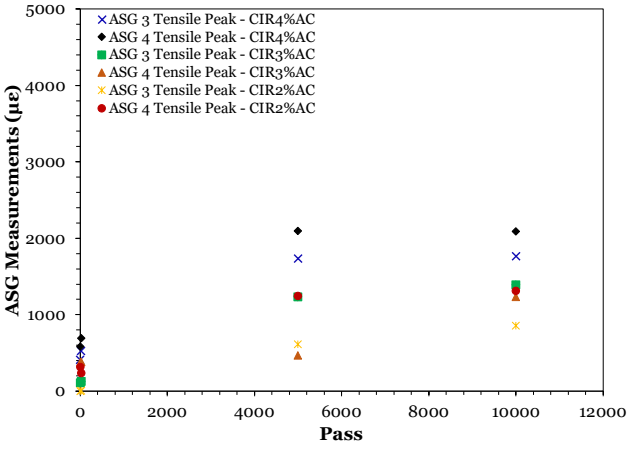

(d) Peak compressive strains from ASG 3 and ASG 4

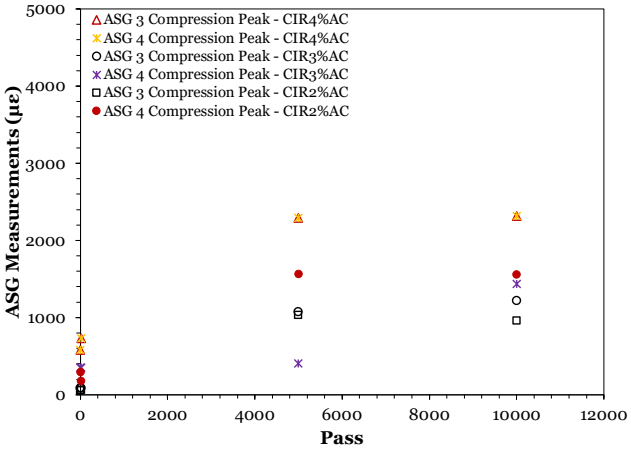

6.5.3.2 Compressive stresses from earth pressure cells

Similar to the ASGs, peak compressive stress as measured using the pressure cells was tracked. Figure 48 presents peak compressive stress as obtained from Pressure Cell 1 and Pressure Cell 2 (PC1 and PC2) during accelerated truck loading. As shown in Figure 48, peak compressive stress seemed to increase slightly (approximately linearly by about 2 psi) as HVS loading passes increased. This was the case for all three sections (Figure 48). The reason for this slight increase in compressive stress under truck loading magnitudes (i.e., 40 kN) is believed to be the densification of the HPTO and CIR layers as HVS loading is applied. By comparing the recorded compressive stresses for all the three CIR sections (Figure 48), one can potentially assess these sections' susceptibility to rutting (i.e., comparing compressive strains at the top of the base course for all sections). Figure 48*a* and *c* shows that the compressive stresses measured from the CIR4%FAC and the CIR2%FAC sections were roughly around 7.5 psi (52 Kpa) (after 145,000 loading passes), which is slightly higher than that observed for the CIR3%FAC section (Figure 48*b*). Since the difference in compressive stresses for the sections is at a maximum of 2 psi (14 Kpa), they are considered similar for all three sections. Therefore, no clear distinction between the sections, with regard to rutting susceptibility, can be made (at least based on truck loading magnitudes).

Figure 49 presents the CIR sections' compressive stress obtained from pressure cells during accelerated aircraft loading (i.e., 100 kN) for 11,000 passes. Unfortunately, compressive-stress data were measured for only the CIR4%FAC and CIR2%FAC sections due to malfunction of both pressure cells embedded in the CIR3%FAC section. As illustrated in Figure 49*a* and *b*, the peak compressive stress, recorded by PC1 and PC2 of the CIR4%FAC section and PC2 of the CIR2%FAC section, considerably increased under the aircraft loading magnitudes by approximately 20 psi. In addition, both sections presented similar compressive stresses, indicating that the CIR2%FAC and CIR4%FAC sections may have the same ability to resist rutting under aircraft loading magnitudes. No clear distinction can be made between the sections based on the recorded compressive stresses.

Figure 48. Peak compressive stress during truck full-scale accelerated loading.

(a) CIR4%FAC section

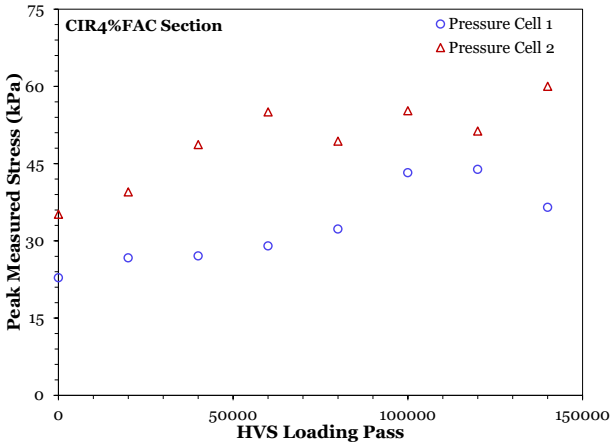

(b) CIR3%FAC section

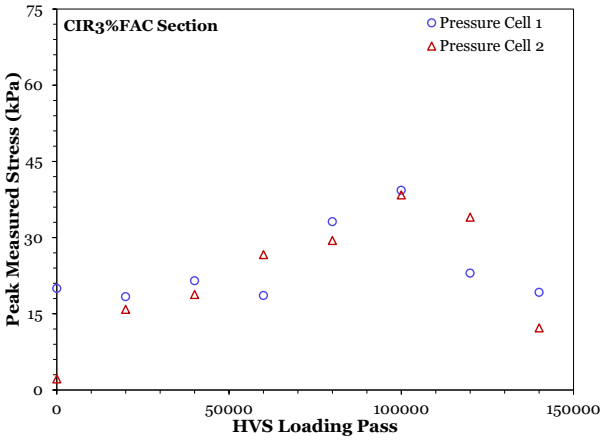

(c) ICIR2%FAC section

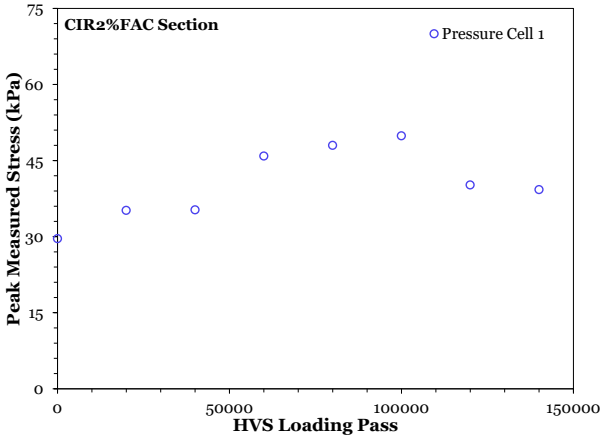

Figure 49. Peak compressive stress during aircraft full-scale accelerated loading.

(a) CIR4%AC section

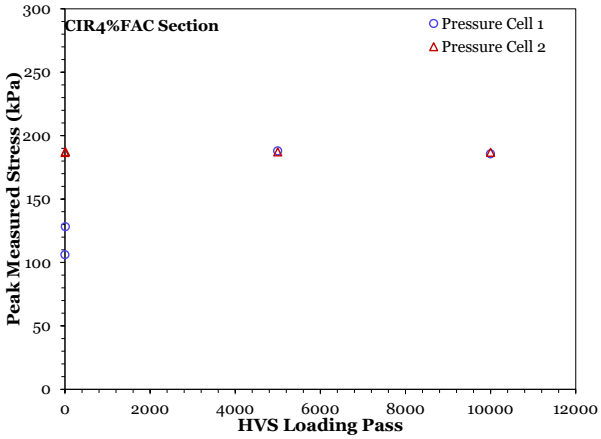

(b) CIR2%AC section

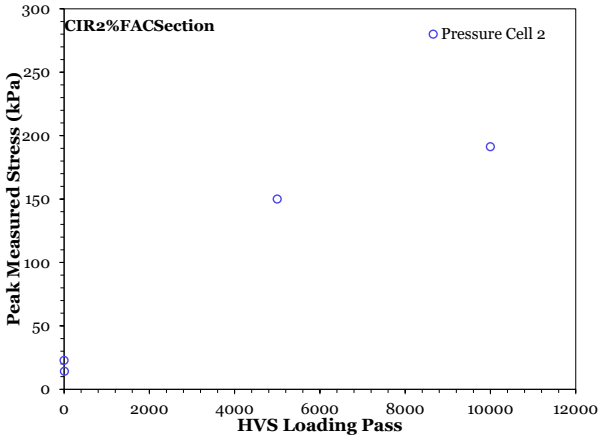

6.5.3.3 Temperature measurements from thermocouples

The target air temperature around the test sections when HVS loading was applied was set to 50°F (10°C). To monitor the difference in temperature, which was caused by variation in weather conditions and limitations of the HVS's cooling and heating systems, the research team installed three thermocouples (labeled top, mid, and bottom) in the CIR layer of each section. For the purposes of this study, temperatures were measured in only the CIR layers. The top thermocouple was placed 0.5 in. (12.5 mm) from the top of the CIR layer, the mid thermocouple was placed in the middle of the layer, and the bottom was placed 0.5 in. (12.5 mm) above the bottom of the CIR layer. Figure 50 presents temperatures at each of these locations along with the air temperature inside the HVS enclosure.

As Figure 50*a–c* shows, the temperature inside the CIR layer for the CIR4%FAC section was lower than that in the CIR3%FAC and CIR2%FAC sections. This is because the CIR4%FAC section was tested in May 2019 (late spring) while the other two sections were tested in June–August 2019 (summer) with increased ambient temperatures. Nonetheless, Figure 50 shows that the temperatures recorded were within 10°F (–12°C) to 15°F (–9°C) of the target air temperature (i.e., 50°F [10°C]). Therefore, the relatively higher temperature recorded at the CIR3%FAC and CIR2%FAC sections can potentially explain why this section presented higher rut-depth values than those measured at the CIR4%FAC section when subjected to accelerated truck loading. With regard to the temperature recorded during the accelerated aircraft loading (Figure 50*d–f*), the three CIR sections presented similar air temperature and temperature of the CIR layer (about 60°F [15.5°C] on average). Thus, this suggests that temperature may not have an impact on trafficking performance during the aircraft loading portion of the HVS testing.

Figure 50. Recorded temperatures at the top, middle, and bottom of the CIR layer.

(a) CIR4%FAC section

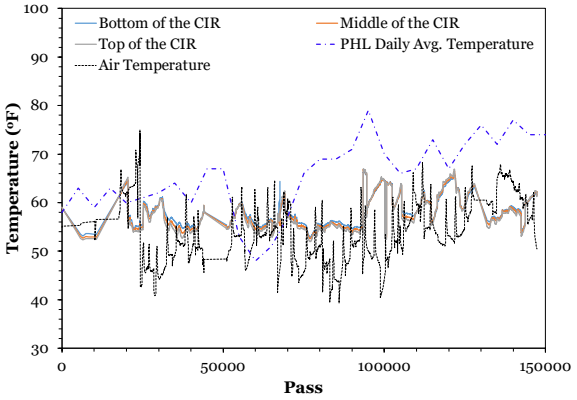

(b) CIR3%FAC section

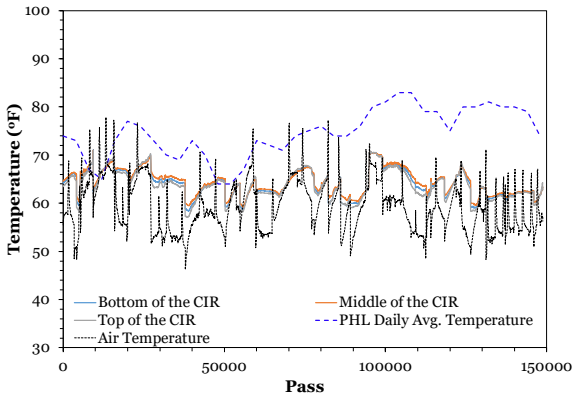

(c) ICIR2%FAC section

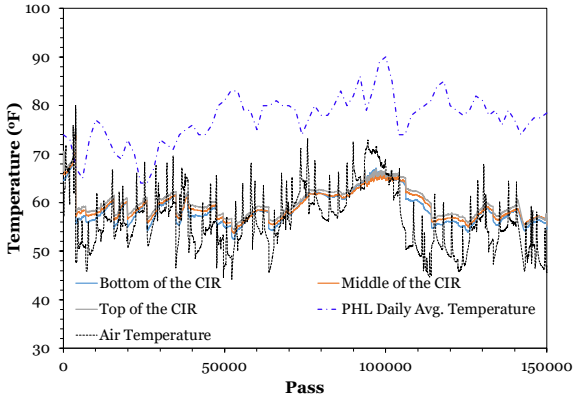

(d) CIR4%FAC section

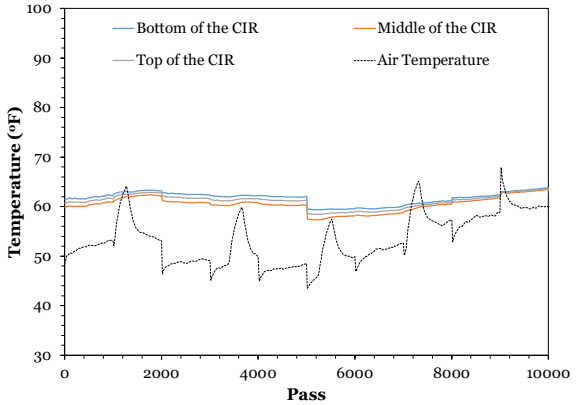

(e) ICIR3%FAC section

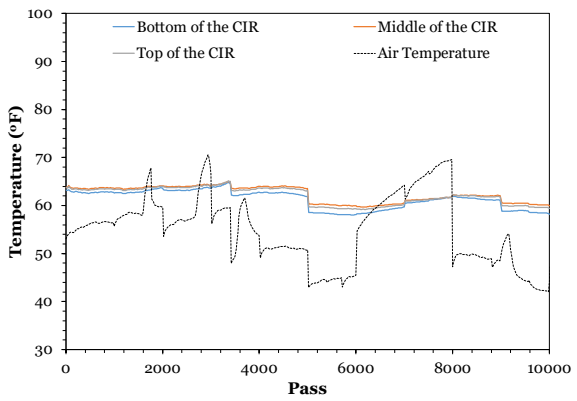

(f) CIR2%FAC section

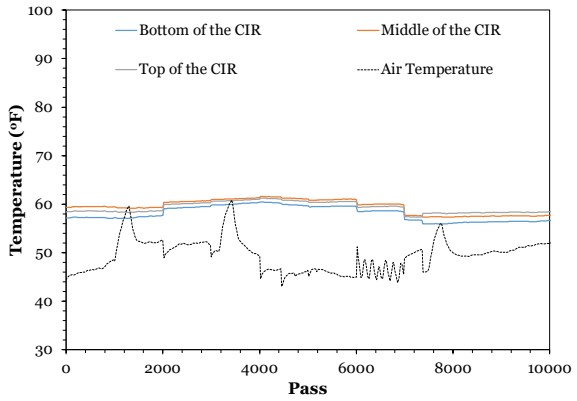

6.5.3.1 Statistical analysis of the measured response data

The research team statistically assessed the impact of CIR binder content on the field performance of CIR sections by using one-way ANOVA and Tukey's HSD post hoc analysis. The analysis was performed on a 95% confidence level: when *p*-values and sigmoid values are less than 0.05, the impact of binder content on the field performance is considered significant. Table 24 presents the ANOVA and Tukey's HSD post hoc analysis for rut depth, estimated CIR layer moduli, and tensile strain values measured after the application of accelerated truck and aircraft loading. ANOVA analysis showed that the estimated layer moduli and tensile strain (at the bottom of the CIR layer) presented *p*-values less than 0.05 (0.026 and 0.038) after the application of accelerated truck loading, while the rut depth presented a *p*-value of 0.356. This suggests that the binder content has a significant impact on the estimated moduli and cracking resistance of CIR sections under truck traffic. Further, varying the binder content by 1% did not cause a significant change in the rutting performance. In addition, post hoc analysis investigated which binder contents caused the significant change in estimated moduli and tensile strain values. Results showed that only the sigmoid values between 3% and 4% binder contents were less than 0.05 (0.022 and 0.035, respectively). Therefore, increasing the binder content from 3% to 4% has a significant impact on both moduli and tensile strain under truck loading. At 3% binder content, the CIR layer presented higher values of estimated moduli and lower cracking susceptibility than the other sections.

With regard to accelerated aircraft loading, ANOVA and post hoc analysis showed that all the performance measures (rut depth, estimated layer moduli, and tensile strain) presented *p*-values higher than 0.05 (Table 24). This indicates that the change in CIR binder contents by 1% has a minor impact on the stiffness, rutting, and cracking performance of CIR layers under accelerated aircraft loading. Based on statistical analyses, the impact of binder content depends on the traffic level applied on the CIR pavement. When the loading magnitude of traffic is low to medium, varying the binder content will result in different performance of the CIR layer, which falls in line with the findings of the BMD design developed as part of this study (see chapter 4). However, when loading magnitude of traffic increases considerably (heavy traffic), it becomes hard to capture the impact of a 1% incremental change of binder content on the stiffness and the performance of CIR.

Table 24. ANOVA and post hoc analysis results.

After the Application of Truck Loading			
Performance Measure	Rut Depth	Estimated Moduli	Tensile Strain
p-Value	0.356	0.026	0.038
Binder Content (%)	Tukey's HSD Post Hoc Analysis (Sig.)		
2 & 3	0.605	0.256	0.596
2 & 4	0.851	0.194	0.125
3 & 2	0.605	0.256	0.596
3 & 4	0.337	0.022	0.035
4 & 2	0.851	0.194	0.125
4 & 3	0.605	0.256	0.035
After the Application of Aircraft Loading			
Performance Measure	Rut Depth	Estimated Moduli	Tensile Strain
p-Value	0.491	0.128	0.416
Binder Content (%)	Tukey's HSD Post Hoc Analysis (Sig.)		
2 & 3	0.68	0.816	0.999
2 & 4	0.478	0.125	0.485
3 & 2	0.68	0.816	0.999
3 & 4	0.929	0.273	0.47
4 & 2	0.478	0.125	0.485
4 & 3	0.68	0.816	0.47

7 Summary of Findings, Conclusions, and Recommendations

7.1 Summary of findings and conclusions

This study presented a method for designing emulsified and foamed asphalt CIR mixtures that balances cracking and rutting performance. To evaluate the feasibility and practicality of the BMD method, eight CIR mixtures were produced in the lab by using a combination of two bituminous additives (foamed asphalt or emulsion), two compaction levels (30 or 70 gyrations), and two curing temperatures (cold curing at 50°F [10°C] or hot curing at 140°F [60°C]). All the laboratory CIR mixtures were prepared using a constant dosage of portland cement and water, 1% and 3%, respectively. Air-void levels were determined for each mixture by using a CoreLok device. APA and dynamic complex modulus tests were conducted to evaluate rutting susceptibility while ITS and SCB-FE tests were conducted to assess strength and cracking resistance. Regression analysis was performed on rutting and cracking performance measures to evaluate the ability of laboratory performance tests to predict the rutting and cracking performances of CIR mixtures at different binder contents. Performance measures exhibiting strong correlations with CIR binder content were then used to select the optimum binder content of the eight CIR mixes. The process of selecting optimum binder contents was demonstrated for all CIR mixes and presented as part of this study.

Based on laboratory results and subsequent ANOVA analyses, the conclusions are the following:

- The BMD approach was used successfully to design eight CIR mixtures. Because of its sensitivity to binder content, performance-testing results highlighted the importance of rutting measures, which currently established CIR mix design methods do not consider, perhaps with the exception of Marshall stability and flow.

- Three of the four rutting and cracking measures (i.e., APA rut depth, ITS, and SCB-FE) presented a strong dependence on CIR binder contents. Regression analysis conducted on CIR performance measures showed that there is a strong correlation between each of these

measures (i.e., APA rut depth, ITS, and SCB-FE) and CIR binder content, therefore, indicating that these measures may be useful for developing a BMD method.

- The results from the dynamic complex modulus, $|E^*|$, conducted at high temperature (i.e., 129°F [54°C]) and a loading frequency of 10 Hz showed a relatively constant trend for all CIR mixtures. The rutting measure determined from the dynamic complex modulus test was, in fact, unable to capture the change in CIR binder content; thus, the $|E^*|$ measure was not considered for the BMD method.

- Three cases for determining ranges of balanced optimum binder contents for CIR mixtures were observed. Each case is related to the trend of the performance measures (i.e., APA rut depth, ITS, and SCB-FE) versus the CIR binder content. The BMD results also indicated that these cases can be dependent on the type of CIR bituminous additive, compaction level, and curing process used in designing CIR mixtures. Based on the results, optimum contents can be selected from APA and SCB-FE plots.

- Bituminous additive type (emulsion or foamed asphalt) showed a minor effect on rutting performance. This can be explained by the fact that, when compacted using the same compaction level, both foamed and emulsified mixtures had similar ability to resist rutting. However, SCB results at optimum binder contents showed that emulsion mixtures exhibited higher fracture energy values than those of foamed asphalt mixtures, indicating that emulsion mixtures are better at resisting cracking than those prepared using foamed asphalt.

- Compaction level had a significant impact on both rutting and cracking performance. APA rut-depth results at optimum binder contents showed that CIR mixtures compacted at 70 gyrations had lower rutting susceptibly than those of CIR mixtures compacted at 30 gyrations.

- Curing process also had a significant impact on rutting and cracking. Performance-test results showed that mixtures subjected to hot curing (i.e., 140°F [60°C] for 3 days) had relatively lower rutting susceptibly (i.e., lower APA rut depths and higher $|E^*|$) and higher cracking resistance (i.e., higher ITS and SCB-FE) than those submitted to cold curing (i.e., 50°F [10°C] for 3 days).

In addition to the laboratory study, an accelerated pavement testing study was conducted on three full-scale CIR sections to evaluate field performance and to verify laboratory results. Specifically, the main purpose of full-scale testing was to verify whether different laboratory-designed CIR mixes (i.e., CIR4%FAC at 4% binder content, CIR3%FAC at 3% binder content, and CIR2%FAC at 2% binder content) will perform similarly under field conditions (e.g., verify that the CIR4%FAC section was the most crack resistant). To characterize the performance of the full-scale sections, truck and aircraft loading (i.e., 9,000 lb [40 kN] and 22,500 lb [100 kN], respectively) was applied. HWD, transverse depth laser profiles, and mechanistic responses from pavement sensors were utilized to collect information about the rutting and cracking responses.

Full-scale accelerated testing results and subsequent analyses conducted resulted in the following conclusions:

- Pavement deflections decreased (by up to 12 mil [0.3 mm] in some cases) after applying HVS truck loading. Applying aircraft loading showed a slight decrease in deflections (by roughly 3 mil [0.08 mm]). This is likely due to the densification of the HMA and CIR materials under HVS loading.

- Applying the truck loading (40 kN) increased the estimated moduli of the upper layers of CIR sections by up to 50%. In addition, the estimated moduli of the upper layers of the CIR section increased by more than 100% after aircraft loading (100 kN).

- Transverse pavement profiles showed that the CIR3%FAC and CIR4%FAC sections had similar rut-depth values (i.e., within 0.04 in. [1 mm] rut depth) after truck loading. The CIR2%FAC section had slightly better rutting resistance (i.e., lower recorded rut-depth values) than the other two sections.

- Under aircraft loading conditions (i.e., 22,480 lb [100 kN]), following the application of accelerated truck loading for 150,000 passes, recorded rut-depth values increased considerably for all three sections, exceeding the 1 in. (25 mm) rutting failure criteria of within 11,000 passes. Rate of failure was fastest for the CIR2%FAC section compared to the other two CIR sections. While the overall trend of the measured permanent deformation shows that lower binder content in the mix results in

better rutting resistance, under high loading the CIR layer might be more like an unbound granular layer as opposed to a bound pavement layer. This may explain why the CIR2%FAC section (i.e., lowest binder content) was the most rutting susceptible under aircraft loading.

- Earth pressure cells installed at the bottom of the CIR layers showed overall equivalent responses in the three CIR sections during repeated HVS loading. A slight ascending trend was observed after 90,000 truck loading passes in all the CIR test sections, which could be due to the stiffening of the CIR layer. An increase of measured peak stress values (by up to 20 psi [138 Kpa]) was observed after aircraft loading, which indicates that the rutting susceptibility decreased.

- During both accelerated truck and aircraft loading, the CIR3%FAC section exhibited lower measured strain values at the bottom of the CIR layer than those of the CIR2%FAC and CIR4%FAC sections. This suggests that the CIR3%FAC section may be the best option for airfields of these materials tested. This finding may be different when different combinations and types of RAP, bituminous, and cementitious additives are used.

- Thermocouple measurements showed that air temperature and the temperature of the CIR layer of the different CIR sections varied between 50°F (10°C) and 70°F (21.1°C) during both truck and aircraft loading.

7.2 Future works

The study team recommends that future CIR research focus on the following:

- Compare mix design methods typically used for CIR techniques by certain agencies (i.e., Pennsylvania mix design, military mix design, and modified Marshall mix design) to the BMD approach developed as part of this study.

- Evaluate the impact of recycling binder type (emulsion vs. foamed asphalts), cementitious additives (cement vs. lime), and water content at varying contents and dosages on CIR mixtures. Further, investigate the impact of these factors on the design approach proposed as part of this study.

- Develop an approach for optimizing the selection of CIR mix constituents other than bituminous additives (e.g., cementitious additives and water).

- Validate the approach for optimizing more than one CIR constituents through controlled, full-scale accelerated pavement testing experiments.

Overall, adopting the BMD approach on multiple CIR ingredients (i.e., bituminous, cementitious additives, and water) will further optimize the ability of CIR mixtures to resist rutting and cracking. This approach will also help to understand the chemical reaction occurring between bituminous and cementitious additives and water at different dosages and to assess their impact on the strength of CIR mixes. Therefore, this research is needed to design longer-lasting, ecofriendly, and economical pavements for different traffic levels, including airfields. A second phase of the current research will address all these recommendations.

References

AASHTO (American Association of State Highway and Transportation Officials). 1986. *Standard Method of Test for Distillation of Creosote and Creosote Coal Tar Solutions*. AASHTO T 62. Washington, DC: American Association of State Highway and Transportation Officials.

AASHTO (American Association of State Highway and Transportation Officials). 1991. *Standard Method of Test for Sampling of Aggregates*. AASHTO T 2. Washington, DC: American Association of State Highway and Transportation Officials.

AASHTO (American Association of State Highway and Transportation Officials). 1998. *Report on Cold Recycling of Asphalt Pavements*. AASHTO-AGC-ARTBA Joint Committee Task Force 38 Report. Washington, DC: American Association of State Highway and Transportation Officials. https://trid.trb.org/view/537167.

AASHTO (American Association of State Highway and Transportation Officials). 2007. *Standard Method of Test for Determining the Creep Compliance and Strength of Hot Mix Asphalt (HMA) Using the Indirect Tensile Test Device*. AASHTO T 322. Washington, DC: American Association of State Highway and Transportation Officials.

AASHTO (American Association of State Highway and Transportation Officials). 2008. *Standard Method of Test for Quantitative Extraction and Recovery of Asphalt Binder from Asphalt Mixtures*. AASHTO T 319. Washington, DC: American Association of State Highway and Transportation Officials.

AASHTO (American Association of State Highway and Transportation Officials). 2010. *Standard Method of Test for Determining Rutting Susceptibility of Hot Mix Asphalt (HMA) Using the Asphalt Pavement Analyzer (APA)*. AASHTO T 340. Washington, DC: American Association of State Highway and Transportation Officials.

AASHTO (American Association of State Highway and Transportation Officials). 2011. *Standard Method of Test for Mineral Matter or Ash in Asphalt Materials*. AASHTO T 111. Washington, DC: American Association of State Highway and Transportation Officials.

AASHTO (American Association of State Highway and Transportation Officials). 2013. *Standard Method of Test for Bulk Specific Gravity (G_{mb}) and Density of Compacted Hot Mix Asphalt (HMA) Using Automatic Vacuum Sealing Method*. AASHTO T 331. Washington, DC: American Association of State Highway and Transportation Officials.

AASHTO (American Association of State Highway and Transportation Officials). 2015a. *Standard Method of Test for Determining the Dynamic Modulus and Flow Number for Asphalt Mixtures Using the Asphalt Mixture Performance Tester (AMPT)*. AASHTO TP 79. Washington, DC: American Association of State Highway and Transportation Officials.

AASHTO (American Association of State Highway and Transportation Officials). 2015b. *Standard Method of Test for Resistance to Plastic Flow of Asphalt Mixtures Using Marshall Apparatus*. AASHTO T 245. Washington, DC: American Association of State Highway and Transportation Officials.

AASHTO (American Association of State Highway and Transportation Officials). 2016. *Standard Method of Test for Emulsified Asphalts*. AASHTO T 59. Washington, DC: American Association of State Highway and Transportation Officials.

AASHTO (American Association of State Highway and Transportation Officials). 2018a. *Standard Method of Test for Determining the Asphalt Binder Content of Hot Mix Asphalt (HMA) by the Ignition Method*. AASHTO T 308. Washington, DC: American Association of State Highway and Transportation Officials.

AASHTO (American Association of State Highway and Transportation Officials). 2018b. *Standard Method of Test for Percent Air Voids in Compacted Dense and Open Asphalt Mixtures*. AASHTO T 269. Washington, DC: American Association of State Highway and Transportation Officials.

AASHTO (American Association of State Highway and Transportation Officials). 2018c. *Standard Method of Test for Resistance of Compacted Asphalt Mixtures to Moisture-Induced Damage*. AASHTO T 283. Washington, DC: American Association of State Highway and Transportation Officials.

AASHTO (American Association of State Highway and Transportation Officials). 2019. *Standard Method of Test for Determining Dynamic Modulus of Hot Mix Asphalt (HMA)*. AASHTO T 342. Washington, DC: American Association of State Highway and Transportation Officials.

AASHTO (American Association of State Highway and Transportation Officials). 2020a. *Standard Method of Test for Materials Finer than 75-µm (No. 200) Sieve in Mineral Aggregates by Washing*. AASHTO T 11. Washington, DC: American Association of State Highway and Transportation Officials.

AASHTO (American Association of State Highway and Transportation Officials). 2020b. *Standard Method of Test for Sieve Analysis of Fine and Coarse Aggregates*. AASHTO T 27. Washington, DC: American Association of State Highway and Transportation Officials.

AASHTO (American Association of State Highway and Transportation Officials). 2020c. *Standard Method of Test for Theoretical Maximum Specific Gravity (G_{mm}) and Density of Asphalt Mixtures*. AASHTO T 209. Washington, DC: American Association of State Highway and Transportation Officials.

AASHTO (American Association of State Highway and Transportation Officials). 2020d. *Standard Method of Test for Moisture–Density Relations of Soils Using a 4.54-kg (10-lb) Rammer and a 457-mm (18-in.) Drop*. AASHTO T 180. Washington, DC: American Association of State Highway and Transportation Officials.

AASHTO (American Association of State Highway and Transportation Officials). 2020e. *Standard Method of Test for Determining the Fracture Energy of Asphalt Mixtures Using the Semicircular Bend Geometry (SCB)*. AASHTO TP 105. Washington, DC: American Association of State Highway and Transportation Officials.

AASHTO (American Association of State Highway and Transportation Officials). 2021. *Standard Method of Test for Bulk Specific Gravity (Gmb) of Compacted Asphalt Mixtures Using Saturated Surface-Dry Specimens*. AASHTO T 166. Washington, DC: American Association of State Highway and Transportation Officials.

Alam, Tashina Binte, Magdy Abdelrahman, and Scott A. Schram. 2010. "Laboratory Characterisation of Recycled Asphalt Pavement as a Base Layer." *International Journal of Pavement Engineering* 11 (2): 123–131. https://doi.org/10.1080/10298430902731362.

Ali, Ayman W., Ala R. Abbas, Munir Nazzal, and David Powers. 2012. "Laboratory Evaluation of Foamed Warm Mix Asphalt." *International Journal of Pavement Research and Technology* 5 (2): 93–101.

Anderson, D. A., D. R. Luhr, and M. Lahr. 1985. *Cold In-Place Recycling of Low-Volume Roads in Susequehanna County*. Volume I: Technical Report. FHWA-PA-84-020. Harrisburg, PA: Pennsylvania Department of Transportation. https://trid.trb.org/View/212995.

Apeagyei, Alex K., and Brian K. Diefenderfer. 2013. "Evaluation of Cold In-Place and Cold Central-Plant Recycling Methods Using Laboratory Testing of Field-Cored Specimens." *Journal of Materials in Civil Engineering* 25, no. 11 (November): 1712–1720. https://doi.org/10.1061/(ASCE)MT.1943-5533.0000717.

ARRA (Asphalt Recycling and Reclaiming Association). 1992. *An Overview of Recycling and Reclamation Methods for Asphalt Pavement Rehabilitation*. Annapolis, MD: Asphalt Recycling and Reclaiming Association. https://trid.trb.org/view/368582.

ARRA (Asphalt Recycling and Reclaiming Association). 1996. *Mixture and Structural Design of Cold Recycled Pavements*. Annapolis, MD: Asphalt Recycling and Reclaiming Association.

ARRA (Asphalt Recycling and Reclaiming Association). 2016. *Recommended Construction Guidelines for Cold In-Place Recycling (CIR) Using Bituminous Recycling Agents*. CR101. Annapolis, MD: Asphalt Recycling and Reclaiming Association. https://cdn.ymaws.com/www.arra.org/resource/resmgr/files/ARRA-CR101.pdf.

ASTM International. 1998. *Test Method for Resistance of Plastic Flow of Bituminous Mixtures Using Marshall Apparatus*. ASTM D1559. West Conshohocken, PA: ASTM International.

ASTM International. 2014. *Standard Test Method for Density of Bituminous Concrete in Place by Nuclear Methods*. ASTM D2950. West Conshohocken, PA: ASTM International.

ASTM International. 2016. *Standard Test Method for Particle-Size Analysis of Soils*. ASTM D422. West Conshohocken, PA: ASTM International.

ASTM International. 2017. *Standard Test Method for Indirect Tensile (IDT) Strength of Asphalt Mixtures*. ASTM D6931. West Conshohocken, PA: ASTM International.

ASTM International. 2018a. *Standard Test Method for Maximum Specific Gravity and Density of Asphalt Mixtures Using Automatic Vacuum Sealing Method*. ASTM D6857. West Conshohocken, PA: ASTM International.

ASTM International. 2018b. *Standard Test Method for Raveling Test of Cold-Mixed Emulsified Asphalt Samples*. ASTM D7196. West Conshohocken, PA: ASTM International.

ASTM International. 2020a. *Standard Specification for Emulsified Asphalt*. ASTM D977. West Conshohocken, PA: ASTM International.

ASTM International. 2020b. *Standard Test Method for Toluene-Insoluble (TI) Content of Tar and Pitch*. ASTM D4318. West Conshohocken, PA: ASTM International.

ASTM International. 2020c. *Standard Test Method for Determining the Resilient Modulus of Asphalt Mixtures by Indirect Tension Test*. ASTM D7369. West Conshohocken, PA: ASTM International.

Asphalt Institute. 1983. "Asphalt Cold-Mix Recycling." In *The Asphalt Institute Manual Series No. 21 (MS-21)*. 2nd ed. College Park, MD: Asphalt Institute.

Bang, Sangchul, Wade Lein, Beth Comes, Leah Nehl, Josh Anderson, Paul Kraft, Michael deStigter, et al. 2011. *Quality Base Material Produced Using Full Depth Reclamation on Existing Asphalt Pavement Structure – Task 4: Development of FDR Mix Design Guide*. FHWA-HIF-12-015. Washington, DC: US Department of Transportation. https://rosap.ntl.bts.gov/view/dot/42788.

Bennett, T., and Maher, A. 2005. *The Development of Performance Specification for Granular Base and Subbase Material.* FHWA-NJ-2005-003. Trenton, NJ: New Jersey Department of Transportation. https://rosap.ntl.bts.gov/view/dot/38119.

Berthelot, Curtis, Brent Marjerison, Gary Houston, Jody McCaig, Stu Warrener, and Rock Gorlick. 2013. "Mechanistic Comparison of Cement- and Bituminous-Stabilized Granular Base Systems." *Transportation Research Record: Journal of the Transportation Research Board* 2026, no. 1 (January): 70–80. https://doi.org/10.3141%2F2026-09.

Bessa, Iuri S., Letícia R. Almeida, K. L. Vasconcelos, and L. L. B. Bernucci. 2016. "Design of Cold Recycled Mixes with Asphalt Emulsion and Portland Cement." *Canadian Journal of Civil Engineering* 43, no. 9 (September): 773–782. https://doi.org/10.1139/cjce-2016-0111.

Black, Kit. 2013. *Cold In-Place Recycling: A Cost Effective Pavement Preservation Treatment*. PowerPoint presentation, October 15, 2013. Amarillo, TX: Texas Department of Transportation. https://businessdocbox.com/Green_Solutions/71240329-Cold-in-place-recycling.html.

Bleakley, Albert M., and Paul J. Cosentino. 2013. "Improving Properties of Reclaimed Asphalt Pavement for Roadway Base Applications through Blending and Chemical Stabilization." *Transportation Research Record: Journal of the Transportation Research Board* 2335, no. 1 (January): 20–28. https://doi.org/10.3141%2F2335-03.

Brovelli, Claudio, and Maurizio Crispino. 2012. "Investigation into Cold Recycled Materials: Influence of Rejuvenant, Mix Design Procedure, and Effects of Temperature on Compaction." *Construction and Building Materials* 37 (December): 507–511. https://doi.org/10.1016/j.conbuildmat.2012.07.070.

Buchanan, M. Shane, Thomas D. White, and Benjamin J. Smith. 2004. *Use of the Asphalt Pavement Analyzer to Study In-Service Asphalt Mixture Performance*. FHWA/MS-DOT-RD-04-155. Jackson, MS: Mississippi Department of Transportation.

Buss, Ashley, Marie Grace Mercado, and Scott Schram. 2017. "Long-Term Evaluation of Cold-In-Place Recycling and Factors Influencing Performance." *Journal of Performance of Constructed Facilities* 31, no. 3 (June): 04016111-1–04016111-10. https://ascelibrary.org/doi/full/10.1061/%28ASCE%29CF.1943-5509.0000985.

Carter, A., B. Feisthauer, D. Lacroix, and D. Perraton. 2010. "Comparison of Cold In-Place Recycling and Full-Depth Reclamation Materials." 10-1325. In *Proceedings, Transportation Research Board 89th Annual Meeting*, Washington, DC.

Charmot, Stephane, Wenlong Dong, and Xiaolei Xu. 2017. "Feasibility of Cold Recycling Asphalt Mixture Design Optimization on the Basis of Fracture Properties Using the Semi-Circular Bending (SCB) at Low Temperature." 17-04716. Paper presented at the Transportation Research Board 96th Annual Meeting, Washington, DC, January 8–12, 2017. https://trid.trb.org/view/1438833.

Chen, Don, Charles T. Jahren, Hosin "David" Lee, R. Chris Williams, Sunghwan Kim, Michael Heitzman, and Jungyong "Joe" Kim. 2010. "Effects of Recycled Materials on Long-Term Performance of Cold In-Place Recycled Asphalt Roads." *Journal of Performance of Constructed Facilities* 24, no. 3 (June): 275–280. https://ascelibrary.org/doi/full/10.1061/%28ASCE%29CF.1943-5509.0000092.

Chesner, Warren H., Christopher W. Stein, Henry G. Justus, Edward R. Kearney, and Stephen A. Cross. 2011. "Evaluation of Factors Affecting the Long-Term Performance of Cold In-Place Recycled Pavements In New York State." *Transportation Research Record: Journal of the Transportation Research* Board 2227, no. 1 (January): 13–22. https://doi.org/10.3141%2F2227-02.

Cohen, Ehud, Arieh Sidess, and Gabriel Zoltan. 1989. Performance of a Full-Scale Pavement Using Cold Recycled Asphalt Mixture. *Transportation Research Record* 1228:88–93. https://onlinepubs.trb.org/Onlinepubs/trr/1989/1228/1228-011.pdf.

Cox, Ben C., and Isaac L. Howard. 2013. *Cold In-Place Recycling and Full Depth Reclamation Literature Review*. White Paper CMRC WP 13-1. Mississippi State, MS: Mississippi State University Construction Materials Research Center. https://www.cee.msstate.edu/downloads/(2013)CoxandHoward-CMRCWP13-1-LitReviewofCIRandFDR.pdf.

Cox, Ben C., and Isaac L Howard. 2015a. *Cold In-Place Recycling Characterization Framework and Design Guidance for Single or Multiple Component Binder Systems*. FHWA/MS-DOT-RD-15-250-Volume 2. Mississippi State, MS: Mississippi State University. https://trid.trb.org/view/1398805.

Cox, Ben C., and Isaac L. Howard. 2015b. "Merits of Asphalt Concrete Durability and Performance Tests When Applied to Cold In-Place Recycling." In *Proceedings of the International Foundations Congress and Equipment Expo 2015*, 369–379. Reston, VA: American Society of Civil Engineers. https://ascelibrary.org/doi/abs/10.1061/9780784479087.037.

Cox, Ben C., and Isaac L. Howard. 2016. "Cold In-Place Recycling Characterization for Single-Component or Multiple-Component Binder Systems." *Journal of Materials in Civil Engineering* 28, no. 11 (November): 04016118-1–04016118-13. https://ascelibrary.org/doi/full/10.1061/%28ASCE%29MT.1943-5533.0001621.

Cox, Ben C., and Isaac L. Howard. 2017. "Points of Consideration for Obtaining Cold In-Place Recycling Theoretical Maximum Specific Gravity." 17-01082. Paper presented at the Transportation Research Board 96th Annual Meeting, Washington, DC, January 8–12, 2017. https://trid.trb.org/view/1437468.

Cross, Stephen A., Edward R. Kearney, Henry G. Justus, and Warren H. Chesner. 2010. *Cold In-Place Recycling in New York State*. C-06-21. Albany, NY: New York State Department of Transportation. https://rosap.ntl.bts.gov/view/dot/18458.

Da Silva, Marcandali, Amanda Helena, Kamilla L. Vasconcelos, Ana Luisa Aranha, Liedi Bariani Bernucci, and José Mario Chaves. 2013. "Laboratory and Field Evaluation of Cold-In-Place Rap Recycling." 13-4178. Paper presented at the Transportation Research Board 92nd Annual Meeting, Washington, DC, January 13–17, 2013. https://trid.trb.org/view/1242429.

Davidson, J. Keith, and Jean-Martin Croteau. 2003. "Best Practices in Cold In-Place Recycling." In *Annual Meeting Asphalt Emulsion Manufacturers Association*, Nashville, March. https://mcasphalt.com/wp-content/uploads/download-manager-files/2003%20-%20Best%20Practices%20in%20Cold%20In-Place%20Recycling%20-%20Croteau%20J.M.%20and%20Davidson%20J.%20Keith.pdf.

Diefenderfer, Brian, and Ben Bowers. 2017. "Renewed Strength: Virginia Is on the Right Track When It Comes to Rap; I-81 Pavement Still Strong Five Years Later." *Roads and Bridges* 55, no. 2 (February): 36–40. https://www.roadsbridges.com/renewed-strength.

Diefenderfer, Brian K., Benjamin F. Bowers, Charles W. Schwartz, Azadeh Farzaneh, and Zhuoyi Zhang. 2016. "Dynamic Modulus of Recycled Pavement Mixtures." *Transportation Research Record: Journal of the Transportation Research Board* 2575, no. 1 (January): 19–26. https://doi.org/10.3141%2F2575-03.

Division of Construction. 2009. *Tack Coat Guidelines*. Sacramento, CA: California Department of Transportation. https://dot.ca.gov/-/media/dot-media/programs/construction/documents/construction-standards/hma-intelligent-compaction-construction/201910-tack-coat-guidelines-a11y.pdf.

Dong, Wenlong, and Stephane Charmot. 2018. "Propose Tests for Cold Recycling Balanced Mixture Design with Measured Impact of Varying Emulsion and Cement Contents." *Journal of Materials in Civil Engineering* 31, no. 2 (November): 04018387-1–04018387-8. https://doi.org/10.1061/(ASCE)MT.1943-5533.0002611.

EI-Basyouny, M. M., M. W. Witczak, and K. Kaloush. 2005. "Development of the Permanent Deformation Models for the 2002 Design Guide." Paper presented at the Transportation Research Board 84th Annual Meeting, Washington, DC, January 9–13, 2005. https://trid.trb.org/view/1157120.

Epps, J. A., and C. L. Monismith. 1986. *Equipment for Obtaining Pavement Condition and Traffic Loading Data*. National Cooperative Highway Research Program Synthesis of Highway Practice 126. Washington, DC: Transportation Research Board. https://trid.trb.org/view/277331.

Epps, Jon A. 1980. "State-of-the-Art Cold Recycling." *Proceedings of the National Seminar on Asphalt Pavement Recycling*, no. 780, 68–100. https://trid.trb.org/view/167827.

Epps, Jon A. 1990. *Cold-Recycled Bituminous Concrete Using Bituminous Materials*. National Cooperative Highway Research Program Synthesis of Highway Practice 160. Washington, DC: Transportation Research Board. http://onlinepubs.trb.org/Onlinepubs/nchrp/nchrp_syn_160.pdf.

Federal Highway Administration. 2018. *Overview of Project Selection Guidelines for Cold In-Place and Cold Central Plant Pavement Recycling*. FHWA-HIF-17-042. Washington, DC: US Department of Transportation. https://www.fhwa.dot.gov/pavement/asphalt/pubs/hif17042.pdf.

Fišer, Jiří, and Michal Varaus. 2004. *Cold Recycling of Pavements in the Czech Republic*. Brno, Czech Republic: Brno University of Technology. https://citeseerx.ist.psu.edu/viewdoc/download?doi=10.1.1.545.8569&rep=rep1&type=pdf.

Forsberg, Al, Erland Lukanen, and Todd Thomas. 2002. "Engineered Cold In-Place Recycling Project: Blue Earth County State Aid Highway 20, Minnesota." *Transportation Research Record: Journal of the Transportation Research Board* 1813, no. 1 (January): 111–123. https://doi.org/10.3141%2F1813-14.

Fu, Pengcheng, David Jones, John T. Harvey, and Felipe A. Halles. 2010. "Investigation of the Curing Mechanism of Foamed Asphalt Mixes Based on Micromechanics Principles." *Journal of Materials in Civil Engineering* 22, no. 1 (January): 29–38. https://ascelibrary.org/doi/full/10.1061/%28ASCE%29MT.1943-5533.0000009.

Gao, Lei, Fujian Ni, Stephane Charmot, and Hailong Luo. 2014. "Influence on Compaction of Cold Recycled Mixes with Emulsions Using the Superpave Gyratory Compaction." Journal of Materials in Civil Engineering 26 (11):04014081. https://doi.org/10.1061/(ASCE)MT.1943-5533.0000987.

Graziane, Andrea, Christian Iafelice, Simone Raschia, Daniel Perraton, and Alan Carter. 2018." A Procedure for Characterizing the Curing Process of Cold Recycled Bitumen Emulsion Mixtures." *Construction and Building Materials* 173 (June): 754–762. https://doi.org/10.1016/j.conbuildmat.2018.04.091.

Harun, M. H., Z. Sufian, N. A. Aziz, M. Y. Matori, M. Z. Hussain, and A. Azmi. 2010. "Challenges in Design and Construction of Cold In-Place Recycling Pavements in Malaysia." Paper presented at the 24th ARRB Conference, Melbourne, Australia, October 12–15, 2010. https://trid.trb.org/view/1096984.

Hicks, R. G., Dale Allen, Telimoye M. Oguara, Randy Davis, and David Foster. 1987. *Development of Improved Mix Design and Construction Procedures for Cold In-Place Recycled Pavements*. Vol. 1 of *1984–86 Construction Projects*. Salem, OR: Oregon Department of Transportation. https://rosap.ntl.bts.gov/view/dot/22832.

Huang, Yang H. 2004. *Pavement Analysis and Design*. 2nd ed. Upper Saddle River, NJ: Pearson Prentice Hall. https://erdclibrary.on.worldcat.org/oclc/53154617.

Kandhal, Prithvi S., and Rajib B. Mallick. 1997. *Pavement Recycling Guidelines for State and Local Governments: Participant's Reference Book*. FHWA-SA-98-042. Washington, DC: US Department of Transportation. https://www.fhwa.dot.gov/pavement/recycling/98042/98042.pdf.

Kavussi, Amir, and Amir Modarres. 2010. "A Model for Resilient Modulus Determination of Recycled Mixes with Bitumen Emulsion and Cement from Its Testing Results." *Construction and Building Materials* 24, no. 11 (November): 2252–2259. https://doi.org/10.1016/j.conbuildmat.2010.04.031.

Kim, Yongjoo, Soohyok Im, and Hosin "David" Lee. 2011. "Impacts of Curing Time and Moisture Content on Engineering Properties of Cold In-Place Recycling Mixtures Using Foamed or Emulsified Asphalt." *Journal of Materials in Civil Engineering* 23, no. 5 (May): 542–553. https://ascelibrary.org/doi/full/10.1061/%28ASCE%29MT.1943-5533.0000209.

Kim, Yongjoo, and Hosin "David" Lee. 2006. "Development of Mix Design Procedure for Cold In-Place Recycling with Foamed Asphalt." *Journal of Materials in Civil Engineering* 18, no. 1 (February): 116–124. https://ascelibrary.org/doi/full/10.1061/%28ASCE%290899-1561%282006%2918%3A1%28116%29.

Kim, Yongjoo, and Hosin "David" Lee. 2011. "Influence of Reclaimed Asphalt Pavement Temperature on Mix Design Process of Cold In-Place Recycling Using Foamed Asphalt." J*ournal of Materials in Civil Enginee*ring 23, no. 7 (July): 961–968. https://ascelibrary.org/doi/full/10.1061/%28ASCE%29MT.1943-5533.0000274.

Kim, Yongjoo, and Hosin "David" Lee. 2012. "Performance Evaluation of Cold In-Place Recycling Mixtures Using Emulsified Asphalt Based on Dynamic Modulus, Flow Number, Flow Time, and Raveling Loss." *KSCE Journal of Civil Engineering* 16, no. 4 (May): 586–593. https://doi.org/10.1007/s12205-012-1376-0.

Kim, Yongjoo, Hosin "David" Lee, and Michael Heitzman. 2007. "Validation of New Mix Design Procedure for Cold In-Place Recycling with Foamed Asphalt." *Journal of Materials in Civil Engineering* 19 (11): 1000–1010. https://doi.org/10.1061/(ASCE)0899-1561(2007)19:11(1000).

Kim, Yongjoo, Hosin "David" Lee, and Michael Heitzman. 2009. "Dynamic Modulus and Repeated Load Tests of Cold In-Place Recycling Mixtures Using Foamed Asphalt." *Journal of Materials in Civil Engineering* 21, no. 6 (June): 279–285. https://ascelibrary.org/doi/full/10.1061/%28ASCE%290899-1561%282009%2921%3A6%28279%29.

Koh, Chulseung, and Reynaldo Roque. 2010. "Use of Nonuniform Stress-State Tests to Determine the Fracture Energy of Asphalt Mixtures Accurately." *Transportation Research Record: Journal of the Transportation Research Board* 2181, no. 1 (January): 55–66. https://doi.org/10.3141%2F2181-07.

Kuna, Kranthi, Gordon Airey, and Nick Thom. 2014. "Laboratory Mix Design Procedure for Foamed Bitumen Mixtures." *Transportation Research Record: Journal of the Transportation Research Board* 2444, no. 1 (January): 1–10. https://doi.org/10.3141%2F2444-01.

Lane, Becca, and Tom Kazmierowski. 2014. "Implementation of Cold In-Place Recycling with Expanded Asphalt Technology in Canada." *Transportation Research Record: Journal of the Transportation Research Board* 1905, no. 1 (January): 17–24. https://doi.org/10.1177%2F0361198105190500102.

Lee, K. Wayne, Todd E. Brayton, Max Mueller, and Ajay Singh. 2016. "Rational Mix-Design Procedure for Cold In-Place Recycling Asphalt Mixtures and Performance Prediction." *Journal of Materials in Civil Engineering* 28, no. 6 (January): 04016008-1–04016008-7. https://ascelibrary.org/doi/full/10.1061/%28ASCE%29MT.1943-5533.0001492.

Lee, Kang-Won Wayne, Max Mueller, and Ajay Singh. 2014. "Cold In-Place Recycling as a Sustainable Pavement Practice." *Journal of Civil Engineering and Architecture* 8, no. 6 (June): 680–692. https://doi.org/10.17265/1934-7359/2014.06.002.

Lewis, A. J. N., and D. C. Collings. 1999. "Cold In Place Recycling: A Relevant Process for Road Rehabilitation and Upgrading." Paper presented at the 7th Conference on Asphalt Pavements for Southern Africa. https://www.viastrade.it/letteratura/bitume/COLD%20IN%20PLACE%20RECYCLING%20A%20RELEVANT%20PROCESS%20FOR%20ROAD.pdf.

Li, Hongmei, Fujian Ni, Qiao Dong, and Yuqin Zhu. 2018. "Application of Analytic Hierarchy Process in Network Level Pavement Maintenance Decision-Making." *International Journal of Pavement Research and Technology* 11, no. 4 (July): 345–354. https://doi.org/10.1016/j.ijprt.2017.09.015.

Martínez, Adriana H., Rodrigo Miró, and Felix Pérez-Jiménez. 2007. "Spanish Experience with Gyratory Compactor and Indirect Tensile Test in Design and Control of Cold Recycled Asphalt Pavement." *Transportation Research Record: Journal of the Transportation Research Board* 2001, no. 1 (January): 163–168. https://doi.org/10.3141%2F2001-18.

Miller, John S., and William Y. Bellinger. 2003. *Distress Identification Manual for the Long-Term Pavement Performance Program*. 4th ed. FHWA-RD 03-031. Washington, DC: US Department of Transportation. https://rosap.ntl.bts.gov/view/dot/40882.

Modarres, Amir, Majid Rahimzadeh, and Mohsen Zarrabi. 2014. "Field Investigation of Pavement Rehabilitation Utilizing Cold In-Place Recycling". *Resources, Conservation, and Recycling* 83 (February): 112–120. https://doi.org/10.1016/j.resconrec.2013.12.011.

Niazi, Y., and M. Jalili. 2009. "Effect of Portland Cement and Lime Additives on Properties of Cold In-Place Recycled Mixtures with Asphalt Emulsion." *Construction and Building Materials* 23, no. 3 (March): 1338–1343. https://doi.org/10.1016/j.conbuildmat.2008.07.020.

Ozer, Hasan. 2015. "Application of Performance-Based Specifications for Mix Designs." PowerPoint presented at Illinois Bituminous Paving Conference, Urbana, IL, February 3, 2015. https://ws.engr.illinois.edu/sitemanager/getfile.asp?id=1252.

Rodezno, Maria Carolina, Randy West, and Adam Taylor. 2015. "Flow Number Test and Assessment of AASHTO TP 79-13 Rutting Criteria, Comparison of Rutting Performance of Hot-Mix and Warm-Mix Asphalt Mixtures." *Transportation Research Record: Journal of the Transportation Research Board* 2507, no. 1 (January): 100–107. https://doi.org/10.3141%2F2507-11.

Rushing, John F., Thomas D. White, E. Ray Brown, and Navneet Garg. 2012. "Criteria for Using the Superpave Gyratory Compactor to Design Airport HMA Mixtures." *International Journal of Pavement Engineering* 13, no. 2 (October): 126–136. https://doi.org/10.1080/10298436.2011.617443.

Salaices Gomez, Berenice. 2017. "Impact of Reclaimed Asphalt Pavement and Recycled Asphalt Shingles on Laboratory and Field Performance of Texas Asphalt Concrete Pavements." MS diss., The University of Texas at El Paso.

Saleh, Mofreh F. 2006. "Effect of Aggregate Gradation, Mineral Fillers, Bitumen Grade, and Source on Mechanical Properties of Foamed Bitumen Stabilized Mixes." *Transportation Research Record: Journal of the Transportation Research Board* 1952, no. 1 (January): 90–100. https://doi.org/10.1177%2F0361198106195200110.

Salomon, Atenea, and David E. Newcomb. 2000. *Cold In-Place Recycling Literature Review and Preliminary Mixture Design Procedure*. MN/RC-2000-21. St. Paul, MN: Minnesota Department of Transportation. https://trid.trb.org/view/672622.

Sanger, Morgan, Renee Olley, Angela Pakes Ahlman, Tuncer Edil, Andrew Baker, and Erik Elliot. 2017. *Environmental Benefits of Cold-In-Place Recycling*. Madison, WI: University of Wisconsin–Madison. https://rmrc.wisc.edu/wp-content/uploads/2017/09/CIR-WisDOT-Draft.pdf.

Scholz, Todd, David F. Rogge, R. Gary Hicks, and Dale Allen. 1991. "Evaluation of Mix Properties of Cold In-Place Recycled Mixes." *Transportation Research Record: Journal of the Transportation Research Board* 1317:77–89. http://onlinepubs.trb.org/Onlinepubs/trr/1991/1317/1317-009.pdf.

Stroup-Gardiner, Mary. 2012. "Selection Guidelines for In-Place Recycling Projects." *Transportation Research Record: Journal of the Transportation Research Board* 2306, no. 1 (January): 3–10. https://doi.org/10.3141%2F2306-01.

Tabaković, Amir, Ciaran McNally, and Eanna Fallon. 2016. "Specification Development for Cold In-Situ Recycling of Asphalt." *Construction and Building Materials* 102, no. 1 (January). 318–328. https://doi.org/10.1016/j.conbuildmat.2015.10.154.

Tario, J. D. 2010. *Cold-In-Place Recycling in New York State*. C-06-21. Albany, NY: New York State Department of Transportation. https://rosap.ntl.bts.gov/view/dot/18458.

Turk, Janez, Alenka Mauko Pranjić, Ana Mladenovič, Zvonko Cotič, and Primož Jurjavčič. 2016. "Environmental Comparison of Two Alternative Road Pavement Rehabilitation Techniques: Cold-In-Place-Recycling Versus Traditional Reconstruction." *Journal of Cleaner Production* 121 (May): 45–55. https://doi.org/10.1016/j.jclepro.2016.02.040.

US Army Corps of Engineers. 1995a. *Standard Test Method For Unit Weight, Marshall Stability, and Flow of Bituminous Mixture*. CRD-C649-95. Washington, DC: US Army Corps of Engineers.

US Army Corps of Engineers. 1995b. *Standard Test Method For Density And Percent Voids In Compacted Bituminous Paving Mixtures*. CRD-C650-95. Washington, DC: US Army Corps of Engineers.

USACE (US Army Corps of Engineers) (Preparing Agency). 2018. *Cold-Mix Reused Asphalt Paving*. UFGS 32 01 16.70. Washington, DC: USACE, Naval Facilities Engineering Command, US Air Force Civil Engineering Center, NASA. https://www.wbdg.org/FFC/DOD/UFGS/UFGS%2032%2001%2016.70.pdf.

VanFrank, Kevin. 2015. *Cold In-Place Recycle Phase III, Supplemental—Field Protocol: Short Term Field Stability*. Supplemental Report. UT-15.08. Salt Lake City, UT: Utah Department of Transportation. https://rosap.ntl.bts.gov/view/dot/29581.

Wegman, Daniel E., and Mohammadreza Sabouri. 2016. *Optimizing Cold In-Place Recycling (CIR) Applications through Fracture Energy Performance Testing*. MN/RC 2016-21. St. Paul, MN: Minnesota Department of Transportation, Research Services and Library. http://www.dot.state.mn.us/research/TS/2016/201621.pdf.

Winke, Jeff. 2014. "Brazilian Contractor Uses Cold-in-Place Recycling in Major Highway Rehab." *Asphalt Contractor*, September 15, 2014. https://www.forconstructionpros.com/asphalt/article/12001350/brazilian-contractor-uses-coldinplace-recycling-in-major-highway-rehab.

Wirtgen. 2006. *Cold Recycling Manual*. 2nd ed. Windhagen, Germany: Wirtgen.

Wirtgen. 2012. *Wirtgen Cold Recycling Technology*: *Recommended Performance Guidelines*. 2nd ed. Windhagen, Germany: Wirtgen.

Wirtgen. 2016. *Cold Recycling for the Rehabilitation of Ayrton Senna Highway*. Windhagen, Germany: Wirtgen. https://www.wirtgen-group.com/binary/full/o5598v77_W_jobreport_AyrtonSennaHighway_0517_EN.pdf.

Wirtgen. n.d. "Cutting-Edge Wirtgen Technology in Successful Operation on Interstate 81." News and Media. https://www.wirtgen-group.com/en-us/news-and-media/wirtgen/job-report-interstate-81/.

Yan, J., F. Ni, J. Jia, and Z. Tao. 2009. "Investigation on the Bulk Performance and Microstructure of Emulsion-Based, Cold In-Place Recycling Mixtures." *Journal of Testing and Evaluation* 37 (5): 436–441. https://doi.org/10.1520/JTE000344.

Acronyms and Abbreviations

AASHTO	American Association of State Highway and Transportation Officials
ANOVA	Analysis of variances
APA	Asphalt pavement analyzer
ARRA	Asphalt Recycling and Reclaiming Association
ASG	Asphalt strain gage
AV	Air voids
BMD	Balanced mix design
CIR	Cold in-place recycling
CMS	Cationic medium-setting emulsion
CREATEs	Center for Research and Education in Advanced Transportation Engineering Systems
CRREL	Cold Regions Research and Engineering Laboratory
CSS	Cationic slow-setting emulsion
DoD	Department of Defense
DOT	Department of Transportation
ERDC	US Army Engineer Research and Development Center
ESAL	Equivalent single-axle load
FN	Flow number
FWD	Falling weight deflectometer
GSL	Geotechnical and Structures Laboratory
HFMS	High-float medium-setting emulsion
HMA	Hot mix asphalt

HPTO	High-performance thin overlay
HVS	Heavy vehicle simulator
HWD	Heavy weight deflectometer
IDT	Indirect tension test
IRI	International Roughness Index
ITS	Indirect tensile strength
MS	Medium-setting emulsion
OWC	Optimum water content
PC	Pressure cell
RAP	Reclaimed asphalt pavement
RUAPTF	Rowan University Accelerated Pavement Testing Facility
SCB	Semicircular bend
SCB-FE	Semicircular bend fracture energy
SGC	Superpave Gyratory Compactor
SS	Slow-setting emulsion
UFGS	Unified Facilities Guide Specifications
USACE	US Army Corps of Engineers
VB	Volume of asphalt binder
VFB	Voids filled with asphalt binder
VMA	Voids in mineral aggregates

REPORT DOCUMENTATION PAGE

Form Approved
OMB No. 0704-0188

1. REPORT DATE (DD-MM-YYYY)	2. REPORT TYPE	3. DATES COVERED (From - To)
October 2022	Technical Report / Final Report	FY18–FY20

4. TITLE AND SUBTITLE

Development and Validation of a Balanced Mix Design Approach for CIR Mixtures Using Full-Scale Testing

5a. CONTRACT NUMBER

5b. GRANT NUMBER

5c. PROGRAM ELEMENT
0602784A

6. AUTHOR(S)

Ayman Ali, Ahmed Saidi, Yusuf Mehta, Christopher J. DeCarlo, Mohamed H. Elshaer, Ben C. Cox, and Wade A. Lein

5d. PROJECT NUMBER
T53

5e. TASK NUMBER
09

5f. WORK UNIT NUMBER

7. PERFORMING ORGANIZATION NAME(S) AND ADDRESS(ES)

Center for Research and Education in Advanced Transportation Engineering Systems (CREATEs)
Rowan University
201 Mullica Hill Rd.
Glassboro, NJ 08028

8. PERFORMING ORGANIZATION REPORT NUMBER
ERDC TR-22-21

9. SPONSORING / MONITORING AGENCY NAME(S) AND ADDRESS(ES)

Headquarters, US Army Corps of Engineers
Washington, DC 20314-1000

10. SPONSOR/MONITOR'S ACRONYM(S)
USACE

11. SPONSOR/MONITOR'S REPORT NUMBER(S)

12. DISTRIBUTION / AVAILABILITY STATEMENT

Approved for public release; distribution is unlimited.

13. SUPPLEMENTARY NOTES

14. ABSTRACT

The main goal of this study was to improve the performance of cold in-place recycling (CIR) mixtures by using a balanced mix design (BMD) approach. This study involved preparing and testing CIR mixtures in the lab at varying contents of bituminous additives and constant content of 1% cement and 3% water. Eight combinations of CIR mixtures were produced for this study using two binders (emulsion and foamed asphalt), compaction efforts (30 and 70 gyrations), and curing processes (72 hours at 140°F and 50°F). Results showed that asphalt pavement analyzer, semicircular bend, and indirect tensile strength tests presented the highest correlation with the change of binder contents. The study successfully used the developed BMD for designing CIR mixtures and selecting their optimum binder contents. It then used three balanced CIR mixtures to construct full-scale pavement sections to validate the BMD approach in the field. A heavy vehicle simulator was used to apply different accelerated loadings on each section. Results showed that the CIR section with 2% binder presented the best rutting performance under truck loading and the highest rutting susceptibility under aircraft loading. Conversely, the CIR section with 3% binder presented the highest cracking resistance under both truck and aircraft loading.

15. SUBJECT TERMS

Aggregates (Building materials); Asphalt emulsion mixtures--Evaluation, Binders (Materials); Bituminous materials; Cement; Pavements, Asphalt--Maintenance and repair; Pavements, Asphalt--Recycling

16. SECURITY CLASSIFICATION OF:			17. LIMITATION OF ABSTRACT	18. NUMBER OF PAGES	19a. NAME OF RESPONSIBLE PERSON
a. REPORT	b. ABSTRACT	c. THIS PAGE			19b. TELEPHONE NUMBER (include area code)
Unclassified	Unclassified	Unclassified	SAR	144	

7 (cont.). PERFORMING ORGANIZATION NAME(S) AND ADDRESS(ES)

US Army Engineer Research and Development Center (ERDC)
Cold Regions Research and Engineering Laboratory (CRREL)
72 Lyme Road
Hanover, NH 03755-1290

US Army Engineer Research and Development Center (ERDC)
Geotechnical and Structure Laboratory (GSL)
3909 Halls Ferry Road
Vicksburg, MS 39180